NTNU

Norwegian University of
Science and Technology

Corrosion and Cathodic Protection of Steel-Aluminium Galvanic Couples in Subsea Structures

Kristin Jacobsen

Chemical Engineering and Biotechnology
Submission date: June 2018
Supervisor: Kemal Nisancioglu, IMA
Co-supervisor: Otto Lunder, IMA
Andreas Erbe, IMA
Roy Johnsen, MTP

Norwegian University of Science and Technology
Department of Materials Science and Engineering

Preface

This master's thesis was written during spring of 2018 at the Department of Materials Science and Engineering at the Norwegian University of Science and Technology (NTNU) in Trondheim, Norway. The thesis is a continuation of the specialization project written during fall 2017 and the master's theses of Harald Solli and Sondre Røstbø.

I would like to give thanks to my supervisor, Professor Kemal Nisancioglu, for guidance and help. Also, I would like to give thanks to my co-supervisors Roy Johnsen, Otto Lunder and Andreas Erbe for their guidance.

A special thanks goes to Staff Engineer Anita Storsve for preparing salt bridges with me, for guidance and technical advice at the lab, and for always respond to my problems. For preparing samples and creating crevice devices for the experimental setup the mechanical workshop at NTNU, *Finmekanisk Verksted*, deserves gratitude. Thanks to Harald Solli for always answering on my questions.

Last but not least, a big thanks goes to Sondre Røstbø for guidance and teaching me the experimental methods for the project. For always respond to my questions and being helpful.

Trondheim, June 11, 2018

Kristin Jacobsen

Summary

An increasing interest for use of aluminium in subsea structures has been seen the resent years, considering replacing some of the heavier steel components with aluminium. Due to good corrosion resistance and strength to weight ratio the aluminium alloys of the 5000-series and 6000-series are of great relevance. Galvanic corrosion and crevice corrosion must be taken into consideration when replacing the more noble steel with aluminium. Cathodic protection of steel is widely used in seawater structures, and the possibility of protecting both steel and aluminium in galvanic couples is therefore of interest.

The aim of the thesis was to investigate whether or not steel-aluminium galvanic couples could be protected against crevice corrosion by applied cathodic protection. Samples of carbon steel X65 and the aluminium alloys 5083 and 6082 were galvanic coupled in a simulated crevice with applied CP by the sacrificial anode AlZnIn. The experiments were performed in artificial seawater at 10°C with exposure time up to twenty days. The affect of crevice sizes of $100\,\mu m$ and $300\,\mu m$ was studied. In addition, galvanic couples of carbon steel X65 and the aluminium alloys 5083, 6005 and 6082 in absence of a crevice were studied to validate the effect of cathodic protection. Open Circuit tests were also performed. Weight loss measurements and surface characterization by SEM and EDS were performed to examine corrosion rates and the formation of deposits.

Cathodic protection of the galvanic couples was possible in the absence of a crevice, where cathodic currents were seen on both steel and the aluminium alloys. The currents on steel were one and two order of magnitude larger than on Al. Galvanic couples in a simulated crevice with size of $300\,\mu m$ showed anodic currents on Al, though cathodic currents were seen on steel. A uniform calcareous deposit layer mainly of $Mg(OH)_2$ was seen on steel with precipitation of Ca-ions near the steel surface. A thin protective oxide layer was observed on Al. In galvanic couples with a crevice of $100\,\mu m$ the aluminium alloys showed initial anodic peak currents which steadily decayed towards zero. The corrosion rates increased as a function of exposure time, and localized corrosion was mainly seen at the crevice mouth on Al. Higher initial cathodic currents were seen on steel which decreased steadily. Reduction reactions on steel increased the pH in the crevice and the oxide film on Al was destabilized. Intermetallic cathodic sites in the Al-matrix were detached due to alkaline etching. Oxygen depletion in the crevice and the formation of calcareous deposits and renewed oxide films stabilized the currents and the corrosion attacks on the alloys with time. Nevertheless, steel-aluminium galvanic couples could be protected in the form of corrosion control against crevice corrosion with applied cathodic protection.

Sammendrag

Det har de siste årene vært en økende interesse for aluminium som materiale i undersjøiske strukturer, med tanke på å erstatte noen av de tyngre stålkomponentene med aluminium. Som følge av god motstandsdyktighet for korrosjon og stor styrke i forhold til vekten er aluminiumlegeringer fra 5000 - og 6000 serier av stor relevans. Ved å erstatte det mer edle stålet med aluminium må galvanisk korrosjon og spaltkorrosjon tas i betraktning. Katodisk beskyttelse av stål er vidt utbredt i strukturer til sjøs, og muligheten for å beskytte både stål og aluminium i galvaniske koblinger er derfor av interesse.

Formålet med oppgaven var å undersøke om det var mulig å beskytte stål-aluminium galvaniske koblinger mot spaltkorrosjon ved katodisk beskyttelse. Prøver av karbonstål X65 og aluminiumlegeringene 5083 og 6082 ble galvanisk koblet i en simulert spalt med tilført katodisk beskyttelse fra offeranoden AlZnIn. Eksperimentene ble utført i kunstig sjøvann ved 10°C eksponert opp til tjue dager. Påvirkningen av spaltstørrelser på $100\,\mu\mathrm{m}$ og $300\,\mu\mathrm{m}$ ble undersøkt. I tillegg ble galvaniske koblinger av karbonstål X65 og aluminiumlegeringene 5083, 6005 og 6082 undersøkt i fraværet av spalt for å validere effekten av katodisk beskyttelse. Åpen krets målinger ble også utført. Vekttapsmålinger og overflate karakterisering i SEM og EDS ble utført for å undersøke korrosjonshastighetene og formasjonen av belegg på overflatene.

Katodisk beskyttelse av de galvaniske koblingene var mulig i fravær av spalt, hvor katodiske strømmer ble observert på både stål og aluminiumlegeringene. Strøm på stålet var en og to størrelsesordener større enn på aluminium. Galvaniske koblinger i spalt på $300\,\mu\mathrm{m}$ viste anodiske strømmer på aluminiumlegeringene, selv om katodiske strømmer var sett på stålet. Et uniformt kalkbelegg bestående hovedsakelig av $Mg(OH)_2$ var sett på stålet, med utfelling av Ca-ioner nær ståloverflaten. Et tynt beskyttende oksidlag ble observert på Al. I galvaniske koblinger med en spalt på $100\,\mu\mathrm{m}$ ble initielle anodiske strømtopper sett på aluminiumlegeringene, hvor av de jevnt avtok mot null. Korrosjonshastighetene økte som funksjon av eksponeringstiden og lokalisert korrosjon var hovedsakelig sett i spaltmunningen på Al. Høyere initielle katodiske strømmer ble sett på stålet hvor av de jevnt avtok. Reduksjonsreaksjoner på stålet bidro til å øke pH i spalten og oksidfilmen på aluminium ble destabilisert. Intermetalliske katodiske seter i Al-matrisen falt av som følge av alkalisk etsning. Uttømming av oksygen i spalten samt formasjonen av kalkbelegg og fornyet oksidfilm bidro til stabilisering av både strømmen og korrosjonsangrepene på legeringene. Stål-aluminium galvaniske koblinger kan likevel bli beskyttet mot spaltkorrosjon i form av korrosjonskontroll ved tilført katodisk beskyttelse.

Contents

List of Symbols

Symbol	Explanation	Unit
E_{couple}	Coupling potential	V
I_{net}	Net current	A
i_{corr}	Corrosion current density	A/cm^2
E_{corr}	Corrosion potential	V
E_p	Protection potential	V

Chapter 1

Introduction

1.1 Background

An increased interest for use of aluminium alloys in subsea structures has been seen the resent years. The 5000-series (AlMg) and 6000-series (AlMgSi) are especially of interest due to good corrosion resistance and strength to weight ratio. Furthermore, these alloys are recommended for seawater structures [1], [2]. A protective oxide film is developed on aluminium when immersed in seawater. In contrary, the frequently used carbon steel in subsea application needs an additional protective system. Replacing some of the heavier steel with aluminium in the structures on the seabed is desired due to weight limitations when installed and maintained. The outcome would be reduced cost due to installation and maintenance, but also safety aspects during installation and fabrication costs [3]. Galvanic corrosion must be taken into account when replacing some of the steel with aluminium, where the less noble aluminium will sacrificially corrode in contact with the nobler steel. Furthermore, joining dissimilar metals in seawater could lead to crevice corrosion.

Sacrificial anodes are often used as cathodic protection (CP) of steel in seawater. Studies have shown that current requirements on aluminium are reduced by an order of magnitude when cathodic protection is applied [4], [5]. A protective system of the galvanic coupling of steel-aluminium is therefore of great relevance. Investigations of steel-aluminium galvanic couples in NaCl solutions at 25°C have shown a protective current on steel [6], however aluminium revealed localized corrosion [6],[7]. However, a significant reduction in corrosion rates of aluminium was seen when cathodic protection was applied to the

galvanic coupling in artificial seawater [7]. Studies in artificial seawater have shown that steel-aluminium galvanic couples in the presence of a crevice experience some localized crevice corrosion due to an increased alkaline environment, especially at the crevice mouth [7],[8],[9]. The formation of calcareous deposit had an impact on the corrosion rates when CP was applied in these short term experiments. Though, fewer studies have been performed of these galvanic couplings with applied cathodic protection in the presence of a crevice at more seawater realistic temperatures and longer exposure time.

1.2 Aim of the master's thesis

The aim of this master's thesis is to investigate whether or not steel-aluminium galvanic couples can be protected against crevice corrosion by application of cathodic protection. The electrochemical behavior of the galvanic couples in a simulated crevice in artificial seawater at 10°C is going to be studied for exposure time up to twenty days. The affect of crevice sizes of $100\,\mu m$ and $300\,\mu m$ will be examined. Galvanic corrosion experiments in absence of a crevice are also going to be studied to validate the effect of cathodic protection of steel-aluminium galvanic couples. In addition, Open Circuit experiments will be performed of the respective alloys. Samples of carbon steel X65 and the aluminium alloys 5083, 6005 and 6082 in addition to the sacrificial anode AlZnIn will be used in the experimental work. Weight loss measurements to determine corrosion rates will be performed. In addition, calculations of the weight losses from the electrochemical data will be performed. Furthermore, surface characterization by Scanning Electron Microscopy (SEM) will be done, in addition to determining the chemical composition of the surface deposits by Electron Dispersive Spectroscopy (EDS). This master's thesis is a continuation of the specialization project of the author in addition to the master's theses of Sondre Røstbø and Harald Solli. The experimental methods in the thesis will be based on the work of Røstbø. Comparisons of the earlier obtained results in this ongoing project are also to be performed.

Chapter 2

Theory

2.1 Galvanic corrosion

Galvanic corrosion will occur when dissimilar metals in metallic contact are in presence of a corrosive environment [10]. The active metal, the less noble metal N, generates a positive net current flow to metal M. Metal N experience thus an increased corrosion rate and dissolves. The potential of metal N and M becomes equal a couple potential, E_{couple}, by the assumption of no ohmic potential drop in the electrolyte nor the closed circuit. Possible oxidation reactions are as follow [10]:

$$M \rightarrow M^{n+} + ne^- \tag{2.1}$$

$$N \rightarrow N^{n+} + ne^- \tag{2.2}$$

And possible reduction reactions are:

$$2H^+ + 2e^- \rightarrow H_2 \tag{2.3}$$

$$2H_2O + 2e^- \rightarrow H_2 + 2OH^- \tag{2.4}$$

$$O_{2(dissolved)} + 2H_2O + 4e^- \rightarrow 4OH^- \tag{2.5}$$

$$O_{2(dissolved)} + 4H^+ + 4e^- \rightarrow 2H_2O \tag{2.6}$$

The total rate of oxidation is equal the total rate of reduction when the circuit is closed and there is no ohmic resistance when the potential equals the coupling potential [10]. The measured current, I_{net}, is the difference between the sum of oxidation and reduction currents. The corrosion current density or the corrosion rate, i_{corr}, is equal the oxidation reaction by assuming that metal dissolution is the only oxidation reaction.

2.2 Cathodic protection

Cathodic protection (CP) is a well-known method of protecting structures against corrosion. It can be achieved by galvanically connecting a more active metal to the structures, a sacrificial anode. Sacrificial anodes are preferred as cathodic protection systems for seawater installations [11]. A protective current is provided from the anode to the more noble structure, where the anode experience anodic dissolution and is consumed. Due to low weight and high electrochemical capacity aluminium based anodes are widely used [11]. AlZnIn is a commonly used anode in marine structures which gives an operating potential of -1100 mV_{SCE}. These anodes are fabricated such that the pits occurring are small and tightly packed during anode consumption. The potential needs to be lowered from the corrosion potential, E_{corr}, to a protection potential, E_p, in order to protect the structure of interest [10].

2.2.1 Cathodic protection of steel

Cathodic protection is applied when carbon steel and low alloy steels are used as structural material in marine environments. Figure 2.1 shows the Pourbaix diagram for iron in water, which shows the potential V_{SCE} as a function of pH. Due to poor corrosion resistance, steel submerged in seawater must be polarized to a potential between -850 mV_{SCE} and -1100 mV_{SCE} by the CP system to be protected [11]. Though, protection of carbon steel should not be considered as a way of stopping corrosion, rather a method of corrosion control [11],[12].

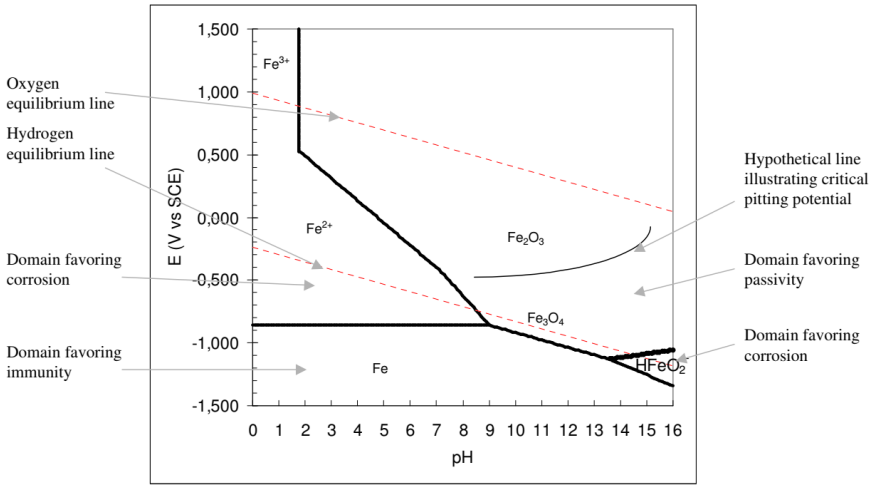

Figure 2.1: Pourbaix diagram for iron in water [13].

Calcareous deposits

Calcareous deposits forms on steel surfaces immersed in seawater when cathodic protection is applied. The formation of hydroxyl-ions according to the reduction reactions equation (2.4) and (2.5) gives an increased pH at the steel surface. Dissolution of CO_2 from the atmosphere into seawater reacts according to [10]:

$$CO_2 + H_2O \rightarrow H_2CO_3 \tag{2.7}$$
$$H_2CO_3 \rightarrow H^+ + HCO_3^- \tag{2.8}$$
$$HCO_3^- \rightarrow H^+ + CO_3^{2-} \tag{2.9}$$

Calcium ions present in seawater react with CO_3^{2-} in equation (2.9) and the hydroxyl-ions react with magnesium-ions and forms calcareous deposits:

$$Ca^{2+} + CO_3^{2-} \rightarrow CaCO_{3(s)} \tag{2.10}$$
$$Mg^{2+} + 2OH^- \rightarrow Mg(OH)_{2(s)} \tag{2.11}$$

The current requirement from the anode is reduced due to calcareous deposits on steel surfaces [10]. The diffusion of oxygen to the metal surface is limited. The Ca/Mg ratio has a significant affect of the reduced current requirement from the anode. The deposition kinetics of calcareous deposits is influenced e.g. by applied potential and current, temperature, flow rate and pH respectively. Okstad [14] found the composition of calcareous deposit to be depending of applied potential and flow velocity. Figure 2.2 shows the Ca/Mg ratio in calcareous deposits as a function of applied potential and flow velocity.

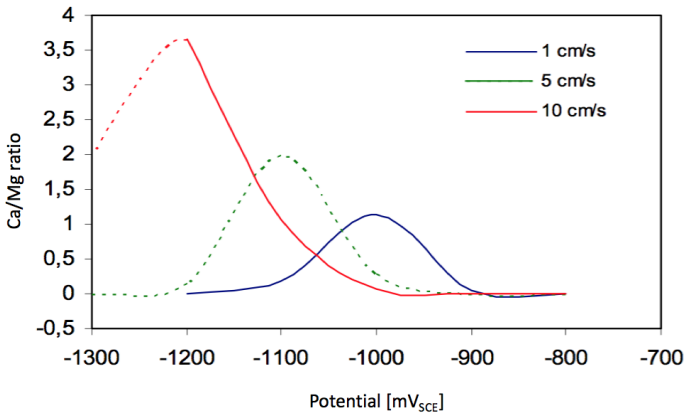

Figure 2.2: Ca/Mg ratio as a function of applied potential [mV$_{SCE}$] and flow velocity [cm/s]. Dashed lines represented assumed data. Adapted from Okstad [14].

The Ca/Mg ratio was reported to decrease with increasing flow velocities at potentials of -900 mV_{SCE} and -1000 mV_{SCE} [14]. At potentials of -1000 mV_{SCE} and -1100 mV_{SCE} $CaCO_3$ precipitated at all flow velocities (1, 5 and 10 cm/s). At temperatures of 8-10°C the kinetics of $CaCO_3$ was found to be slow at the steel surface. The deposition kinetics of $Mg(OH)_2$ was reported to be faster than for $CaCO_3$, and the precipitation of $CaCO_3$ was inhibited of Mg-ions at high pH and more negative potentials [14]. Elbeik et al. reported that a $CaCO_3$ film on mild steel could lead to a reduction in corrosion current by a factor of five for the oxygen reduction [15].

Barchiche et al. [16] investigated the formation of $CaCO_3$ and $Mg(OH)_2$ on steel surfaces in artificial seawater at different potentials and temperatures by chronoamperometry and electrochemical impedance spectroscopy (EIS). The calcareous deposit obtained at a potential of -1000 mV_{SCE} and a temperature of 10°C was the aragonite structure of $CaCO_3$ [16]. The study also indicated that sulphate-ions inhibited the formation of aragonite, possibly by promoting the magnesium gel layer at potentials of -1000 mV_{SCE} and 20°C. Barchiche et al. stated that brucite appeared as a homogeneous layer and aragonite crystals were smaller at a potential of -1200 mV_{SCE} and 10°C. In addition, aragonite crystals were observed on the brucite layer [16]. Yang et al. studied the calcareous deposits on cathodic protected mild steel in artificial seawater and calculated a pH of 7.58 for the $CaCO_3$ precipitation and 10 for $Mg(OH)_2$ [17]. On the other hand, in natural seawater Okstad reported a pH of 6.0 for the precipitation of $CaCO_3$ and 9.1 for $Mg(OH)_2$ [14].

2.2.2 Cathodic protection of aluminium

The 5000-series (AlMg) and 6000-series (AlMgSi) of the aluminium alloys are of interest in marine structural applications due to corrosion resistance properties and strength to weight ratio. Furthermore, aluminium alloy 5083 and 6082 are preferred alloys for seawater structures [1], [2]. Due to Mg and its increased passivity in slightly alkaline environment the 5000-series have significant corrosion resistance [10]. Small particles of the Mg_2Si-phase in 6000-series give these alloys their strength. Caution has to be made for alloys with a high amount of Si, where the Mg/Si ratio gets small and the alloy become susceptible to intergranular corrosion [10]. The 6000-series are enriched with a higher content of Cu. The more noble Cu will act as cathodic sites in the Al-matrix, leading to dissolution of the surrounding matrix and enrich the matrix with the noble Cu. Small amounts of Cu could also lead to the susceptibility for intergranular corrosion [10].

The passivating aluminium oxide formed on the aluminium surface is unstable in both acidic and alkaline solutions, it is an amphoteric component [18]. The Pourbaix diagram in figure 2.3a shows that the passive region is in the pH range of 4 - 8.5, and an immune

region is indicated for potentials more negative than -2.0 V_{SCE} [19]. On the other hand, figure 2.3b shows the experimental potential-pH diagram for AA5086 in sodium chloride solution, indicating a passive region of pH 4 - 8.5 and a narrower passive potential range [20]. An immune region is not indicated in the latter diagram. The oxides of the alloy elements Mn and Mg, which becomes more passive with increased pH, could influence the passive region of aluminium alloys [4].

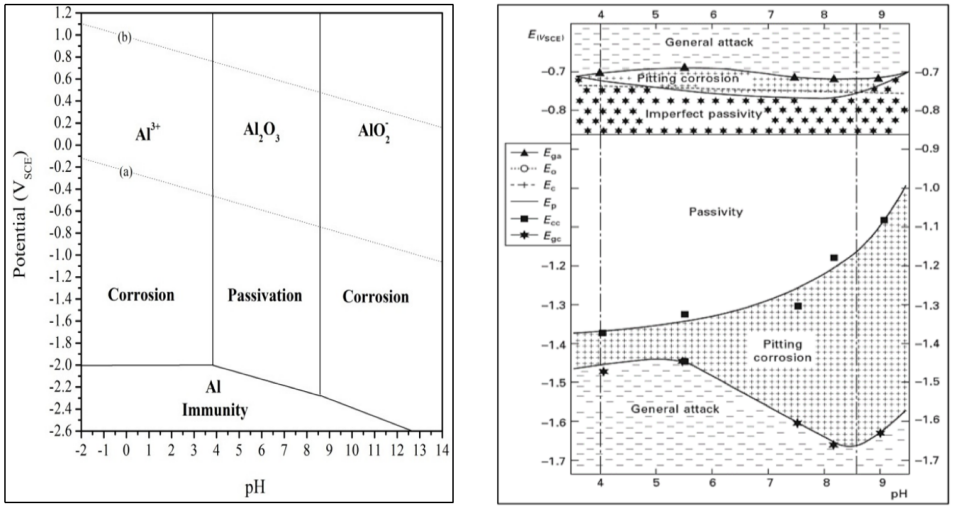

(a) **(b)**

Figure 2.3: (a) Pourbaix diagram for pure aluminium in aqueous solution at 25°C, where line (a) and (b) corresponds to reduction of hydrogen and oxygen [19]. (b) Experimental potential-pH diagram for aluminium alloy 5086 in sodium chloride solution [20].

Johnsen and Nese [21], studied the effect of potential on corrosion behavior of aluminium alloy 5083 and 6082 exposed in natural seawater at 10°C. Investigations of both the Open Circuit Potential and the effect of cathodic protection were made. The OCP was measured for freely exposed samples over a period of thousand hours. The OCP of AA5083 and AA6082 was -710 $mV_{Ag/AgCl}$ and -880 $mV_{Ag/AgCl}$ respectively after two hours [21]. After thousand hours the OCP of the samples had developed to be -790 $mV_{Ag/AgCl}$ and -890 $mV_{Ag/AgCl}$ respectively [21]. The cathodic polarization when connected to a sacrificial anode at -1050 $mV_{Ag/AgCl}$ showed a cathodic current on both alloys. The AA5083 showed an increasing cathodic current before it decreased exponentially. The cathodic current on AA6082 varied during the test period. Pitting potentials of the respective alloys were obtained by polarization curves of the freely exposed samples involved in the OCP. A pitting potential of -620 $mV_{Ag/AgCl}$ and -590 $mV_{Ag/AgCl}$ was obtained on AA5083 and

A6082 respectively after thousand hours [21]. Johnsen and Nese concluded that the experimental potential-pH diagram for aluminium alloy 5086, shown in figure 2.3b, is valid for AA5083 and AA6082 in seawater at 10°C [21]. Though, cathodic polarization at a potential of -1050 $mV_{Ag/AgCl}$ initiated pits on the sample surfaces.

Increased reduction reactions give rise to increasing pH due to formation of hydroxyl-ions when cathodic protection is applied. The oxide layer on aluminium may become destabilized in more alkaline environment [4]. The Al-matrix consist of less cathodic areas compared to steel, hence aluminium requires lower currents from the sacrificial anode. Reduction reactions occur at intermetallic particles in the Al-matrix, figure 2.4a, such as the more noble Fe, which acts as cathodic sites [5]. The oxide layer surrounding the intermetallic particles starts to dissolve due to increased alkaline pH at these cathodic sites, as shown in figure 2.4b. An alkaline etching of the Al-matrix surrounding the intermetallic particles initiates. As a consequence, the intermetallic particles may be detached and the particle sites will probably be covered with calcareous deposits, corrosion products and a renewed oxide layer as shown in figure 2.4c, as there will be less cathodic sites left [5].

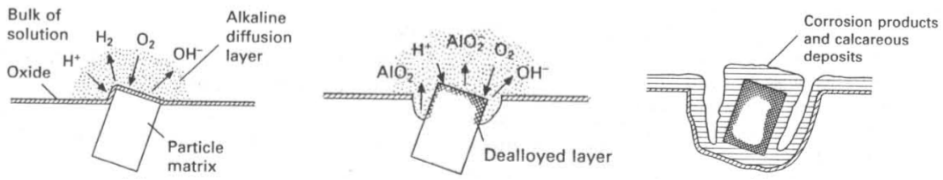

Figure 2.4: Mechanism of cathodic protection of aluminium alloys in seawater: (a) Alkaline diffusion layer developed according to hydrogen and oxygen reduction reactions at intermetallic particles in the aluminium matrix. (b) Dissolution of aluminium oxide film, causing a dealloyed layer. (c) Alkaline etching of the aluminium matrix leads to detachment of the particle [5].

The current requirements are reduced by an order of magnitude when cathodic protection is applied due to detachment of cathodic intermetallic particles from the Al-matrix [4]. Gundersen and Nisancioglu [5] investigated cathodic protection of aluminium alloys from the 1000-series, 5000-series and 6000-series in natural seawater at 9±2°C and flow rates of 2.5 and 8 cm/s. Cathodic polarization curves were obtained on the three different aluminium alloys as well as carbon steel at a flow rate of 8 cm/s. The current density on steel was given by the limiting current for oxygen reduction [5]. The polarization curve for the 6000-series indicated a cathodic reaction rate an order of magnitude smaller than for steel. This indicated the reduction reactions on aluminium to be on the intermetallic sites. The

requirement of the steady state current for the 1000-series and 5000-series was lower than for the 6000-series due to less particles on the surface of these alloys [5]. Johnsen and Nese [21] also studied the surfaces of the cathodic polarized AA5083 and AA6082 after exposed to seawater at 10°C. Investigations in SEM revealed pitting corrosion on both samples with pit depths of $5\,\mu\mathrm{m}$. The pitting was assumed to occur due to detachment of intermetallic particles as a consequence of alkaline etching [21].

2.2.3 Steel-aluminium galvanic couples

Pryor and Keir [6], studied galvanic couples of aluminium - mild steel and zinc - mild steel in NaCl solution at 25°C. The electrochemical behavior of the couples in addition to weight loss measurements were investigated. Steel showed a cathodic electrochemical behavior when coupled to both Al and Zn, and weight loss measurements of steel revealed complete protection against corrosion from the coupling [6]. Al and Zn both revealed anodic currents when coupled to steel. In static solutions were both Al and Zn uniformed corroded [6]. Pryor and Keir calculated the weight losses of Al and Zn from the currents, and found that measured weight losses were higher due to local attacks [6].

Røstbø studied steel-aluminium galvanic couples and the possibility of applying cathodic protection to the coupling [7]. Due to reduction reactions occurring only on Fe-rich intermetallic particles in the Al-matrix, the reduction rate on aluminium was found to be one and two orders of magnitude smaller than the rate on steel [7]. Weight loss measurements of both steel and AA6005 showed decreased corrosion rates when galvanic coupled with the sacrificial anode AlZnIn in artificial seawater compared to the open circuit experiments [7]. On the other hand, AA6005 experienced an increased corrosion rate in NaCl solution at 25°C when galvanic coupled to steel and the anode, where AA6005 revealed localized corrosion. Røstbø stated cathodic protection of steel-aluminium galvanic couples to be possible [7].

2.3 Crevice corrosion

Narrow gaps or cavities between two metals joined together in the presence of an electrolyte give rise to crevice corrosion. Concentration differences between the inside and the outside of the narrow gaps arises with time [10]. Crevice corrosion is a localized attack which often occurs at active-passive metals because of their susceptibility [10]. Furthermore, it is often seen between metals, washers, screws and flanges of pipes. Localized attacks are especially observed at the crevice mouth. Initially, there are no concentration difference of the solution inside a crevice and the bulk solution. However, as a consequence of depleted dissolved oxygen on the inside of the crevice, which can not be replenished from the bulk solution fast enough, a potential difference arises between the inside of the crevice and the bulk solution [10]. The dominating reaction in the bulk then becomes the oxygen reduction. Dissolved metal equation (2.12) as well as hydrolysis equation (2.13) becomes the dominating reactions on the inside of the crevice

$$M \rightarrow M^+ + e^- \tag{2.12}$$

$$M^+ + H_2O \rightleftharpoons MOH_s + H^+ \tag{2.13}$$

where the hydrolysis results in an excess of positive charge [10]. Migration of negative ions like Cl^- from the bulk solution into the crevice causes an increased corrosive environment, inducing crevice corrosion. The potential differ in accordance to enhanced ohmic potential drop which changes over the crevice length [10]. The potential difference is nonuniform and promotes nonuniform current distribution in the crevice [10]. Joma et al. [22], studied crevice corrosion of AISI 316L Stainless Steel coupled with an inert plan by use of a thin-layer cell. A decreasing cathodic current was seen on the steel at a potential of -1.1 V_{SSE} as a consequence of depleted oxygen in the crevice of $150\,\mu m$ [22]. Joma et al. also investigated crevice corrosion of Al and Cu in a thin layer cell in 0.1 M Na_2SO_4 solution. The increased pH due to oxygen reduction reaction initiated cuprous oxide dissolution and copper replating in the crevice [22].

2.3.1 Effect of cathodic protection on crevice corrosion

Cathodic protection of crevices has been studied by Li et al [23]. Figure 2.5 shows the recorded potential and cathodic current on steel along a crevice of 1.0 mm in diluted NaCl solution. Figure 2.5a shows a decreasing potential gradient in the crevice, stabilizing after 25 hours [23]. An anodic peak was measured 65 mm into the crevice, as shown in figure 2.5b. The anodic current was measured after one hour and disappeared with time. Heterogeneity of the steel and chemical environment generated a local corrosion cell which the anodic peak arose from [23]. Nevertheless, applied cathodic protection to prevent local corrosion in crevices seemed possible. Li et al. also reported that the pH in the crevice

increased from the initial value of 6.6 to a final value of 8.6-10.6 [23]. The pH increased due to formation of hydroxyl-ions from the oxygen reduction in the crevice. At a potential of -1.25 V_{SCE} Li et al. observed that hydrogen evolution on the steel surface blocked the current flow into the crevice [23].

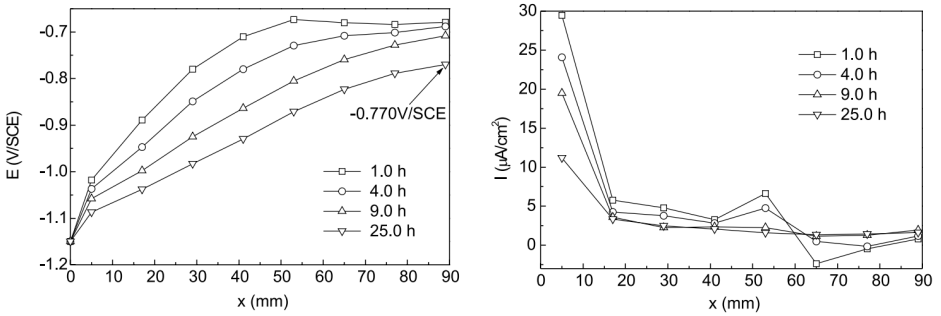

(a) **(b)**

Figure 2.5: Recorded potential and current distribution on steel along the crevice of 1.0 mm in diluted NaCl solution: (a) Potential in the crevice, where the potential at the crevice mouth was -1.15 V_{SCE}, (b) current in the crevice [23].

The effect of cathodic protection on crevice corrosion of steel-aluminium galvanic couples has been investigated by Røstbø [7] and Solli [8]. Røstbø studied the effect of galvanic crevice corrosion of the couples in a simulated crevice of $100\,\mu m$ in both artificial seawater and a NaCl solution at 25°C [7]. An anodic current was observed on aluminium though connected to the sacrificial anode in artificial seawater. Steel however, revealed a cathodic current and was thus protected in the crevice. A coupling potential of -1100 mV_{SCE} was recorded and thus controlled by the anode [7]. The current densities on steel and aluminium made symmetric shapes. Current densities on both AA6005 and steel were higher in the NaCl solution as a result of the more corrosive environment caused by Cl^- ions. Røstbø stated the anodic current on Al to be related to the increased pH in the crevice due to high local reduction rates on steel [7]. The hydroxyl-ions in the crevice caused dissolution of Al at a sufficiently high rate, which gave the anodic current [7]. The pH was measured to be 10 in both solutions. Applied cathodic protection gave no measurable weight loss of steel. Aluminium on the other hand, suffered a weight loss in the same order as self corrosion in artificial seawater [7].

Solli [8] investigated the couples in the same crevice in artificial seawater at both 10°C and 25°C in long term tests up to 120 hours. Current densities on AA6005 showed initial anodic peaks which decreased with time and turned cathodic at both temperatures for some of the tests [8]. Weight loss measurements of Al showed slightly increasing corrosion

rates at 10°C. Lower corrosion rates of Al at 25°C were due to formation of calcareous deposits. The formation of the deposits was concluded to form faster with the presence of the sacrificial anode [8]. No measurable weight loss was found for steel at 25°C. Though, at 10°C slightly increasing corrosion rates were found. A test without CP at 25°C showed an increased weight loss of steel, though Al showed similar corrosion rates as with applied CP. A more acidic environment in the crevice was found, approximately pH 5 [8]. When cathodic protection was applied to the crevice the pH was measured to be 9-10. Investigations indicated the possibility of the calcareous deposits to seal the crevice mouth and thereby prevent further corrosion when CP was applied [8].

Further studies of the work of Solli were made in the specialization project of the author [9]. Galvanic crevice couples of steel and the aluminium alloys 5083 and 6082 in addition to 6005 were investigated both with and without applied CP. A slightly higher anodic current was seen on AA6005 at 10°C compared to AA5083 and AA6082 at 25°C [9]. The anodic currents on Al decayed towards zero, though never turning cathodic when CP was applied. Cathodic currents were seen on steel in all of the couplings. The measured pH in the crevice was 9-10. Calcareous deposits and corrosion products was seen on Al, the former on steel. Microscopic characterization in SEM confirmed the faster kinetics of calcareous deposits at 25°C. The corrosion rates of steel and the aluminium alloys were relatively low [9].

2.4 Summary of theory

Cathodic protection of steel in seawater is widely investigated, especially the study of the calcareous deposits formed on steel surfaces. Comprehensive studies of the alkaline etching mechanisms of the Al-matrix surrounding intermetallic particles when CP is applied to Al have also been found in the literature. It is limited published articles regarding CP of AA5083, AA6005 and AA6082, especially for the latter two. Galvanic corrosion is thoroughly investigated, but less studies regarding the specific steel-Al galvanic couples is reported. Also, most of the studies of galvanic couples is performed in NaCl solutions, which does not give the protective effect from calcareous deposits which forms in artificial and natural seawater. Furthermore, Cl^- ions have been shown to be a contributing factor of the corrosion attacks on Al. Studies of the effect of CP on crevice corrosion of galvanic steel-aluminium couples is limited covered in the literature, except from the earlier studies in this project. Uncertainties regarding the corrosion rates of both steel and Al is shown. The mechanisms of the increased alkaline environment in the crevice with applied CP and the affect on Al at lower temperatures more comparable to the environment on the seabed is less reported. In addition, studies with long term exposure is also lacking.

Chapter 3

Experimental

The experimental methods in this master's thesis follows the methods and work performed in the master's thesis of Røstbø [7] and the specialization project of the author [9]. The methods for cleaning and weight loss measurements were inspired by the project work of Bergin [24] and the ASTM G1 standard [25], the electrolyte was artificial seawater made in accordance to the ASTM D1141-98 standard [26].

3.1 Materials

The aluminium alloys 5083, 6005 and 6082 were used in the experimental work of the thesis. AlZnIn was used as the sacrificial anode. AA5083 and AA6082 were chosen in accordance to NORSOK Standard M-121 [1]. Carbon steel X65 and aluminium alloy 6005 were chosen based on the experimental work performed in the master's theses of Røstbø [7] and Solli [8].

3.1.1 Carbon steel X65

The chemical composition of carbon steel X65 is shown in table 3.1.

Table 3.1: Chemical composition of carbon steel X65 [7].

Element [wt%]								
C	Si	Mn	P	S	V	Nb	Ti	Fe
0.16	0.45	1.65	0.02	0.01	0.09	0.05	0.06	Bal.

3.1.2 Aluminium alloys; 5083, 6005 and 6082

The chemical composition of the aluminium alloys is shown in table 3.2. AA5083 was made by Alcoa, AA6082 by Sapa Profiles kft.

Table 3.2: Chemical composition of AA5083, AA6005 and AA6082.

	Element [wt%]									
	Mg	Si	Fe	Mn	Cr	Cu	Ni	Zn	Ti	Al
AA5083	4.66	0.29	0.35	0.53	0.058	0.035	0.0076	0.11	0.020	Bal.
AA6005	0.51	0.59	0.41	0.14	0.02	0.18	-	-	-	Bal.
AA6082	0.63	0.73	0.24	0.43	0.04	0.07	-	0.04	0.02	Bal.

3.1.3 Sacrificial anode AlZnIn

The chemical composition of the sacrificial anode AlZnIn is shown in table 3.3. The anode was made by Skarpenord Corrosion A.S.

Table 3.3: Chemical composition of sacrificial anode AlZnIn.

Element [wt%]						
Zn	In	Cd	Si	Fe	Cu	Al
4.7397	0.0240	0.0001	0.0956	0.0701	0.0018	Bal.

3.2 Setup

Experimental setup for the Open Circuit Potential (OCP), galvanic corrosion and galvanic crevice corrosion experiments with applied cathodic protection is shown in figure 3.1 and figure 3.2 respectively. The experimental setups were based on the master's thesis of Røstbø [7].

3.2.1 Open Circuit Potential

The Open Circuit Potential (OCP) of the metals was measured with a Gamry Potentiostat. The reference electrode (RE) and the counter electrode (CE) were connected to a standard calomel electrode (SCE) immersed in saturated KCl-solution, as shown in figure 3.1. The metal of interest was connected as working electrode (WE) in artificial seawater. Ionic contact was made by a salt bridge filled with KCl and Agar.

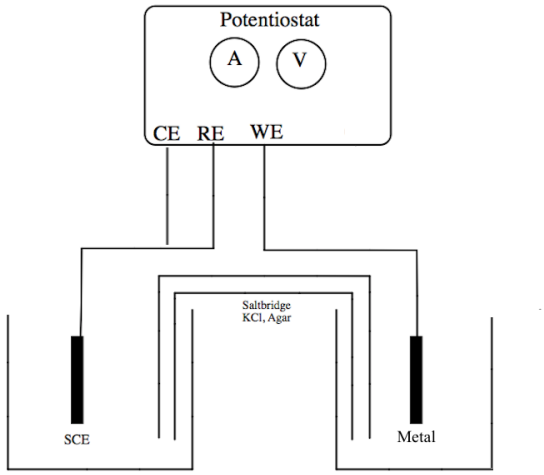

Figure 3.1: The experimental setup for the Open Circuit Potential (OCP). A Gamry Potentiostat measured the potential between the reference electrode, SCE, and the metal sample. A salt bridge containing KCl and Agar made the ionic contact between the two solutions. The metal sample was immersed in artificial seawater, the reference electrode was immersed in saturated KCl solution. Adapted figure from [7].

3.2.2 Galvanic corrosion and galvanic crevice corrosion

The experimental setup for the galvanic corrosion and galvanic crevice corrosion experiments is shown in figure 3.2. The metal samples were freely immersed in the artificial seawater in galvanic corrosion experiments after coating. In galvanic crevice corrosion experiments were the samples placed in the crevice device prior immersion in the artificial seawater.

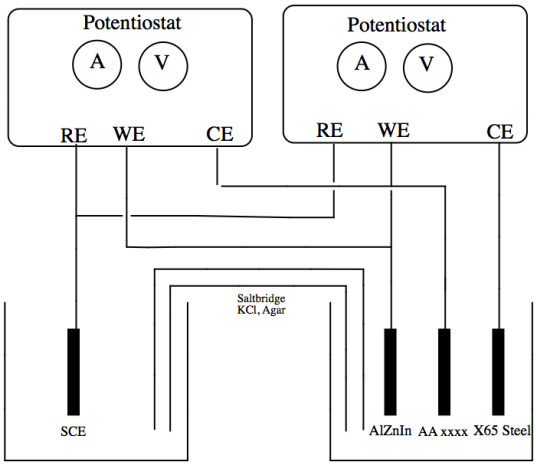

Figure 3.2: Setup for galvanic corrosion and galvanic crevice corrosion experiments indicating the metallic connections between the metal samples and the potentiostats: the working electrode (WE), counter electrode (CE) and reference electrode (RE). The circuit was closed by a salt bridge filled with KCl and Agar. Adapted figure from [7].

The electrochemical cell was a glass beaker filled with artificial seawater, point 1 in figure 3.3, which was made in accordance to the ASTM D1141-98 standard [26] as described in section 3.2.4. The electrochemical cell was immersed into a water bath containing distilled water where the temperature was regulated to 10°C by use of a cooling element. The water bath, point 2 as shown in figure 3.3, needed to be filled up to a water level over the thermometer and had to be refilled as the water evaporated with time. Plastic balls were filled on top of the water surface, as shown at point 3 in figure 3.3, to prevent evaporation and to maintain the temperature in the water bath. The crevice device used for galvanic crevice experiments was immersed into the electrolyte in the electrochemical cell, as shown at point 4 in figure 3.3. For galvanic corrosion experiments were the samples immersed freely in the cell. The wires, point 5 in figure 3.3, were connected to the potentiostats as described for the respective experiments.

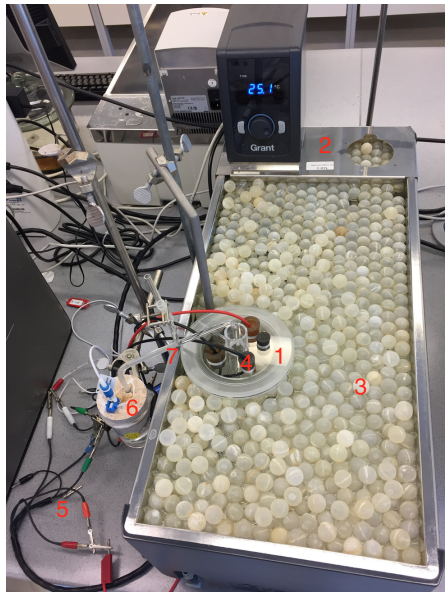

Figure 3.3: Setup for galvanic corrosion and galvanic crevice corrosion experiments in water bath: The electrochemical cell (1) was immersed into the water bath (2) and covered with plastic balls (3). The cell was filled with artificial seawater and contained the samples (4). Wires connected the samples to the potentiostats (5). Ionic contact between the reference electrode (6) immersed into the KCl-solution and the elctrochemical cell containing artificial seawater was made by a salt bridge (7) [9].

A saturated calomel electrode (SCE), point 6 in figure 3.3, was used as reference electrode. A salt bridge filled with KCl solution and Agar, point 7 in figure 3.3, was used to make ionic contact between the reference electrode and the electrolyte in the electrochemical cell. Before the salt bridge was placed in the beakers, the KCl solution was removed. Electrolyte was sucked up in the salt bridge by using a Peleus balloon.

3.2.3 Crevice device

The crevice device (sample holders) for galvanic crevice corrosion experiments were made of polyoxymethylene (POM) by the Mechanical workshop, *Finmekanisk verksted*. The sample holders were designed to fit the metal samples, as shown in figure 3.6b. The dimensions of the metal samples of carbon steel X65 and the aluminium alloys were 40·40·2mm (width·height·depth) and the dimensions of the AlZnIn sacrificial anodes were 20·60·2mm. Teflon strips (5·40·0.1mm) placed on top of one of the metal samples, as shown in figure 3.6g, were used to simulate a crevice of $100\,\mu\mathrm{m}$ when two sample holders were forced together. Teflon strips (5·40·0.3mm) were used to simulate a crevice of $300\,\mu\mathrm{m}$.

3.2.4 Electrolyte

Artificial seawater was used as electrolyte in the experiments and was made in accordance to the ASTM D1141-98 standard [26]. Due to Health, Safety and the Environment (HSE) reasons the KBr was excluded when making the artificial seawater. In accordance to the ASTM standard the pH shall be 8.2±0.1. To adjust the pH was 0.1M NaOH and 0.1M HCl added to achieve the right pH, and measured by a pH-meter. The chemicals used in the artificial seawater is shown in table 3.4.

Table 3.4: Chemical composition of the artificial seawater in accordance to the ASTM D1141-98 standard [26].

Compound	Concentration [g/L]
$MgCl_2 \cdot 6H_2O$	11.112
$CaCl_2$	1.158
$SrCl_2 \cdot 6H_2O$	0.042
KCl	0.695
$NaHCO_3$	0.201
H_3BO_3	0.027
NaF	0.003
NaCl	24.534
Na_2SO_4	4.094

3.3 Sample preparation

The Mechanical workshop at NTNU, *Finmekanisk Verksted*, assisted with the sample preparation regarding fitting of the sample dimensions. The samples of the aluminium alloys and carbon steel were sawed and milled to the proper dimension of 40·40·2mm (width·height·depth). First, the sacrificial anode AlZnIn was turned flat, then sawed and milled to the proper dimension of 20·60·2mm. All the samples needed to be strictly cleaned, dried and weight measured before use in the experiments. First, all the samples were cleaned in distilled water, acetone and ethanol (96%) thoroughly. An electrical heating gun was used to dry the samples. The samples were then left to cool to avoid static friction on the analytical weight. The samples were weighted on the analytical weight with an error of $\pm$ 0.1 mg. The AlZnIn samples were coated with bee wax, as shown in figure 3.4c. First, masking tape was placed on the area that was going to be exposed, before immersing the samples in the bee wax and then left to dry. The masking tape was removed prior the experiment by cutting outside the tape before carefully ripping it off. A metal area of 20·38mm (width of sample·width of masking tape) was then exposed.

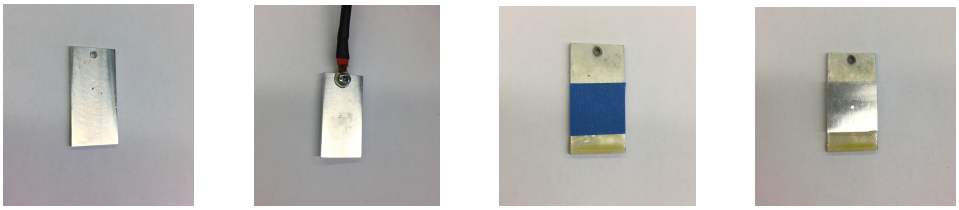

(a) **(b)** **(c)** **(d)**

Figure 3.4: (a) Sacrificial anode AlZnIn metal. (b) AlZnIn connected to a wire by a cable shoe and a screw. (c) AlZnIn covered with masking tape at the supposed exposed area, coated with bee wax. (d) AlZnIn without masking tape, coated with bee wax [9].

A masking tape was placed on the surface which was going to be exposed regarding the samples involved in OCP and galvanic corrosion experiments. A metallic wire was connected to the samples by use of a cable shoe and a screw, as shown in figure 3.5. The samples involved in OCP was dipped in bee wax to protect the areas which were not supposed to be exposed during the experiments. The aluminium alloys involved in galvanic corrosion experiments was prepared the same way. The steel however, was coated with Miccro lacquer, as shown in figure 3.5. The masking tape was gently ripped off prior the experiments.

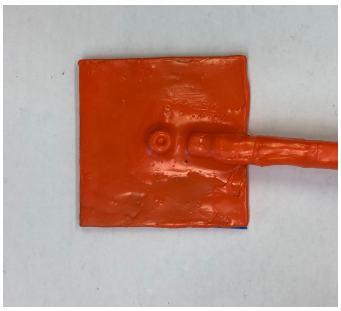

Figure 3.5: Preparation of the samples involved in OCP and galvanic corrosion experiment: The sample was connected to a wire by a cable shoe and a screw. The exposed area was covered with masking tape to prevent spill of the coating. The backside and edges in addition to the wire were coated by Miccro lacquer (steel samples), bee wax (sacrificial anode and the aluminium alloys).

The sample holders involved in galvanic crevice corrosion experiments were coated with Miccro lacquer at the area where the steel sample was going to be placed. The steel was then forced into the sample holder, as shown in figure 3.6f. The metallic contact with the wire and cable shoe on the steel were first coated with nail polish followed by Miccro lacquer, to prevent electrolyte to intrude into the metallic contact and the back of the steel samples. The samples were left to dry for approximately 24 hours before they were coated

again and left to dry. The samples of the aluminium alloys 5083 and 6082 were forced into the sample holders, which first were coated with nail polish. Nail polish was also coated at the sample edges. The backside with the metallic contact between the cable shoe and the wire were then coated with nail polish, followed by Miccro lacquer. The backside of the crevice device was coated twice with the Miccro lacquer.

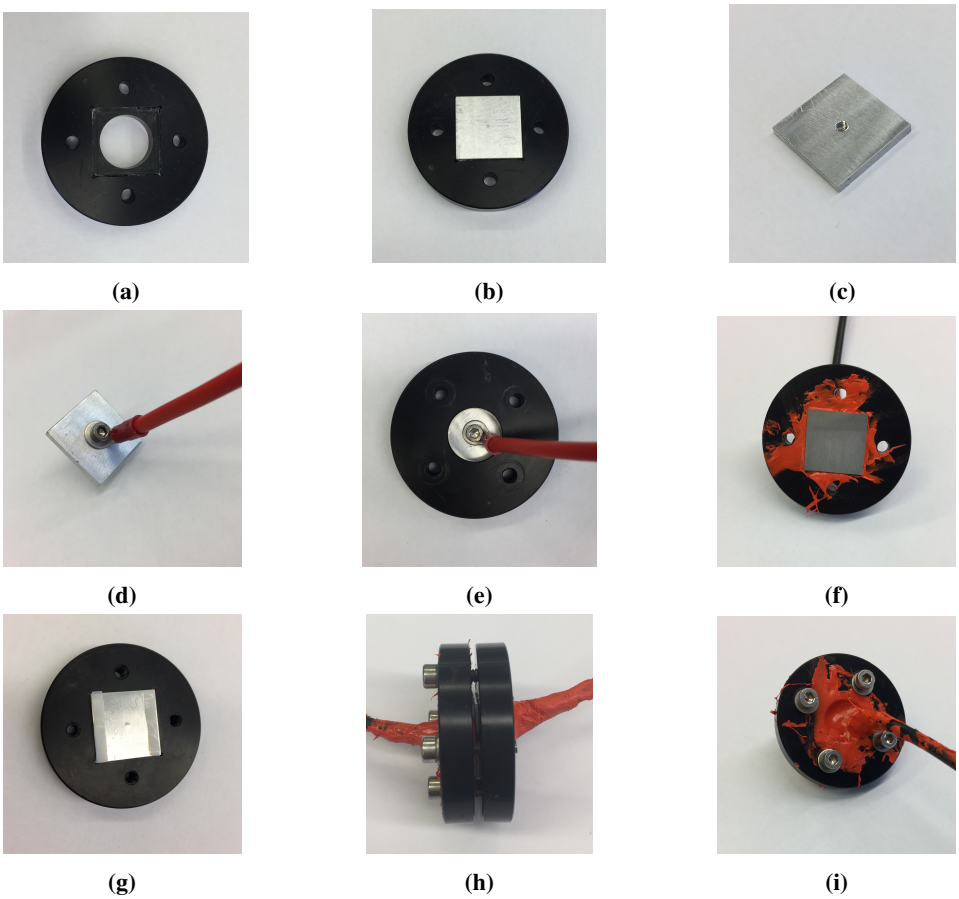

Figure 3.6: (a) The sample holder made of polyoxymethylene (POM), with four screw holes for connecting with the other sample holder. (b) Metal sample forced into the sample holder. (c) Metal sample with dimensions of 40·40·2mm with a screw hole in the middle. (d) Metallic connection of the backside of the sample by a wire, cable shoe and a screw. (e) Backside of the sample holder where the metal sample was connected with the wire by the cable shoe. (f) Coated sample holder with the steel forced into it. (g) Teflon strips placed on top of one of the metal samples, making a crevice when two sample holders are forced together. (h) The entire crevice device: Two sample holders making the crevice device with Teflon strips in between are forced and screwed together. (i) Backside of both sample holders were coated with Miccro Lacquer [9].

3.4 Procedure

The experimental procedure for the different experiments follows. Open Circuit Potential (OCP) was performed for 24 hours. Galvanic corrosion experiments ran for 3 days. Galvanic crevice corrosion experiments ran for 3 days, 5 days and 20 days. The temperature was 10°C inn all of the experiments.

3.4.1 Open Circuit Potential

The Open Circuit Potential (OCP) of the metal samples was recorded by a Gamry Potentiostat, as shown in figure 3.1. The beaker with the artificial seawater was connected to the beaker with the reference electrode by a salt bridge filled with KCl and Agar. The OCP was recorded for 24 hours.

3.4.2 Galvanic corrosion and galvanic crevice corrosion

Galvanic corrosion experiments were performed according to the setup in figure 3.2. The samples hang freely in the artificial seawater in the beaker. The potentials and currents were recorded every five minutes by the Gamry Potentiostats and logged by the Gamry Framework program. The pH was measured on the metal surfaces by a pH paper after the experiment was finished. The coating was then removed and the metals were disconnected from the cable shoes and wires.

In galvanic crevice corrosion experiments, the crevice device (sample holders) was vertically immersed in the electrolyte in the glass beaker, with the opening of the crevice pointing upwards allowing gas to escape. A pipette was used to force electrolyte into the crevice. The metallic wires were connected to the potentiostats as shown in figure 3.2. The Gamry Framework program was opened, and a galvanic corrosion test was chosen. Initial values for currents were set to 1, and a delay for which the first measurement would start was set to 300 seconds. The measurements was then logged every five minutes. After the experiment was finished, the metallic contacts were disconnected from the potentiostat and the crevice device was carefully taken up and opened. The pH was measured on the metal surfaces by a pH paper. The coating was then removed and the metals were disconnected from the cable shoes and wires.

3.5 Cleaning and weight loss measurements

The metal samples had to be thoroughly cleaned to remove corrosion products and other impurities on the samples. The cleaning procedure was performed in accordance to the ASTM G1 standard [25]. Different cleaning processes were used for the samples. The cleaning process regarding carbon steel X65 is shown in table 3.5. The cleaning process regarding the aluminium alloys and the anode is shown in table 3.6. The metal samples were weighted on an analytical weight with an error of $\pm$ 0.1 mg after the cleaning process. Weight loss was determined and corrected for metal loss by using the initial weight of the sample before the experiment.

3.5.1 Carbon steel X65

The Miccro lacquer was peeled off from the samples. The steel samples were washed with distilled water, followed by acetone to remove nail polish from the backside and other contamination. Ethanol (96%) was used to prevent the acetone from evaporating. A heating gun was used to dry the sample. Then the steel samples were chemically cleaned with the solution of hexamethylenetetramin and hydrochloric acid, as shown in table 3.5, in five cycles of 30 seconds immersion.

Table 3.5: Chemical cleaning solution and duration of the carbon steel X65 [25].

Alloy	Cleaning solution	Time [s]	Temperature [°C]
Carbon steel X65	500 mL HCl (SG.1.16) 3.5 g Hexamethylenetetramin Distilled water to make 1000 mL	30	25

The cycles were performed due to the steel samples suffers some weight loss while immersed in the hydrochloric solution. The samples were washed with distilled water and acetone followed by ethanol to remove the chemical cleaning solution. After drying with a heat gun the samples were left to cool. After cooling, the samples were weighted on an analytical weight before a new cycle with chemical cleaning was performed. The procedure of the calculations of weight loss regarding the steel is shown in appendix A.

3.5.2 Aluminium alloys and sacrificial anode

The bee wax on the sacrificial anodes was peeled off before boiled in distilled water. The aluminium alloys and the anode was washed with distilled water, followed by acetone and ethanol (96 %). A heating gun was used to dry the samples before they were left to cool. The chemical cleaning regarding the samples was a solution of chromium(VI)oxide and

phosphoric acid, as shown in table 3.6. The samples were immersed into the solution and left for 10 minutes while boiling at 90°C.

Table 3.6: Chemical cleaning solution and duration of the aluminium alloys and anode [25].

Alloy	Cleaning solution	Time	Temperature [°C]
5083, 6005, 6082 AlZnIn	50 mL Phosphoric acid (SG 1.69) 20 g Chromium(VI)oxide Distilled water to make 1000 mL	10 min	90

3.6 Surface characterization

Microscopic surface characterization was performed by a Scanning Electron Microscopy (SEM) and was used before and after chemical cleaning. An Energy Dispersive Spectroscopy (EDS) was used to examine the chemical composition of the metal samples and their corrosion products and deposits. The SEM used was Hitachi S-3400N. An accelerating voltage of 15 kV was used in addition to a probe current of 40-60. A working distance of 10 mm was used for EDS analysis.

Chapter 4

Results

The results from the electrochemical experiments of OCP, galvanic corrosion and galvanic crevice corrosion will be presented, in addition to comparisons of earlier obtained results, weight loss measurements, macroscopic surface photographs and microscopic surface characterization. All experiments were performed at 10°C.

4.1 Open Circuit Potential

The results from Open Circuit Potential (OCP) experiments of carbon steel X65, AA5083, AA6005, AA6082 and sacrificial anode AlZnIn follows in figure 4.1 - 4.5.

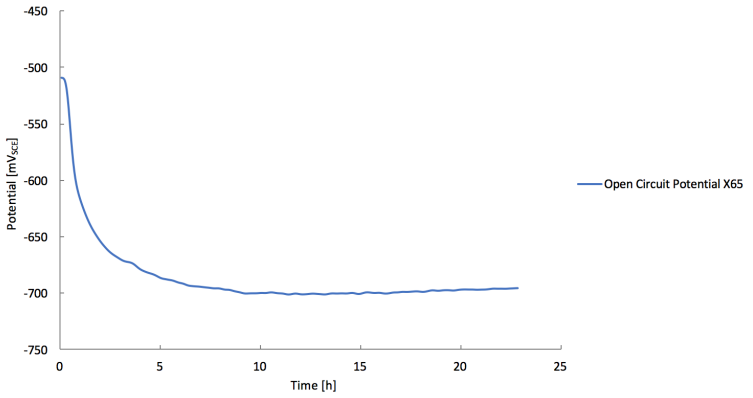

Figure 4.1: Open Circuit Potential (OCP) experiment of carbon steel X65 in artificial seawater at 10°C. Open Circuit Potential [mV$_{SCE}$] as a function of time [h].

The Open Circuit Potential of carbon steel X65 is shown in figure 4.1. An initial potential of -510 mV_{SCE} was measured before the potential dropped and got stable at -700 mV_{SCE}. An increasing (more positive) Open Circuit Potential can be seen in figure 4.2 regarding aluminium alloy 5083. The potential was stable at -755 mV_{SCE} after 4 hours.

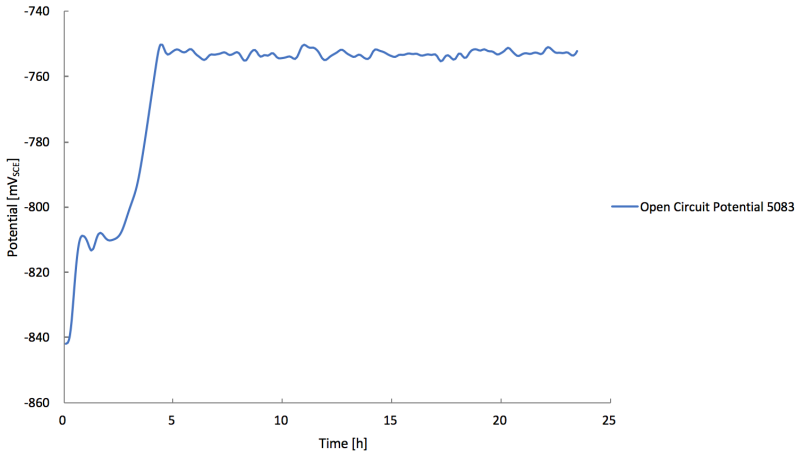

Figure 4.2: Open Circuit Potential (OCP) experiment of aluminium alloy 5083 in artificial seawater at 10°C. Open Circuit Potential [mV_{SCE}] as a function of time [h].

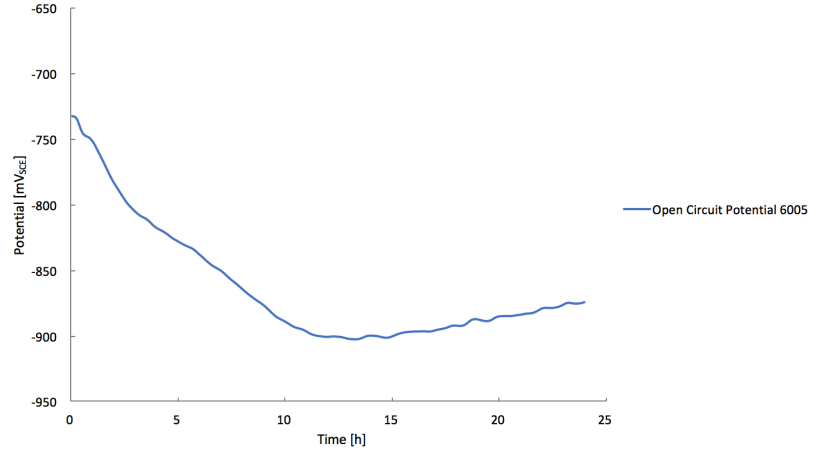

Figure 4.3: Open Circuit Potential (OCP) experiment of aluminium alloy 6005 in artificial seawater at 10°C. Open Circuit Potential [mV_{SCE}] as a function of time [h].

An initial Open Circuit Potential of aluminium alloy 6005 at -730 mV_{SCE} can be seen in figure 4.3. The potential decreased to -900 mV_{SCE} before it increased to a potential

of - 875 mV_{SCE} after 24 hours immersed in artificial seawater. An initial potential of -835 mV_{SCE} can be seen for aluminium alloy 6082 in figure 4.4. A linear decrease in the potential can be seen the first six hours before the potential reached -940 mV_{SCE}. An increased potential of -910 mV_{SCE} can be seen at the end of the experiment.

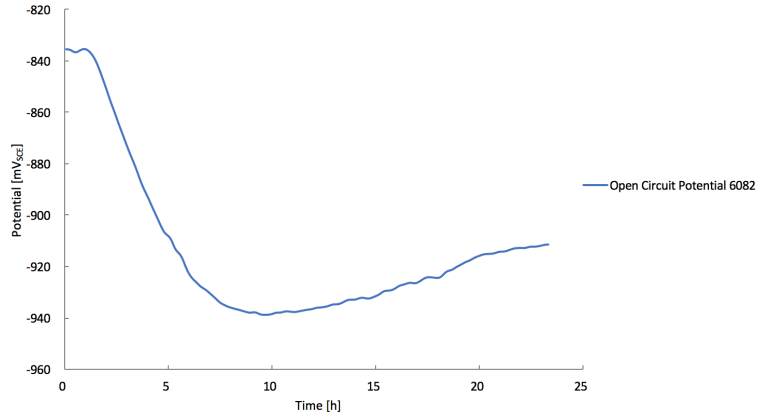

Figure 4.4: Open Circuit Potential (OCP) experiment of aluminium alloy 6082 in artificial seawater at 10°C. Open Circuit Potential [mV_{SCE}] as a function of time [h].

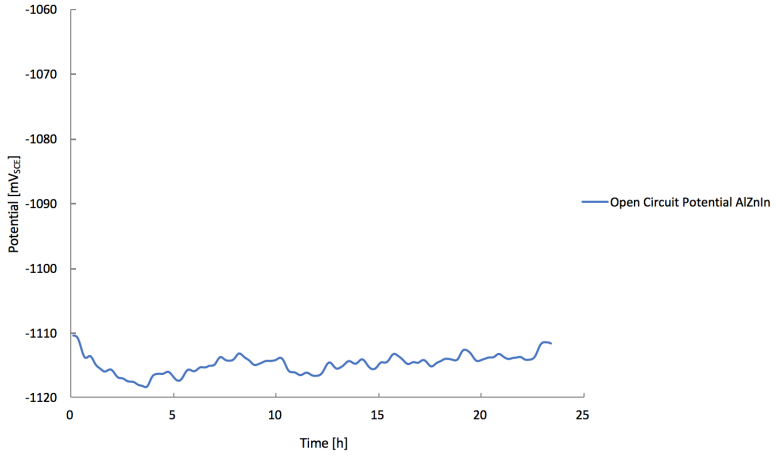

Figure 4.5: Open Circuit Potential (OCP) experiment of sacrificial anode AlZnIn in artificial seawater at 10°C. Open Circuit Potential [mV_{SCE}] as a function of time [h].

The potential of the sacrificial anode AlZnIn can be seen in figure 4.5. The potential jumped throughout the experiment but was approximately stable around a potential of -1114 mV_{SCE}.

4.2 Galvanic corrosion

Galvanic corrosion experiments with applied cathodic protection were in accordance to the setup in figure 3.2 where two potentiostats were used to record the current and potential between carbon steel X65 and the respective aluminium alloy. All the measured currents on both steel and the aluminium alloys were cathodic. As a consequence of the considerable differences in measured current densities on steel and on the aluminium alloys a logarithmic scale was used, and currents are because of the latter given in absolute values.

4.2.1 Coupling of carbon steel X65 and aluminium alloy 5083

Galvanic corrosion experiment involving carbon steel X65 and aluminium alloy 5083 with applied cathodic protection can be seen in figure 4.6. The current density on steel increased in the cathodic direction approximately for ten hours before it was stabilized, and was almost two orders of magnitude larger than the current on AA5083. A stable potential of -1108 mV_{SCE} was measured. A pH - paper was used to measure the pH on the metal samples immediately after they were taken up from the artificial seawater. Measured pH on the steel sample was 11. Measured pH on the AA5083 was 7.

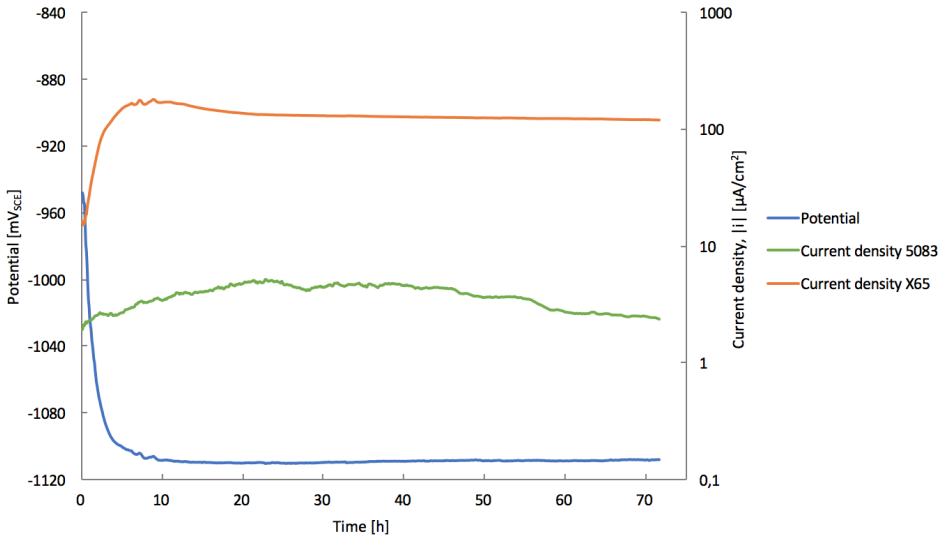

Figure 4.6: Galvanic corrosion experiment of carbon steel X65 and aluminium alloy 5083 with cathodic protection by sacrificial anode AlZnIn in artificial seawater at 10°C. Galvanic coupling potential [mV_{SCE}] and current density [µA/cm^2] as a function of time [h]. Recorded data for 3 days.

4.2.2 Coupling of carbon steel X65 and aluminium alloy 6005

Figure 4.7 shows the galvanic corrosion experiment which involved carbon steel X65 and AA6005 with applied cathodic protection. The steel showed the same tendency as when coupled to AA5083, and AA6005 behaved in the same order of magnitude as AA5083. The potential was stable at -1107 mV_{SCE}. The measured pH on the steel sample was 10. Measured pH on the AA6005 was 7.

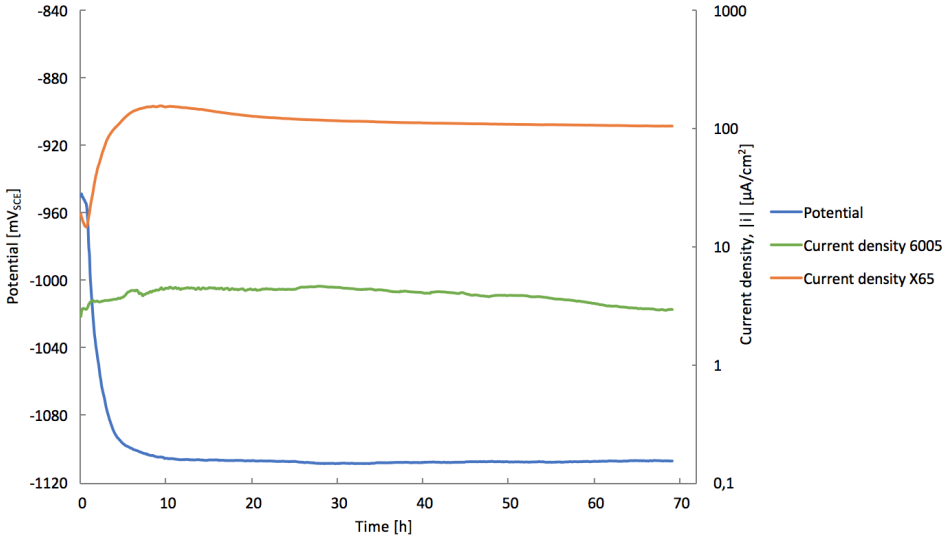

Figure 4.7: Galvanic corrosion experiment of carbon steel X65 and aluminium alloy 6005 with cathodic protection by sacrificial anode AlZnIn in artificial seawater at 10°C. Galvanic coupling potential [mV_{SCE}] and current density [µA/cm^2] as a function of time [h]. Recorded data for 3 days.

4.2.3 Coupling of carbon steel X65 and aluminium alloy 6082

Galvanic corrosion experiment involving carbon steel X65 and AA6082 can be seen in figure 4.8. The current on carbon steel was in the same order of magnitude as seen before in figure 4.6 and figure 4.7, but the current on AA6082 differed from AA5083 and AA6005. An increasing cathodic (more negative) current was seen the first ten hours before it increased in the anodic (more positive) direction. The current on the steel was two orders of magnitude larger than the current on AA6082. The potential was stable at -1108 mV_{SCE}. The pH measured on carbon steel X65 was approximately 10. A pH of 7 was measured on AA6082.

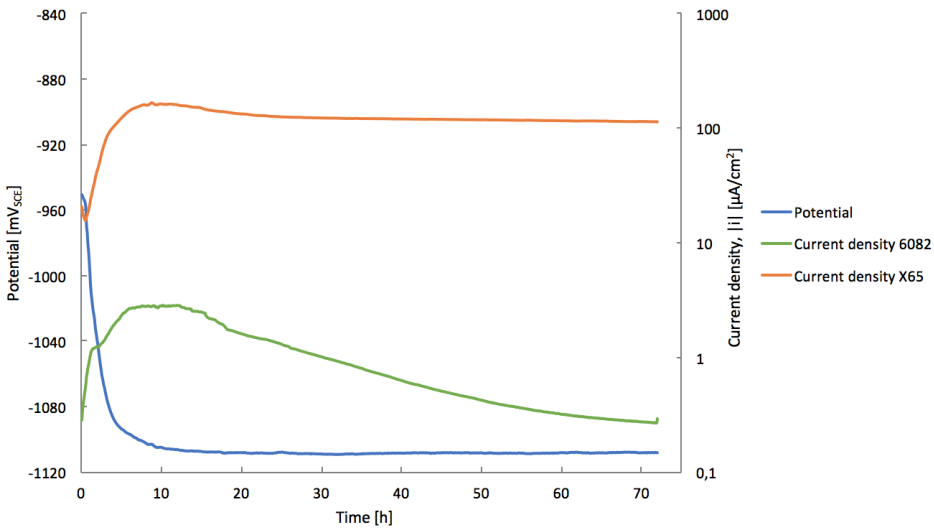

Figure 4.8: Galvanic corrosion experiment of carbon steel X65 and aluminium alloy 6082 with cathodic protection by sacrificial anode AlZnIn in artificial seawater at 10°C. Galvanic coupling potential [mV$_{SCE}$] and current density [µA/cm^2] as a function of time [h]. Recorded data for 3 days.

4.3 Galvanic crevice corrosion

Galvanic crevice corrosion experiments with applied cathodic protection were in accordance to the setup in figure 3.2 where the steel and the respective aluminium alloy were placed in the crevice device before immersed in the beaker containing artificial seawater. Aluminium alloy 6005 was not used in the galvanic crevice corrosion experiments in this master's thesis. A comparison of the galvanic crevice corrosion experiments involving AA6005 from the earlier master's theses of Røstbø [7] and Solli [8] and the specialization project of the author [9] will be presented at the end of the chapter about galvanic crevice corrosion.

Galvanic crevice corrosion experiments with applied CP were performed at different exposure times including 3 days, 5 days and 20 days. For each of the aluminium alloys (5083 and 6082) one experiment was performed for 3 days with a crevice size of 300 µm. A crevice size of 100 µm was used in the other exposure times. Two parallel experiments were performed for AA5083 and AA6082 for 20 days. The parallels will sometimes be denoted as P1 and P2 for the respective aluminium alloy.

4.3.1 Coupling of carbon steel X65 and aluminium alloy 5083

Galvanic crevice corrosion experiments with applied cathodic protection involving carbon steel X65 and aluminium alloy 5083 will be presented in this section. First, a galvanic crevice corrosion experiment with a crevice size of $300\,\mu m$ for 3 days, followed by galvanic crevice corrosion experiments with a crevice size of $100\,\mu m$ for both 5 days and 20 days.

Cathodic protection at 10°C for 3 days

Galvanic crevice corrosion experiment with applied CP and a crevice size of $300\,\mu m$ involving carbon steel X65 and aluminium alloy 5083 can be seen in figure 4.9. An initial anodic peak in current density on aluminium alloy 5083 can be seen the first two hours. A stable current density decreasing towards zero can be seen the rest of the experiment. The current density on carbon steel X65 showed an increasing cathodic peak approximately the first ten hours before it started to decrease to $-15\,\mu A/cm^2$. A stable potential of -1108 mV_{SCE} was observed during the experiment. A pH paper was used to measure the pH on the metal surfaces. On both steel and AA5083 the pH was measured to be 10.

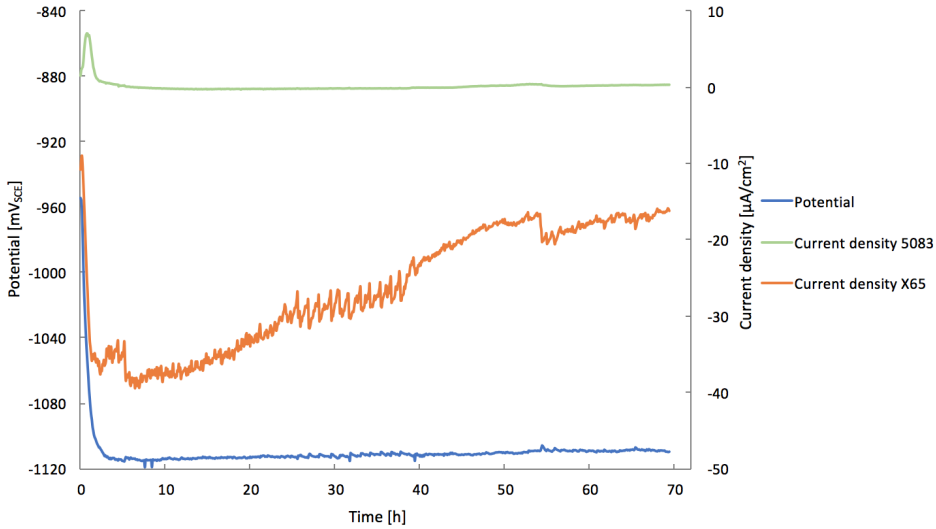

Figure 4.9: Galvanic crevice corrosion experiment of carbon steel X65 and aluminium alloy 5083 with cathodic protection by sacrificial anode AlZnIn in artificial seawater at 10°C in a simulated crevice of $300\,\mu m$. Galvanic coupling potential [mV_{SCE}] and current density [$\mu A/cm^2$] as a function of time [h]. Recorded data for 3 days.

Cathodic protection at 10°C for 5 days

Galvanic crevice corrosion experiment with applied CP and a crevice size of $100\,\mu m$ involving carbon steel X65 and aluminium alloy 5083 can be seen in figure 4.10. The current density on both steel and AA5083 had an increasing peak in the cathodic and anodic direction respectively. The highest peaks were after seventy hours before the currents were stable. After 5 days the current densities on AA5083 and carbon steel X65 were $2.5\,\mu A/cm^2$ and $-4\,\mu A/cm^2$ respectively. The potential was approximately stable at -1116 mV_{SCE}. The measured pH on both metal samples was 9-10.

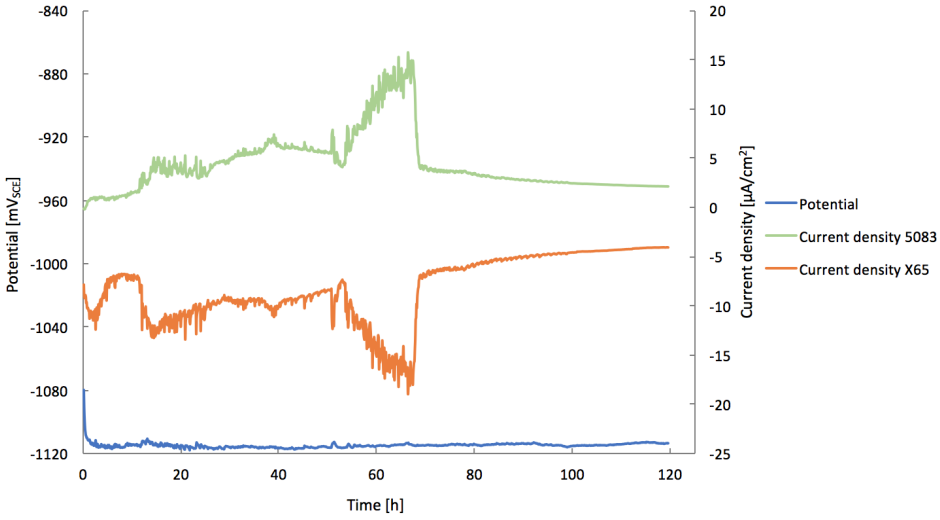

Figure 4.10: Galvanic crevice corrosion experiment of carbon steel X65 and aluminium alloy 5083 with cathodic protection by sacrificial anode AlZnIn in artificial seawater at 10°C in a simulated crevice of $100\,\mu m$. Galvanic coupling potential [mV_{SCE}] and current density [$\mu A/cm^2$] as a function of time [h]. Recorded data for 5 days.

Parallel 1 and 2: cathodic protection at 10°C for 20 days

Parallel galvanic crevice experiments with applied CP and a crevice of $100\,\mu m$ ran for 20 days, as seen in figure 4.11. The current densities on AA5083 was in both parallels in the anodic direction, with a peak the first hours. The steel showed in both parallels a cathodic peak the first hours before steadily decreasing. A small jump in the current on steel in parallel 1 was seen at the end. A potential of approximately - 1108 mV_{SCE} was seen on parallel 1. A slightly more anodic potential was seen for parallel 2 at approximately -1088 mV_{SCE}. The measured pH on both steel and AA5083 was 9-10 in both parallels.

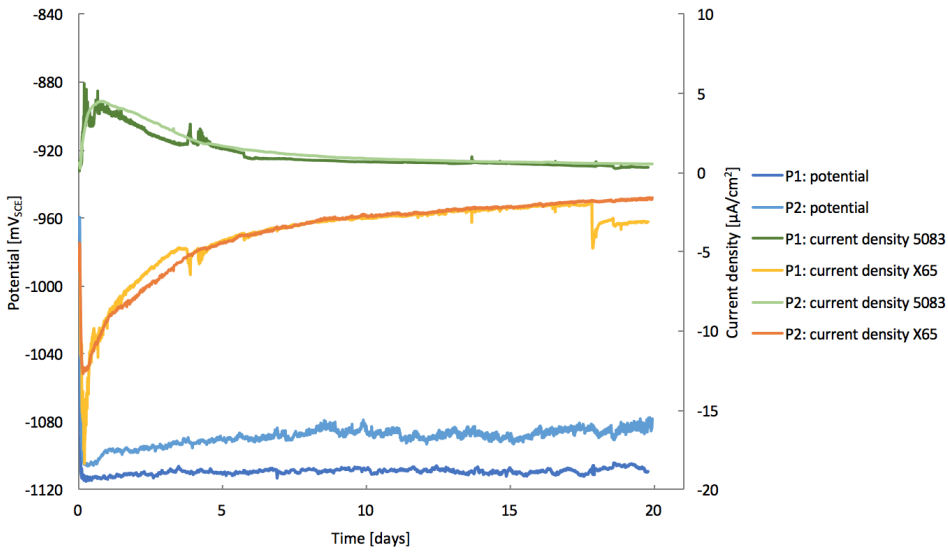

Figure 4.11: Galvanic crevice corrosion experiments of carbon steel X65 and aluminium alloy 5083 with cathodic protection by sacrificial anode AlZnIn in artificial seawater at 10°C in a simulated crevice of $100\,\mu m$. Galvanic coupling potential [mV_{SCE}] and current density [$\mu A/cm^2$] as a function of time [h]. Recorded data for 20 days.

4.3.2 Coupling of carbon steel X65 and aluminium alloy 6082

Cathodic protection at 10°C for 3 days

Galvanic crevice corrosion experiment with applied CP and a crevice size of 300 µm involving carbon steel X65 and aluminium alloy 6082 can be seen in figure 4.12. A stable current density on AA6082 can be seen the first forty hours before an increasing anodic peak. The steel on the other hand, showed a decreasing cathodic current density after five hours until an increasing cathodic peak can be seen at the end of the experiment. The potential was approximately stable at -1106 mV_{SCE}. The measured pH on both metal samples was 10.

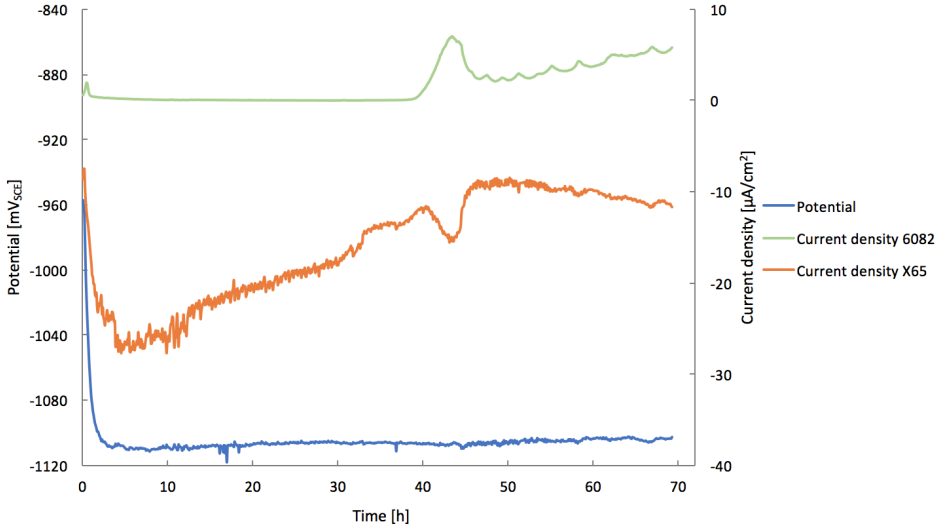

Figure 4.12: Galvanic crevice corrosion experiment of carbon steel X65 and aluminium alloy 6082 with cathodic protection by sacrificial anode AlZnIn in artificial seawater at 10°C in a simulated crevice of 300 µm. Galvanic coupling potential [mV_{SCE}] and current density [µA/cm^2] as a function of time [h]. Recorded data for 3 days.

Cathodic protection at 10°C for 5 days

Galvanic crevice corrosion experiment with applied CP and a crevice of $100\,\mu m$ for 5 days can be seen in figure 4.13. The current density on both AA6082 and on steel was almost stable with time. Both currents at the end of the experiment were small, $0.70\,\mu A/cm^2$ and $-2.1\,\mu A/cm^2$ on AA6082 and carbon steel X65 respectively. On both steel and AA6082 the measured pH was 10.

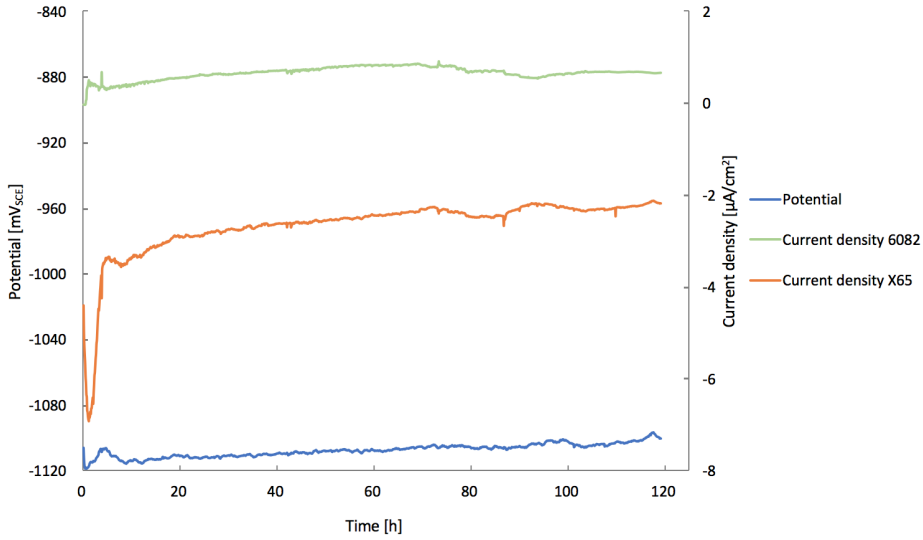

Figure 4.13: Galvanic crevice corrosion experiment of carbon steel X65 and aluminium alloy 6082 with cathodic protection by sacrificial anode AlZnIn in artificial seawater at 10°C in a simulated crevice of $100\,\mu m$. Galvanic coupling potential [mV_{SCE}] and current density [$\mu A/cm^2$] as a function of time [h]. Recorded data for 5 days.

Parallel 1 and 2: cathodic protection at 10°C for 20 days

Parallel experiments involving AA6082 and carbon steel X65 can be seen in figure 4.14. The parallels of the current densities on AA6082 did not overlap as much to each other as seen for the parallels on AA5083 earlier. Though, the current densities on AA6082 have an anodic peak the first hours, and only differ from each other with $3\,\mu A/cm^2$ at the most. The parallels on steel did not overlap each other either, where parallel 2 had a larger cathodic current density than parallel 1. Average potentials of approximately -1090 mV_{SCE} and -1105 mV_{SCE} corresponded to parallel 1 and parallel 2 respectively. The measured pH on both metal samples was 11 in parallel 1. In parallel 2 was the measured pH 10.

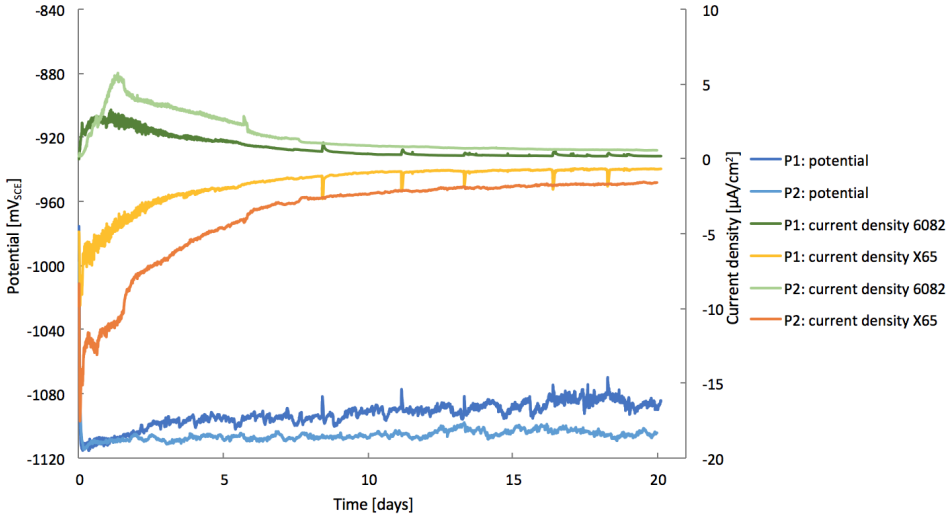

Figure 4.14: Galvanic crevice corrosion experiments of carbon steel X65 and aluminium alloy 6082 with cathodic protection by sacrificial anode AlZnIn in artificial seawater at 10°C in a simulated crevice of 100 µm. Galvanic coupling potential [mV$_{SCE}$] and current density [µA/cm^2] as a function of time [h]. Recorded data for 20 days.

4.3.3 Comparison of the electrochemical behavior of aluminium alloy 6005 at 25°C

One of the purposes of this master's thesis were to compare and investigate the earlier obtained results of this project from the master's theses of Røstbø [7] and Solli [8]. In accordance to this, the electrochemical data recorded in those master's has been adapted and plotted together with the result from the specialization project of the author [9] to compare the electrochemical behavior of aluminium alloy 6005 when coupled to carbon steel X65 in a crevice with applied cathodic protection at 25°C. Røstbø [7] had only one experiment involving galvanic crevice corrosion of AA6005 and steel with applied CP in artificial seawater at 25°C. Solli [8] on the other hand, managed results at temperatures of both 10°C and 25°C for different time intervals. Though, the best fitted experiments of Solli, parallel 1 and parallel 3 at 25°C, were chosen to be compared with the work of Røstbø [7] and the author [9]. The electrochemical data from the specialization project of the author was originally for 96 hours, but was only plotted for 72 hours in the comparison.

Figure 4.15 shows the adapted electrochemical data of the galvanic crevice corrosion experiments of AA6005 coupled to carbon steel X65 with applied CP at 25°C for 72 hours [7], [8], [9].

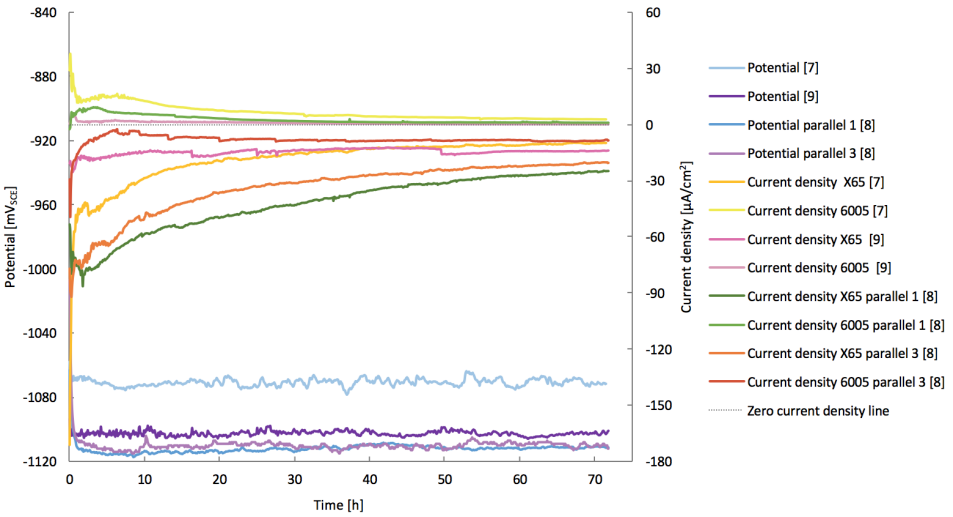

Figure 4.15: Galvanic crevice corrosion experiments of carbon steel X65 and aluminium alloy 6005 with cathodic protection by sacrificial anode AlZnIn in artificial seawater at 25°C in a simulated crevice of 100 µm. Galvanic coupling potential [mV$_{SCE}$] and current density [µA/cm^2] as a function of time [h]. Recorded data for 72 hours. Adapted electrochemical data from [7], [8], [9].

The current density on AA6005 showed the same trend with an anodic peak the first hours for [7], parallel 1 [8], [9]. The current density on AA6005 for parallel 3 from [8] showed a cathodic current density during the experiment, which was an interesting result. All current densities on steel showed an increasing cathodic peak in the beginning before they showed a decreasing cathodic current. The comparison in figure 4.15 shows that the magnitude of the current densities on both steel and AA6005 vary a lot between the different authors [7], [8], [9]. A slightly more anodic potential can be seen from the experiment of Røstbø [7], where the other potentials were in the range of -1106 mV$_{SCE}$ to - 1113 mV$_{SCE}$. The measured pH was 10 in the specialization project of the author [9] on both steel and AA6005. Røstbø [7] measured a pH in the crevice of 10. Solli [8] measured a pH of 10 in parallel 1 and a pH of 9 in parallel 3.

4.4 Weight loss

Weight loss was measured on an analytical weight and the calculations of steel were performed in accordance to ASTM G1 standard [25], which can be seen in appendix A. The weight loss was also calculated from the anodic current densities of the aluminium alloys by the Trapezoidal method and Faraday's law as described in appendix B. Weight loss measured on the analytical weight will be referred to as measured, and weight loss calculated will be referred to as Faraday's law in table 4.1 - 4.5. The weight loss was not calculated by Faraday's law regarding the Open Circuit Potential and galvanic corrosion experiments.

Both measured and calculated weight loss given in table 4.2 and table 4.4 was plotted as a function of time for both AA5083 and AA6082, which can be seen in figure 4.16 and figure 4.17 respectively. The purpose was to investigate and verify the correlation between the measured and calculated weight loss regarding uncertainties in measurements on the analytical weight. Recall that the temperature in all the experiments was 10°C.

A comparison of the measured weight loss and the calculated weight loss by Faraday's law regarding AA6005 from earlier master's theses [7], [8] and the specialization project of the author [9] in addition to the OCP and galvanic corrosion experiment performed in this master's thesis can be seen in figure 4.18 and figure 4.19 respectively. In the comparison of measured weight loss of AA6005 were all experiments from earlier work at both 10°C and 25°C plotted. Though, calculated weight loss by Faraday's law of AA6005 was only at 25°C and corresponds to the electrochemical data given in figure 4.15. Parallel 3 from figure 4.15 was not included in the calculations since the current on AA6005 was cathodic throughout the whole experiment.

4.4.1 Carbon steel X65

The measured weight loss of carbon steel X65 can be seen in table 4.1. One of the highest weight losses of steel can be seen for the OCP. The weight losses from both galvanic and galvanic crevice corrosion experiments were very small and similar to each other. One exception was parallel 2 regarding the coupling of AA5083 with applied CP in galvanic crevice corrosion experiment. Hydrogen gas was seen in the beginning of the experiment before it was stopped and restarted. The samples in the crevice device were not replaced when the experiment was restarted, and the weight loss of the steel in this parallel was much higher as a consequence of the gas evolution.

Table 4.1: Weight loss of carbon steel X65 $\left[\frac{mg}{cm^2}\right]$.

Type	Coupling	Measured	Faraday's law
OCP	X65 (24 h)	0.16	-
Galvanic	X65 / AA5083 / AlZnIn (3 d)	0.05	-
	X65 / AA6005 / AlZnIn (3 d)	0.13	-
	X65 / AA6082 / AlZnIn (3 d)	0.08	-
Crevice	X65 / AA5083 / AlZnIn (300 µm, 3 d)	0.05	-
	X65 / AA6082 / AlZnIn (300 µm, 3 d)	0.04	-
	X65 / AA5083 / AlZnIn (5 d)	0.01	-
	X65 / AA6082 / AlZnIn (5 d)	0.04	-
	P1: X65 / AA5083 / AlZnIn (20 d)	0.02	-
	P2: X65 / AA5083 / AlZnIn (20 d)	0.42	-
	P1: X65 / AA6082 / AlZnIn (20 d)	0.02	-
	P2: X65 / AA6082 / AlZnIn (20 d)	0.05	-

4.4.2 Aluminium alloy 5083

The measured and calculated weight loss of AA5083 can be seen in table 4.2. The smallest weight loss of AA5083 can be seen for the Open Circuit Potential and galvanic corrosion experiment. A crevice size of 300 µm in galvanic crevice corrosion experiment also gave a small weight loss of AA5083. The highest weight loss regarding AA5083 can be seen for the long term parallels for 20 days. AA5083 experienced hydrogen evolution in parallel 2 as described earlier. This parallel should be excluded when comparing the weight loss of AA5083. Though, it showed the detrimental consequences of hydrogen gas evolution in crevice corrosion experiments.

Table 4.2: Weight loss of aluminium alloy 5083 $\left[\frac{mg}{cm^2}\right]$.

Type	Coupling	Measured	Faraday's law
OCP	AA5083 (24 h)	0.04	-
Galvanic	X65 / AA5083 / AlZnIn (3 d)	0.04	-
Crevice	X65 / AA5083 / AlZnIn (300 µm, 3 d)	0.05	0.01
	X65 / AA5083 / AlZnIn (5 d)	0.20	0.17
	P1: X65 / AA5083 / AlZnIn (20 d)	0.22	0.18
	P2: X65 / AA5083 / AlZnIn (20 d)	0.95	0.22

When comparing the measured and calculated weight loss one can see that the calculated weight loss is lower than the measured. This was expected since the calculated values from the electrochemical data do not take into account the localized corrosion which the

measured values does. Nevertheless, the calculated weigh losses corresponded well to the measured values.

4.4.3 Aluminium alloy 6005

Table 4.3 shows the measured weight loss of aluminium alloy 6005 involved in the OCP and galvanic corrosion experiment. A very similar and low weight loss can be seen regarding these experiments.

Table 4.3: Weight loss of aluminium alloy 6005 $\left[\frac{mg}{cm^2}\right]$.

Type	Coupling	Measured	Faraday's law
OCP	AA6005 (24 h)	0.02	-
Galvanic	X65 / AA6005 / AlZnIn (3 d)	0.01	-

4.4.4 Aluminium alloy 6082

Table 4.4 shows the measured and calculated weight loss of aluminium alloy 6082 for the different experiments. The lowest weight loss was regarding the OCP. If comparing the weight loss of 0.06 mg/cm^2 after 5 days with the weight loss of parallel 1, one can see that the weight loss was four times higher in parallel 1 for 20 days than of 5 days. Calculated weight losses corresponded good to the measured values, and were as described earlier as expected slightly smaller than the measured weight losses.

Table 4.4: Weight loss of aluminium alloy 6082 $\left[\frac{mg}{cm^2}\right]$.

Type	Coupling	Measured	Faraday's law
OCP	AA6082 (24 h)	0.02	-
Galvanic	X65 / AA6082 / AlZnIn (3 d)	0.02	-
Crevice	X65 / AA6082 / AlZnIn (300 µm, 3 d)	0.04	0.04
	X65 / AA6082 / AlZnIn (5 d)	0.06	0.03
	P1: X65 / AA6082 / AlZnIn (20 d)	0.24	0.12
	P2: X65 / AA6082 / AlZnIn (20 d)	0.32	0.25

4.4.5 Sacrificial anode AlZnIn

Table 4.5 shows the measured and calculated weight loss of the sacrificial anode AlZnIn for the different type of experiments. The lowest weight loss was regarding the OCP which was in the same magnitude as the other aluminium alloys as described earlier. The highest weight losses can be seen for the galvanic corrosion experiments. The correspondence between measured and calculated weight loss was weaker regarding the AlZnIn compared to the other aluminium alloys. One explanation could be how the values of AlZnIn was calculated by Faraday's law. The current density of AlZnIn was a subtraction of the current density of the AA's and carbon steel X65, the remaining calculation was performed in the same way as earlier. Also for simplicity, the same molar mass was used for both the AA's and the AlZnIn in Faraday's law, which could have been a contributing factor.

Table 4.5: Weight loss of sacrificial anode AlZnIn $\left[\frac{mg}{cm^2}\right]$.

Type	Coupling	Measured	Faraday's law
OCP	AlZnIn (24 h)	0.03	-
Galvanic	X65 / AA5083 / AlZnIn (3 d)	7.60	-
	X65 / AA6005 / AlZnIn (3 d)	6.60	-
	X65 / AA6082 / AlZnIn (3 d)	7.30	-
Crevice	X65 / AA5083 / AlZnIn (300 µm, 3 d)	1.09	0.27
	X65 / AA6082 / AlZnIn (300 µm, 3 d)	0.60	0.41
	X65 / AA5083 / AlZnIn (5 d)	0.50	0.50
	X65 / AA6082 / AlZnIn (5 d)	0.55	0.13
	P1: X65 / AA5083 / AlZnIn (20 d)	1.11	0.80
	P2: X65 / AA5083 / AlZnIn (20 d)	0.89	0.82
	P1: X65 / AA6082 / AlZnIn (20 d)	0.65	0.38
	P2: X65 / AA6082 / AlZnIn (20 d)	1.22	0.85

4.4.6 Comparison of measured weight loss of aluminium alloy 5083 and 6082

The measured weight losses [mg/cm^2] in table 4.2 and table 4.4 of AA5083 and AA6082 respectively were plotted as a function of time [days], as shown in figure 4.16. The purpose was to give a better view of the trend in weight loss with time. If excluding the weight loss of parallel 2 from the galvanic crevice corrosion experiment involving AA5083 and steel with applied CP, one can see a linear trend in the weight loss as a function of time for the remaining experiments.

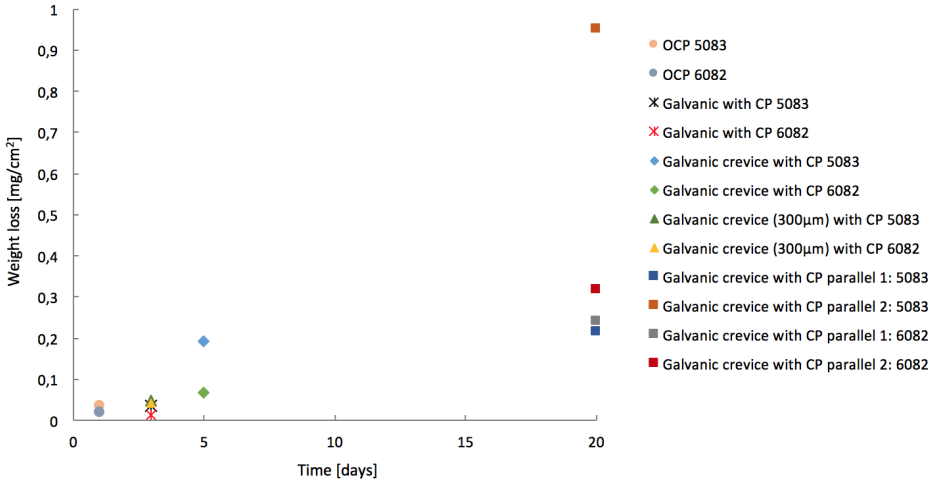

Figure 4.16: Measured weight loss [mg/cm^2] as a function of time [days] of aluminium alloy 5083 and 6082 involved in Open Circuit Potential, galvanic corrosion and galvanic crevice corrosion experiments with applied cathodic protection (CP) at 10°C. Crevice sizes of 100 µm and 300 µm.

4.4.7 Comparison of weight loss by Faraday's law of aluminium alloy 5083 and 6082

The calculated weight losses [mg/cm^2] by Faraday's law from the electrochemical data involving AA5083 and AA6082 were plotted as a function of time [days], as shown in figure 4.17. The last data point in the curves correspond to the calculated weight loss given in table 4.2 and table 4.4 of AA5083 and AA6082 respectively. Since parallel 2 involving AA5083 was stopped and restarted because of the hydrogen gas evolution, the electrochemical data represented do not show the problems regarding the gas evolution. It is likely that the measured weight loss would correspond better to the calculated weight loss of this parallel if the metal samples had been replaced with new samples before restarting

the experiment. For the parallels of both metals one can see a steep curve the first five days before they steadily started to flatten out. Since the calculated weight loss correspond to the earlier represented electrochemical data, one can see a much higher weight loss of galvanic crevice corrosion experiment with applied CP of AA5083 for 5 days - which corresponded to the increasing peak in anodic current density in this experiment.

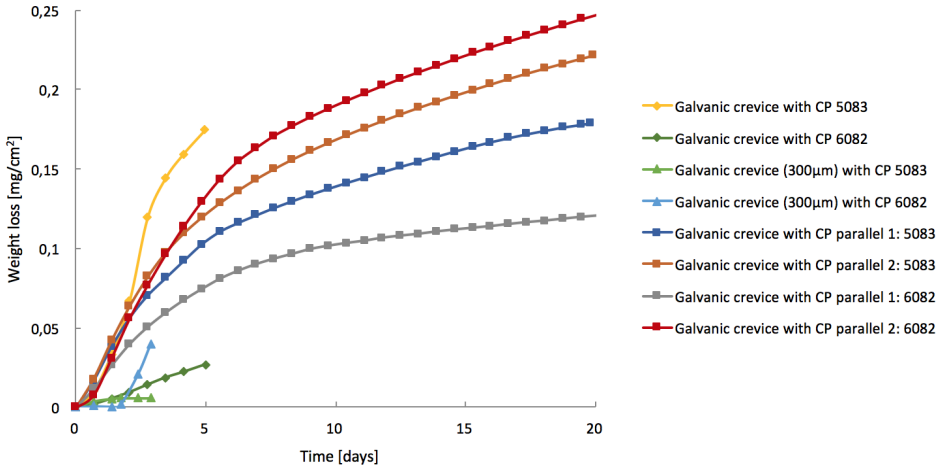

Figure 4.17: Faraday's law weight loss [mg/cm^2] as a function of time [days] of aluminium alloy 5083 and 6082 involved in galvanic crevice corrosion experiments with applied cathodic protection (CP) at 10°C. Crevice sizes of 100 µm and 300 µm.

4.4.8 Comparison of measured weight loss of aluminium alloy 6005

A comparison of the measured weight losses of AA6005 from OCP, galvanic corrosion experiments and galvanic crevice corrosion experiments when coupled to carbon steel X65 with and without cathodic protection can be seen in figure 4.18. The temperatures were both 10°C and 25°C as indicated for the different experiments and authors [7], [8], [9]. The results from Røstbø [7] and the specialization project of the author [9] were given in [mg/cm$^2\cdot$ 24h] and have been adapted to [mg/cm^2]. The weight losses of AA6005 represented in table 4.3 regarding OCP and galvanic corrosion experiment were also included in the comparison in figure 4.18. It can be seen from the figure that temperature differences did not significantly affect the weight loss of AA6005 regarding galvanic crevice corrosion experiments. The lowest weight loss at both temperatures was the OCP and galvanic corrosion experiments. Nevertheless, a fitted linear trend can be seen regarding the measured weight loss of AA6005 in the figure.

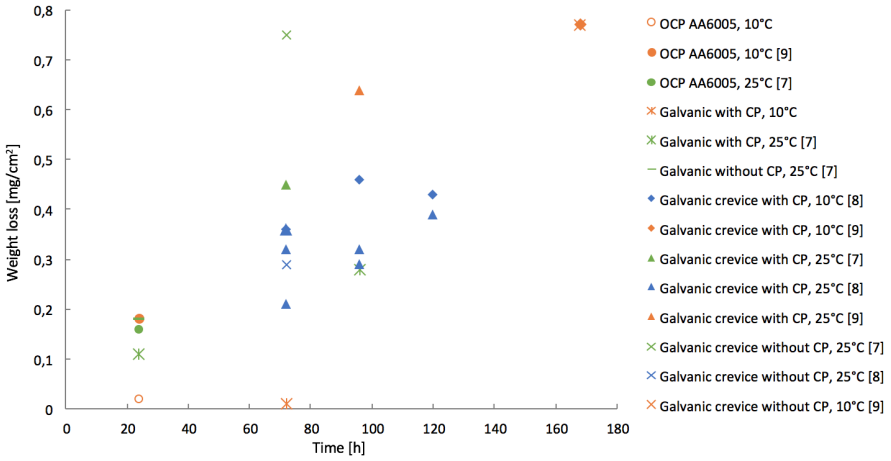

Figure 4.18: Measured weight loss [mg/cm^2] as a function of time [h] of aluminium alloy 6005 involved in Open Circuit Potential, galvanic corrosion and galvanic crevice corrosion experiments with and without cathodic protection (CP). Crevice size of 100 µm. Adapted data from [7], [8], [9].

4.4.9 Comparison of weight loss by Faraday's law of aluminium alloy 6005

A comparison of the calculated weight loss by Faraday's law of AA6005 can be seen in figure 4.19 which corresponds to the adapted electrochemical data in figure 4.15.

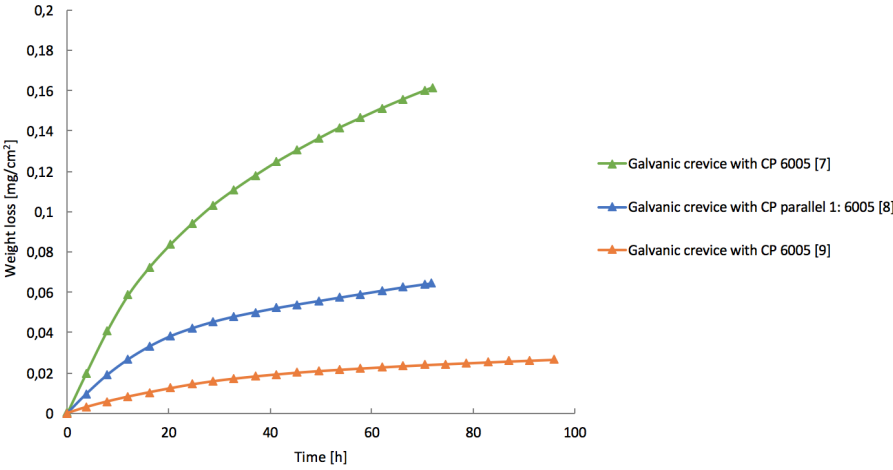

Figure 4.19: Faraday's law weight loss [mg/cm^2] as a function of time [h] of aluminium alloy 6005 involved in galvanic crevice corrosion experiments with applied cathodic protection (CP) at 25°C. Crevice size of 100 µm. Adapted electrochemical data from [7], [8], [9].

Note that the calculations of [9] were done at the original test duration of ninety six hours. Parallel 3 from the work of Solli [8] was not included since the current density on AA6005 was cathodic throughout the experiment. If comparing the Faraday's curves in figure 4.19 with the corresponded measured weight losses at 25°C for the given type of experiment in figure 4.18 one can see clear differences between measured and calculated values.

4.5 Macroscopic surface characterization

The samples were photographed after they were disconnected from the setup equipment. First, they were washed in distilled water, acetone and ethanol followed by drying with a heating gun. Photographs of the samples from Open Circuit experiment were not taken. All of the metal samples involved in galvanic crevice corrosion experiments were photographed such that the crevice mouth is pointing up, and marks from the Teflon strips can be seen at the left and right edges on the steel and the aluminium alloys.

4.5.1 Coupling of carbon steel X65 and aluminium alloy 5083

Galvanic corrosion: cathodic protection at 10°C for 3 days

Images of carbon steel X65, AA5083 and AlZnIn involved in galvanic corrosion experiment can be seen in figure 4.20. A white uniform calcareous deposit can be seen on steel. Some of the deposit started to flake of when touching it. AA5083 had a uniform grey deposit covering almost the entire the surface. The sacrificial anode had suffered from pitting corrosion which can be seen as the pits on the surface. A grey deposit covered the rest of the sample surface.

(a) **(b)** **(c)**

Figure 4.20: Photographs of the samples involved in galvanic corrosion experiment with cathodic protection in artificial seawater at 10°C. (a) carbon steel X65, (b) aluminium alloy 5083, (c) sacrificial anode AlZnIn.

Crevice corrosion: cathodic protection at 10°C for 3 days

The samples involved in galvanic crevice corrosion experiment with a crevice size of $300\,\mu m$ can be seen in figure 4.21. A white/grey deposit covered the exposed sample surface on the steel, where clear marks from the Teflon strips can be seen on the left and right edges. A thicker calcareous deposit layer was observed at the upper crevice mouth on the sample. AA5083 revealed a thin grey uniform deposit layer where the sample surface had been exposed to the seawater.

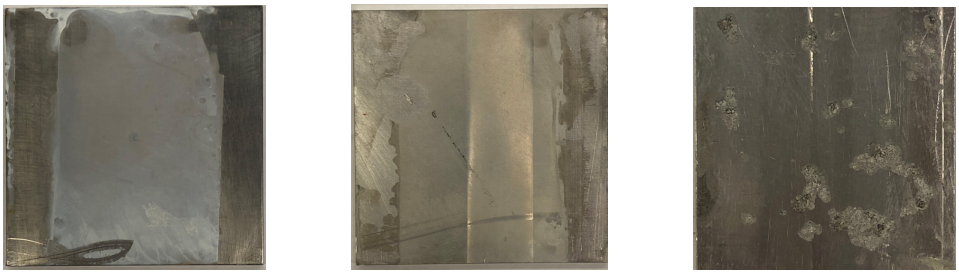

(a) **(b)** **(c)**

Figure 4.21: Photographs of the samples involved in galvanic crevice corrosion experiment with cathodic protection in artificial seawater at 10°C in a simulated crevice of $300\,\mu m$. (a) carbon steel X65, (b) aluminium alloy 5083, (c) sacrificial anode AlZnIn.

Crevice corrosion: cathodic protection at 10°C for 5 days

Images of the samples exposed for 5 days can be seen in figure 4.22. Both steel and AA5083 revealed that the entire sample surface had not been exposed to seawater. A white calcareous deposit can be seen mainly at the lower crevice mouth of X65. Some orange/brown deposit was revealed under the left Teflon.

(a) **(b)** **(c)**

Figure 4.22: Photographs of the samples involved in galvanic crevice corrosion experiment with cathodic protection in artificial seawater at 10°C in a simulated crevice of $100\,\mu m$. (a) carbon steel X65, (b) aluminium alloy 5083, (c) sacrificial anode AlZnIn.

Crevice corrosion parallel 1: cathodic protection at 10°C for 20 days

Minor deposit was revealed on both steel and AA5083 from the long term parallel 1, as shown in figure 4.23. White deposit can be seen mainly at the lower crevice mouth on X65 and a white/grey deposit covered the middle and down on AA5083.

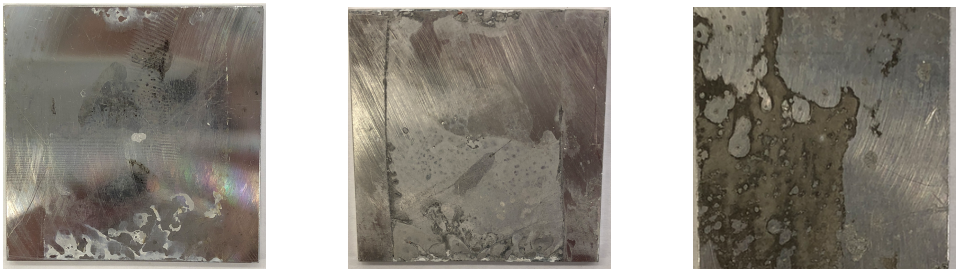

(a) **(b)** **(c)**

Figure 4.23: Photographs of the samples involved in galvanic crevice corrosion experiment with cathodic protection in artificial seawater at 10°C in a simulated crevice of 100 µm. (a) carbon steel X65, (b) aluminium alloy 5083, (c) sacrificial anode AlZnIn.

Crevice corrosion parallel 2: cathodic protection at 10°C for 20 days

AA5083 from parallel 2 in the long term galvanic crevice experiment showed that the sample had suffered of corrosion due to the hydrogen gas evolution, as shown in figure 4.24b. The entire exposed surface revealed corrosion products. The steel surface on the other hand seemed fine, but brown deposit could be seen on the edges. Note that the exposed surface did not show calcareous deposits. The sacrificial anode showed dark grey deposit in addition to white deposit around the pitting attacks.

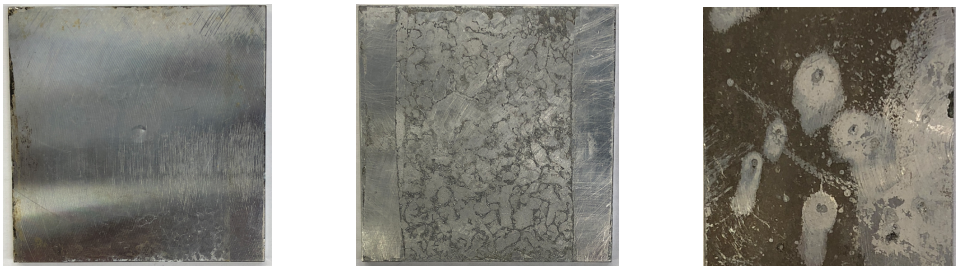

(a) **(b)** **(c)**

Figure 4.24: Photographs of the samples involved in galvanic crevice corrosion experiment with cathodic protection in artificial seawater at 10°C in a simulated crevice of 100 µm. (a) carbon steel X65, (b) aluminium alloy 5083, (c) sacrificial anode AlZnIn.

4.5.2 Coupling of carbon steel X65 and aluminium alloy 6005

Galvanic corrosion: cathodic protection at 10°C for 3 days

Carbon steel X65, AA6005 and AlZnIn involved in the galvanic corrosion experiment can be seen in figure 4.25. A uniform white calcareous deposit covered the steel sample and a thin light grey deposit layer covered the AA6005. Note the heavy pitting attack of the sacrificial anode.

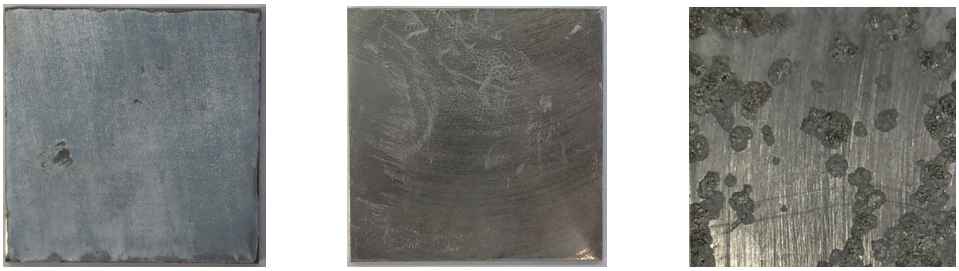

(a) **(b)** **(c)**

Figure 4.25: Photographs of the samples involved in galvanic corrosion experiment with cathodic protection in artificial seawater at 10°C. (a) carbon steel X65, (b) aluminium alloy 6005, (c) sacrificial anode AlZnIn.

4.5.3 Coupling of carbon steel X65 and aluminium alloy 6082

Galvanic corrosion: cathodic protection at 10°C for 3 days

Carbon steel X65, AA6082 and AlZnIn from the galvanic experiment is shown in figure 4.26. A white uniform calcareous deposit covered the steel surface. AA6082 showed a very thin white deposit covering the surface. AlZnIn revealed heavy pitting attacks.

(a) **(b)** **(c)**

Figure 4.26: Photographs of the samples involved in galvanic corrosion experiment with cathodic protection in artificial seawater at 10°C. (a) carbon steel X65, (b) aluminium alloy 6082, (c) sacrificial anode AlZnIn.

Crevice corrosion: cathodic protection at 10°C for 3 days

Images from the galvanic crevice corrosion involving CSX65, AA6082 and AlZnIn with a crevice size of 300 µm can be seen in figure 4.27. An almost uniform deposit layer was revealed on the steel with a white horizontal calcareous deposit at the upper crevice mouth. A white/grey deposit covered the exposed AA6082 sample.

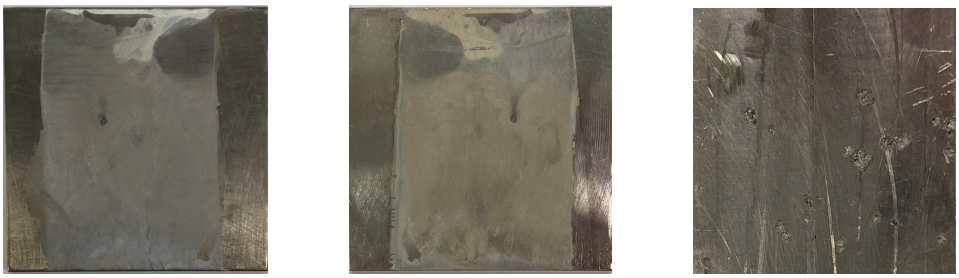

(a) **(b)** **(c)**

Figure 4.27: Photographs of the samples involved in galvanic crevice corrosion experiment with cathodic protection in artificial seawater at 10°C in a simulated crevice of 300 µm. (a) carbon steel X65, (b) aluminium alloy 6082, (c) sacrificial anode AlZnIn.

Crevice corrosion: cathodic protection at 10°C for 5 days

Minor deposit was revealed on both steel and AA6082 involved in the galvanic crevice corrosion experiment for 5 days, as shown in figure 4.28. From looking at the samples it can be assumed that the sample surfaces have not been properly exposed to seawater. The sacrificial anode revealed a dark grey deposit around the pits.

(a) **(b)** **(c)**

Figure 4.28: Photographs of the samples involved in galvanic crevice corrosion experiment with cathodic protection in artificial seawater at 10°C in a simulated crevice of 100 µm. (a) carbon steel X65, (b) aluminium alloy 6082, (c) sacrificial anode AlZnIn.

Crevice corrosion parallel 1: cathodic protection at 10°C for 20 days

Images of the long term parallel 1 involving carbon steel X65, AA6082 and AlZnIn is shown in figure 4.29. When looking at the samples, it seemed like both the steel and AA6082 have not been exposed to the seawater properly. A minor calcareous deposit layer can be seen at the lower crevice mouth on the steel. A grey deposit of corrosion products was revealed on AA6082.

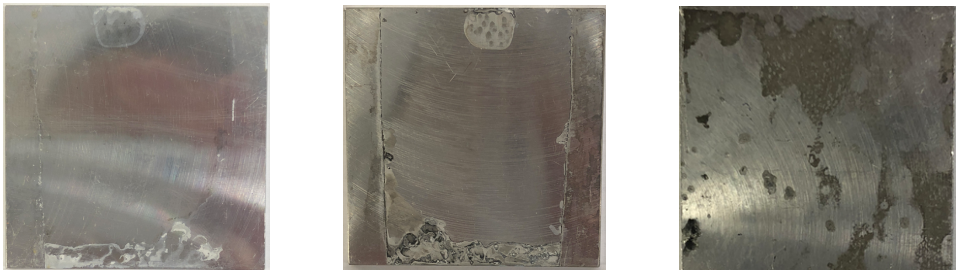

(a) **(b)** **(c)**

Figure 4.29: Photographs of the samples involved in galvanic crevice corrosion experiment with cathodic protection in artificial seawater at 10°C in a simulated crevice of 100 µm. (a) carbon steel X65, (b) aluminium alloy 6082, (c) sacrificial anode AlZnIn.

Crevice corrosion parallel 2: cathodic protection at 10°C for 20 days

Images from parallel 2 shown in figure 4.30 revealed a more exposed sample surface of AA6082 than seen in parallel 1. AA6082 had a thicker layer of corrosion products in addition to calcareous deposits. The anode revealed larger corroded areas around the pits.

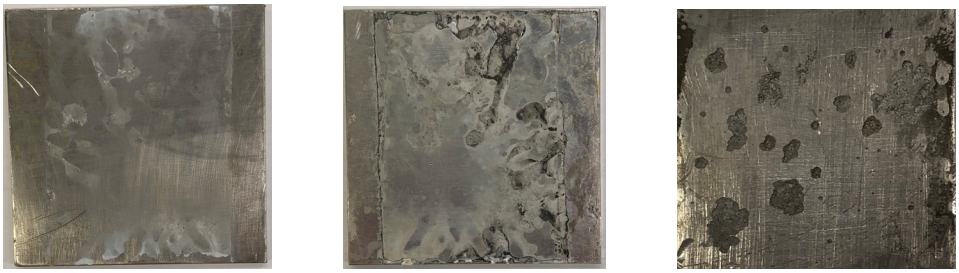

(a) **(b)** **(c)**

Figure 4.30: Photographs of the samples involved in galvanic crevice corrosion experiment with cathodic protection in artificial seawater at 10°C in a simulated crevice of 100 µm. (a) carbon steel X65, (b) aluminium alloy 6082, (c) sacrificial anode AlZnIn.

4.6 Microscopic surface characterization

Surface characterization was performed with a Scanning Electron Microscopy (SEM). An Energy Dispersive Spectroscopy (EDS) was used to analyze the chemical composition of the deposits on the sample surfaces. Additional SEM images and EDS data may be found in appendix C. All samples were analyzed except those from OCP experiments and the AlZnIn anodes. Figure 4.31 shows the samples as received from the Mechanical workshop.

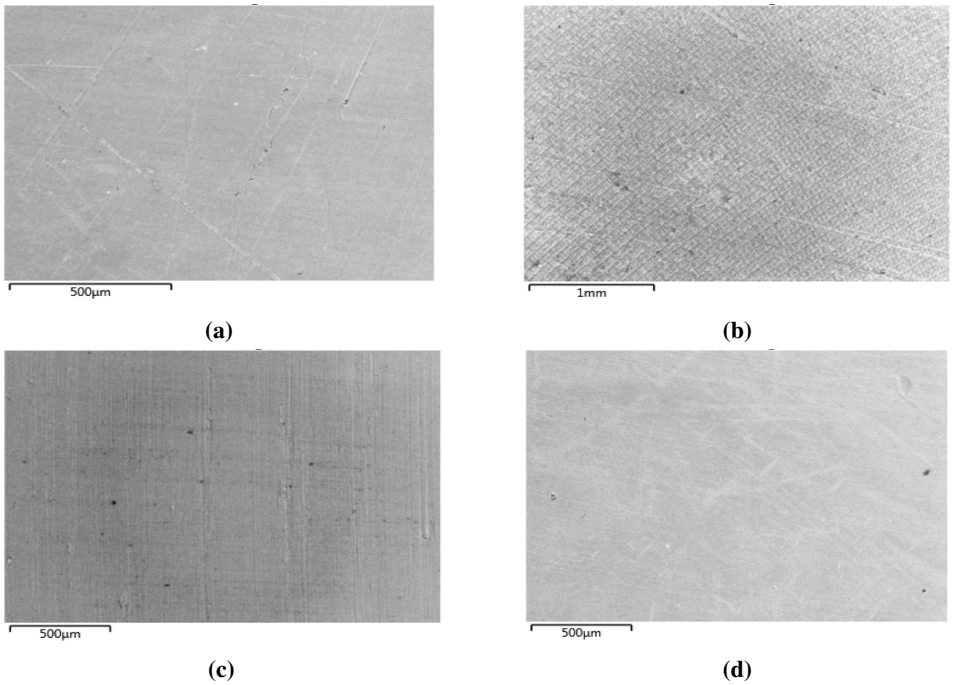

Figure 4.31: SEM images of the samples (a) carbon steel X65, (b) aluminium alloy 5083, (c) aluminium alloy 6005, (d) aluminium alloy 6082, as received from the Mechanical workshop [9].

4.6.1 Coupling of carbon steel X65 and aluminium alloy 5083

Galvanic corrosion: cathodic protection at 10°C for 3 days

A SEM image of the middle of the AA5083 sample prior chemical cleaning can be seen in figure 4.32. By comparing this image with the AA5083 sample as received from the Workshop in figure 4.31b one can see the same pattern in the surface. Not surprisingly was the revealing of Al, Mn, Si and Mg in the EDS analysis of spectrum 1 as shown in table 4.6. A higher content of oxygen appeared which presumably indicated a thin oxide layer of both Al and Mg.

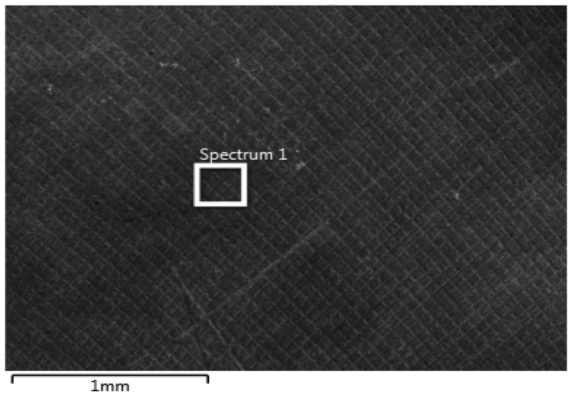

Figure 4.32: SEM image of the middle of aluminium alloy 5083 sample prior chemical cleaning.

Table 4.6: EDS analysis for spectrum 1 in figure 4.32 prior chemical cleaning.

Element	Spectrum 1 [wt%]
Mg	3.72
Al	83.71
Mn	0.77
O	11.38
Si	0.42

A SEM image of the calcareous deposits on carbon steel X65 is shown in figure 4.33a. The EDS analysis of spectrum 1 in table 4.7 revealed that the highest content was of Mg and O. The calcareous deposit was presumably mainly of $Mg(OH)_2$ when looking on the stoichiometrics of this deposit.

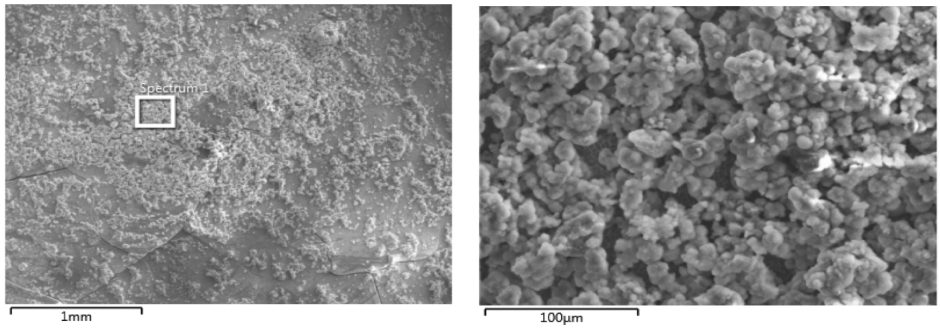

(a) **(b)**

Figure 4.33: SEM images prior chemical cleaning (a) SEM image of the middle of carbon steel X65 sample, (b) close up of the calcareous deposits on carbon steel X65 sample.

Table 4.7: EDS analysis for spectrum 1 in figure 4.33a prior chemical cleaning.

Element	Spectrum 1 [wt%]
Mg	36.76
Cl	3.06
Ca	0.89
O	51.65
Na	0.90
C	6.76

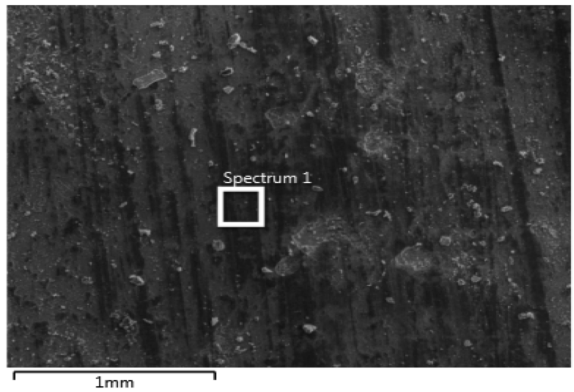

Figure 4.34: SEM image of the middle of carbon steel X65 sample prior chemical cleaning where the calcareous deposits have been scraped off.

The calcareous deposit shown in figure 4.33a was gently scraped off with a knife to examine the deposits close to the surface, as shown in figure 4.34.

The EDS analysis of spectrum 1 is shown in table 4.8, which revealed that mainly Mg and O was near the surface.

Table 4.8: EDS analysis for spectrum 1 in figure 4.34 prior chemical cleaning.

Element	Spectrum 1 [wt%]
Mg	44.19
Cl	0.89
O	53.68
Fe	1.25

SEM images of AA5083 and carbon steel X65 post chemical cleaning is shown in figure C.1 in appendix C. CS X65 revealed some corrosion while AA5083 did not.

Crevice corrosion: cathodic protection at 10°C for 3 days

SEM images prior chemical cleaning of aluminium alloy 5083 involved in galvanic crevice corrosion experiment with a crevice size of $300\,\mu\mathrm{m}$ is shown in figure C.2 in appendix C. No major deposits could be seen except a thin layer of oxide film.

SEM images prior chemical cleaning of carbon steel X65 is shown in figure 4.35 where a thicker layer of calcareous deposits could be seen. The EDS analysis in table 4.9 showed that the thicker white layer in spectrum 2 in figure 4.35a mainly consisted of $Mg(OH)_2$ but also a mix of other salts like NaCl. The thinner deposit layer close to the metal surface in spectrum 1 revealed a higher content of Ca.

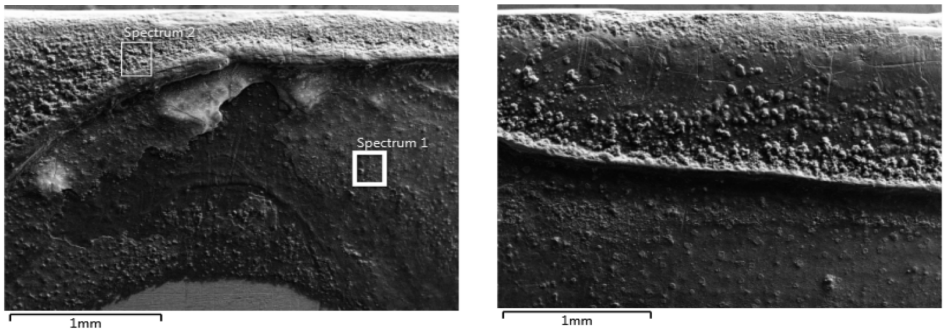

(a) **(b)**

Figure 4.35: SEM image of the carbon steel X65 sample prior chemical cleaning (a) left side of the upper crevice mouth, (b) middle of the upper crevice mouth.

Table 4.9: EDS analysis for spectrum 1 and 2 in figure 4.35a prior chemical cleaning.

Element	Spectrum 1 [wt%]	Spectrum 2 [wt%]
C	4.86	8.70
O	51.67	45.74
Na	0.86	3.33
Mg	36.13	33.26
Cl	1.49	6.64
Ca	3.93	0.74
Fe	1.06	0.84
Al	-	0.42
Si	-	0.14
K	-	0.19

Figure C.4 in appendix C shows AA5083 and carbon steel X65 post chemical cleaning where some changes in the surface morphology could be seen.

Crevice corrosion: cathodic protection at 10°C for 5 days

A SEM image of aluminium alloy 5083 prior chemical cleaning is shown in figure 4.36. Spectrum 2 in the image revealed a higher content of Ca, as shown in table 4.10. Taking the stoichiometrics into account it seemed like the white small round calcareous deposits were $CaCO_3$. The thicker deposit layer in spectrum 1 seemed to be a mix of corrosion products and Mg oxide.

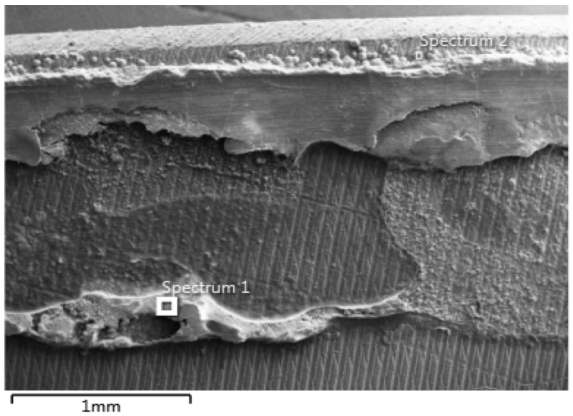

Figure 4.36: SEM image of the upper crevice mouth of aluminium alloy 5083 sample prior chemical cleaning.

Table 4.10: EDS analysis for spectrum 1 and 2 in figure 4.36 prior chemical cleaning.

Element	Spectrum 1 [wt%]	Spectrum 2 [wt%]
O	59.98	50.71
Mg	8.49	2.19
Al	31.1	0.65
Ca	0.43	33.27
C	-	13.17

The aluminium alloy 5083 sample post chemical cleaning showed localized corrosion at the upper crevice mouth, as shown in figure 4.37. The image was taken at the same spot as the image in figure 4.36 and by comparing these images it seemed like the localized corrosion was on the surface where the calcareous deposits was thickest prior chemical cleaning.

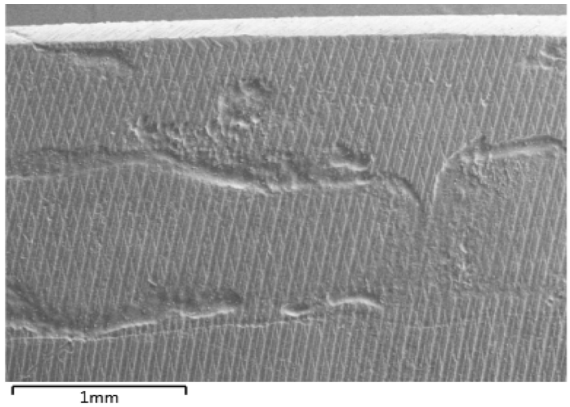

Figure 4.37: SEM image of the upper crevice mouth of aluminium alloy 5083 sample post chemical cleaning.

Crevice corrosion parallel 1: cathodic protection at 10°C for 20 days

Figure 4.38 shows SEM images of the upper crevice mouth on aluminium alloy 5083 from parallel 1 prior chemical cleaning. The round white deposits were investigated by EDS analysis as shown for spectrum 1 in table 4.11. A higher content of Ca was seen in addition to O and C. Spectrum 2 on the other hand, revealed a higher content of Mg and O, which presumably indicated that the darker deposit layer was $Mg(OH)_2$. Both of the spectres indicated different ions from the artificial seawater.

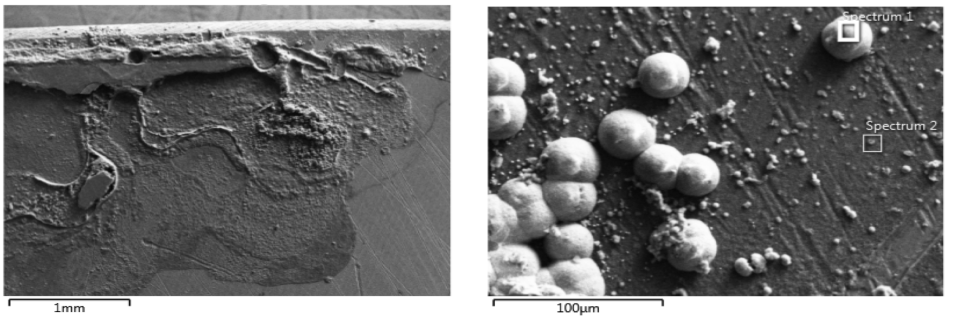

(a) **(b)**

Figure 4.38: SEM images prior chemical cleaning: (a) the upper crevice mouth of aluminium alloy 5083 sample, (b) zoomed SEM image of the upper crevice mouth of aluminium alloy 5083 sample.

Table 4.11: EDS analysis for spectrum 1 and 2 in figure 4.38b prior chemical cleaning.

Element	Spectrum 1 [wt%]	Spectrum 2 [wt%]
C	22.76	4.61
O	48.70	41.80
Mg	1.65	31.24
Al	0.24	9.19
Cl	0.89	2.11
Ca	19.95	0.17
Na	1.41	0.85
S	0.45	0.16
Sr	2.44	-
F	1.52	9.75
Si	-	0.13

SEM images of carbon steel X65 prior chemical cleaning can be seen in figure C.5 in appendix C. The EDS analysis in table C.1 of the upper crevice mouth of X65 indicated that the deposits were mainly of corrosion products from Al in addition to Al - and Mg oxides.

SEM images post chemical cleaning of both the upper and lower crevice mouth of AA5083 revealed localized corrosion. Pitting corrosion in addition to alkaline etching around intermetallic particles can be seen in figure 4.39.

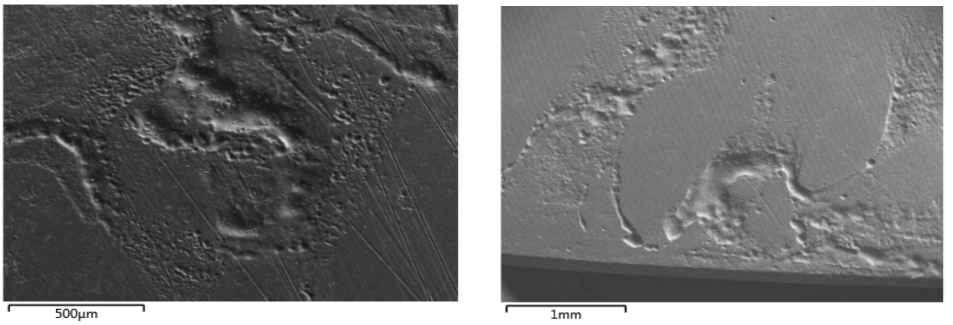

(a) **(b)**

Figure 4.39: SEM images post chemical cleaning: (a) the upper crevice mouth of aluminium alloy 5083 sample, (b) the lower crevice mouth of aluminium alloy 5083 sample.

Crevice corrosion parallel 2: cathodic protection at 10°C for 20 days

SEM images of AA5083 from parallel 2 is shown in figure 4.40.

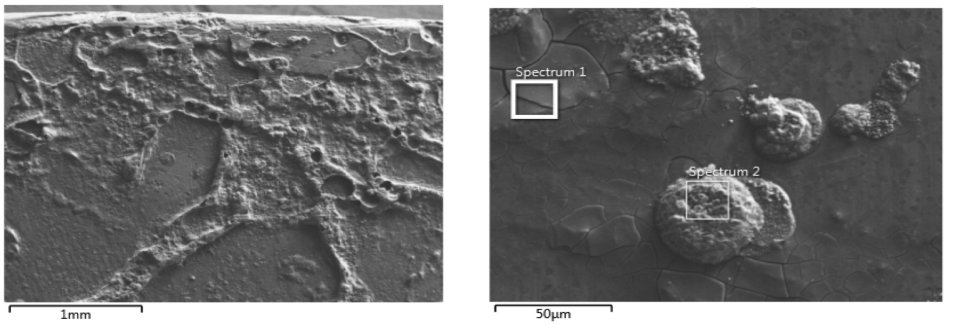

(a) **(b)**

Figure 4.40: SEM images prior chemical cleaning: (a) the upper crevice mouth of aluminium alloy 5083 sample, (b) close up of the deposits at the upper crevice mouth of aluminium alloy 5083 sample.

Table 4.12: EDS analysis for spectrum 1 and 2 in figure 4.40b prior chemical cleaning.

Element	Spectrum 1 [wt%]	Spectrum 2 [wt%]
C	5.48	4.89
O	53.50	63
Mg	1.46	0.57
Al	38.99	31.54
Na	0.39	-
Si	0.18	-

Recall that parallel 2 experienced gas evolution before the experiment was restarted. The deposits on the surface were corrosion products in addition to a Al oxide layer as shown in table 4.12 from the EDS analysis of figure 4.40b. SEM images of carbon steel X65 from parallel 2 prior chemical cleaning is shown in figure C.7 in appendix C.

SEM images of AA5083 post chemical cleaning revealed alkaline etching around intermetallic particles in the matrix, as shown in figure 4.41. A SEM image of carbon steel post chemical cleaning indicated that pieces of the edges on the metal has corroded, as shown in figure 4.42.

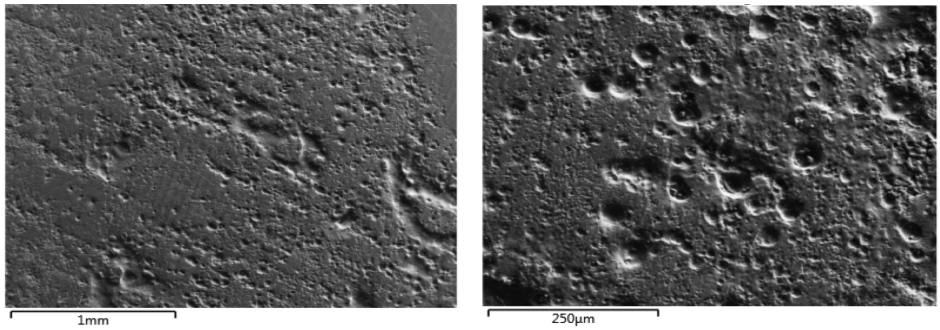

(a) **(b)**

Figure 4.41: SEM image of aluminium alloy 5083 sample post chemical cleaning (a) SEM of the upper middle of the sample, (b) extra close up of the upper middle of the sample.

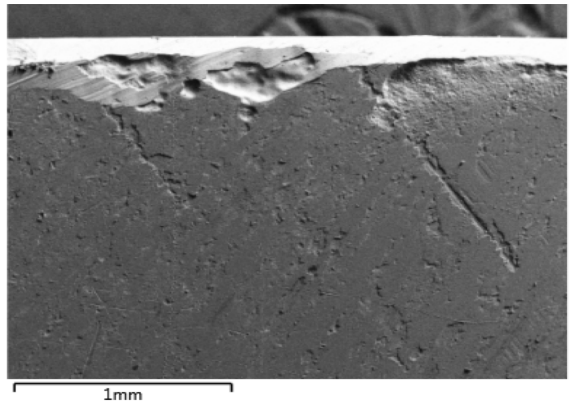

Figure 4.42: SEM image of the upper crevice mouth of carbon steel X65 sample post chemical cleaning.

4.6.2 Coupling of carbon steel X65 and aluminium alloy 6005

Galvanic corrosion: cathodic protection at 10°C for 3 days

SEM images prior chemical cleaning of aluminium alloy 6005 and carbon steel X65 from galvanic corrosion experiment is shown in figure 4.43 and figure 4.44 respectively. AA6005 showed no other deposits than a very thin Al oxide layer. The steel on the other hand revealed calcareous deposits in the form of $Mg(OH)_2$ and other salt deposits, as shown in the EDS analysis in table 4.13. Figure C.9 in appendix C shows the steel surface where calcareous deposits were scraped off, indicating that a Mg oxide layer surrounded Ca-ions and other intermetallic particles, as shown in table C.3. SEM images post chemical cleaning of both AA6005 and the steel did not show any corrosion.

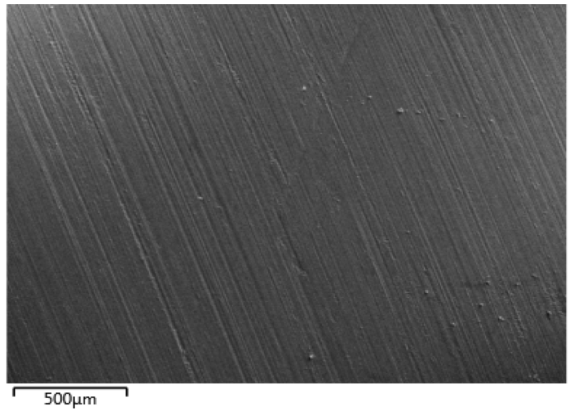

Figure 4.43: SEM image of the middle of aluminium alloy 6005 sample prior chemical cleaning.

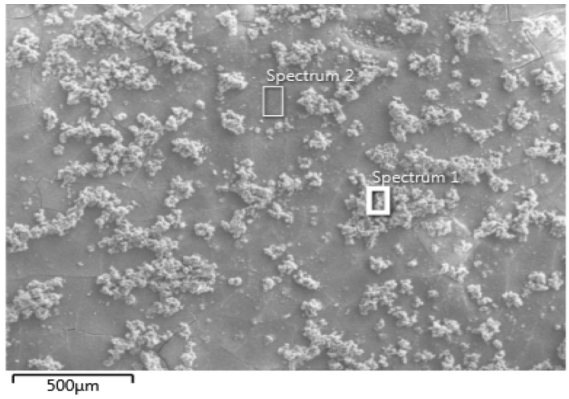

Figure 4.44: SEM image of the middle of carbon steel X65 sample prior chemical cleaning.

Table 4.13: EDS analysis for spectrum 1 and 2 in figure 4.44 prior chemical cleaning.

Element	Spectrum 1 [wt%]	Spectrum 2 [wt%]
O	50.72	53.52
Al	1.74	-
Ca	0.59	0.37
Zn	2.31	-
Mg	40.32	43.62
Fe	1.25	0.84
Na	0.65	0.45
Cl	2.43	1.19

4.6.3 Coupling of carbon steel X65 and aluminium alloy 6082

Galvanic corrosion: cathodic protection at 10°C for 3 days

A SEM image prior chemical cleaning of aluminium alloy 6082 from galvanic corrosion experiment is shown in figure 4.45. The associated EDS analysis in table 4.14 indicated a thin Al oxide layer on the surface in addition to the intermetallic particles in the metal matrix. SEM images of the calcareous deposits on carbon steel X65 is shown in figure C.10 in appendix C.

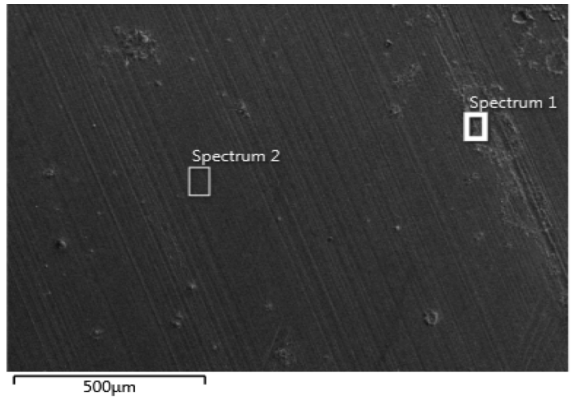

Figure 4.45: SEM image of the middle of aluminium alloy 6082 sample prior chemical cleaning.

Table 4.14: EDS analysis for spectrum 1 and 2 in figure 4.45 prior chemical cleaning.

Element	Spectrum 1 [wt%]	Spectrum 2 [wt%]
O	16.81	2.36
Al	82.03	96.50
Si	0.56	0.56
Mn	0.60	-
Mg	-	0.58

A SEM image of the middle of carbon steel X65 where the calcareous deposits have been gently scraped off is shown in figure 4.46 with EDS analysis in table 4.15. The analysis indicated that a Mg-oxide layer with Ca-ions covered the surface. The SEM images post chemical cleaning did not show any noticeable corrosion and are not presented.

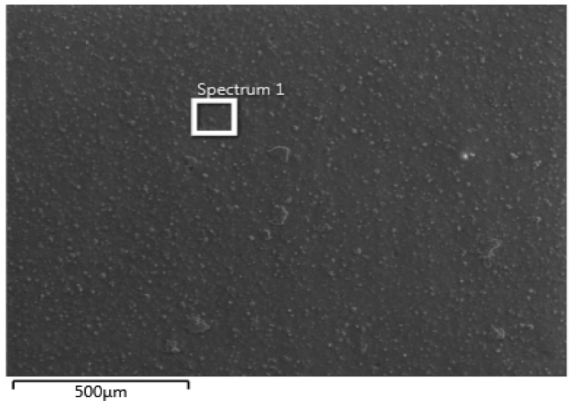

Figure 4.46: SEM image of the middle of carbon steel X65 sample prior chemical cleaning where the calcareous deposits were scraped off.

Table 4.15: EDS analysis for spectrum 1 in figure 4.46 prior chemical cleaning.

Element	Spectrum 1 [wt%]
Mg	44.71
Ca	0.29
O	53.65
Fe	1.34

Crevice corrosion: cathodic protection at 10°C for 3 days

A SEM image prior chemical cleaning of the upper crevice mouth of AA6082 involved in galvanic crevice corrosion experiment with a crevice size of 300 µm is shown in figure 4.47. Looking at the EDS analysis in table 4.16 one can see that the deposit layer on AA6082 was mainly of Al - and Mg oxide.

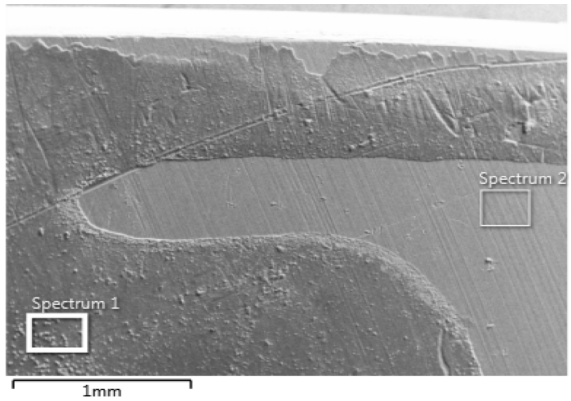

Figure 4.47: SEM image of the upper crevice mouth of aluminium alloy 6082 sample prior chemical cleaning.

Table 4.16: EDS analysis for spectrum 1 and 2 in figure 4.47 prior chemical cleaning.

Element	Spectrum 1 [wt%]	Spectrum 2 [wt%]
C	5.18	8.24
O	54.43	1.44
Mg	36.98	0.66
Al	0.70	89.07
Ca	2.71	-
Si	-	0.58

Figure 4.48 shows SEM images of carbon steel X65 prior chemical cleaning. A thicker deposit layer could be seen at the upper crevice mouth than the rest of the surface. Though, the whole exposed surface was covered with deposits. The SEM images post chemical cleaning did not show any noticeable corrosion and is not presented.

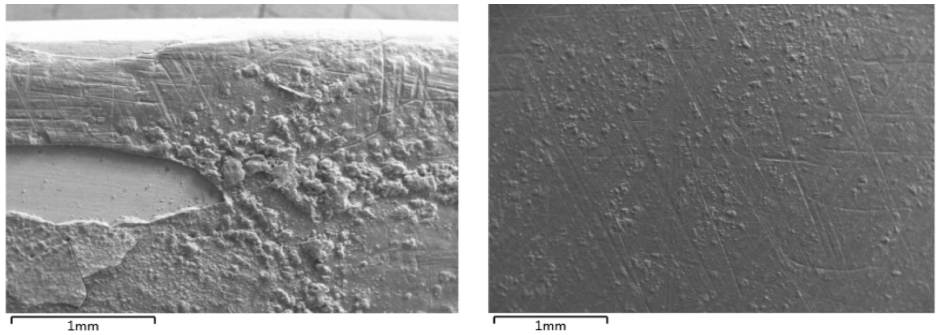

Figure 4.48: SEM image of carbon steel X65 sample prior chemical cleaning (a) SEM of the upper crevice mouth, (b) SEM of the middle of the sample.

Crevice corrosion: cathodic protection at 10°C for 5 days

The aluminium alloy 6082 and carbon steel X65 involved in the galvanic crevice corrosion experiment for 5 days did not show any major deposits, as earlier described in the part of the macroscopic photographs. The only deposits were seen at the lower crevice mouth on both metals as shown in figure 4.49. SEM images post chemical cleaning is not presented.

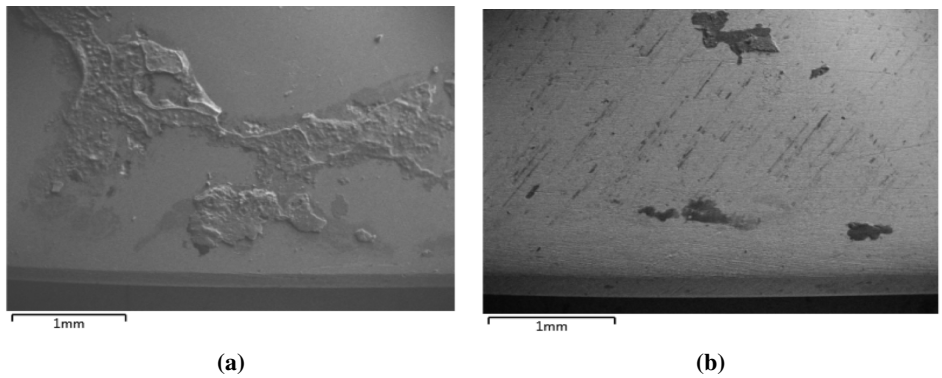

Figure 4.49: SEM images prior chemical cleaning (a) SEM of the lower crevice mouth of aluminium alloy 6082 sample, (b) SEM of the lower crevice mouth of carbon steel X65 sample.

Crevice corrosion parallel 1: cathodic protection at 10°C for 20 days

SEM images prior chemical cleaning of the upper and lower crevice mouth on aluminium alloy 6082 from parallel 1 is shown in figure 4.50 where thicker deposit layers were seen. On carbon steel X65 could a deposit layer be seen at the lower crevice mouth, as shown in figure C.14 in appendix C.

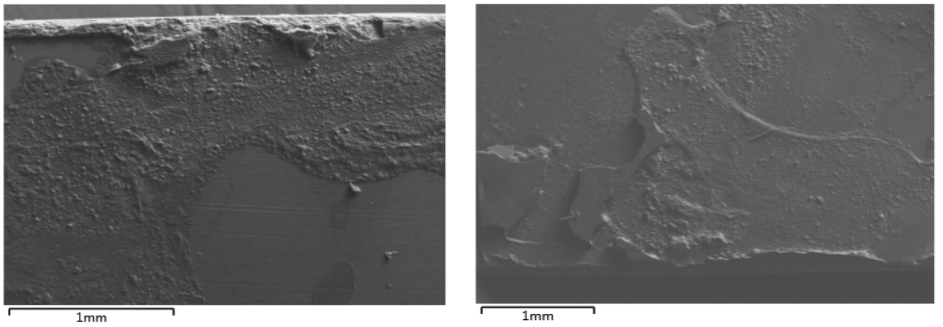

(a) **(b)**

Figure 4.50: SEM images prior chemical cleaning (a) the upper crevice mouth of aluminium alloy 6082 sample (b) the lower crevice mouth of aluminium alloy 6082 sample.

SEM images post chemical cleaning showed localized corrosion at the upper crevice mouth of AA6082, as shown in figure 4.51. Furthermore, alkaline etching around intermetallic particles was also seen at the lower crevice mouth on AA6082, as shown in figure 4.52. Carbon steel X65 did not show any corrosion and SEM images is not presented.

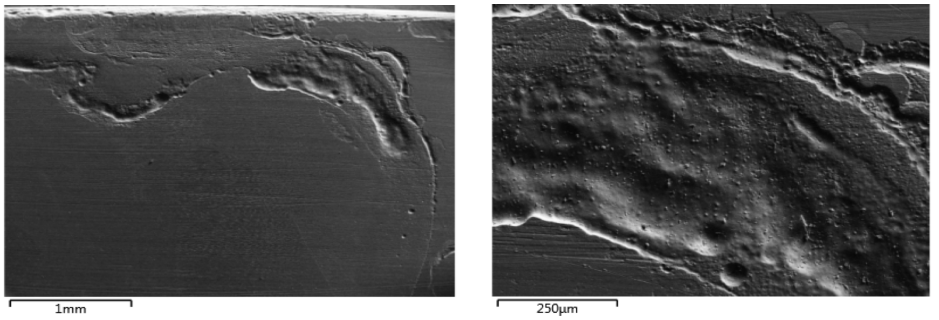

(a) **(b)**

Figure 4.51: SEM images post chemical cleaning (a) the upper crevice mouth of aluminium alloy 6082 sample (b) close up of the upper crevice mouth of aluminium alloy 6082 sample.

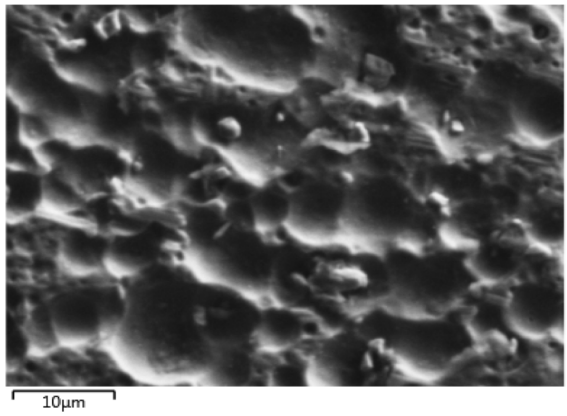

Figure 4.52: SEM image of the lower crevice mouth of aluminium alloy 6082 sample post chemical cleaning.

Crevice corrosion parallel 2: cathodic protection at 10°C for 20 days

SEM images prior chemical cleaning of the upper and lower crevice mouth of AA6082 from parallel 2 is shown in figure 4.53. Spectrum 1 in the image of the upper crevice showed more round particles in the deposit than spectrum 2. The EDS analysis in table 4.17 indicated that these particles presumably were $CaCO_3$, where the surrounding deposit was $Mg(OH)_2$.

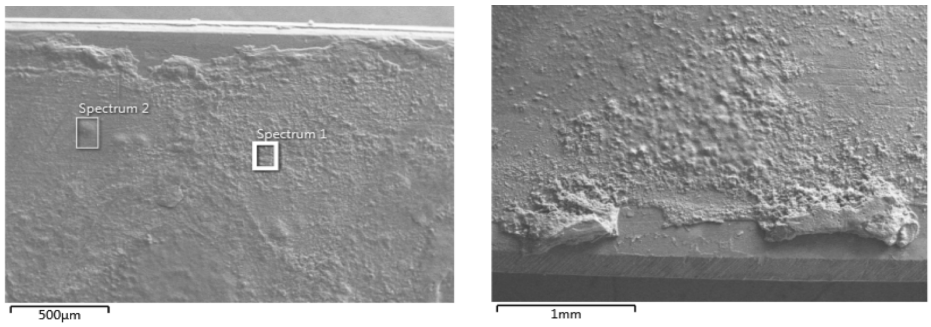

(a) **(b)**

Figure 4.53: SEM images prior chemical cleaning (a) the upper crevice mouth of aluminium alloy 6082 sample (b) lower crevice mouth of aluminium alloy 6082 sample.

Table 4.17: EDS analysis for spectrum 1 and 2 in figure 4.53a prior chemical cleaning.

Element	Spectrum 1 [wt%]	Spectrum 2 [wt%]
C	10.63	9.43
O	52.55	53.09
Mg	25.29	27.21
Al	4.43	8.47
Ca	7.10	1.81

SEM images post chemical cleaning of aluminium alloy 6082 and carbon steel X65 is shown in figure 4.54. Localized corrosion could be seen at the upper crevice mouth of AA6082 with alkaline etching around intermetallic particles. It seemed like the localized corrosion had occurred where the deposits were thickest when comparing the images prior and post chemical cleaning. The SEM image of carbon steel X65 did not show any significant corrosion attacks.

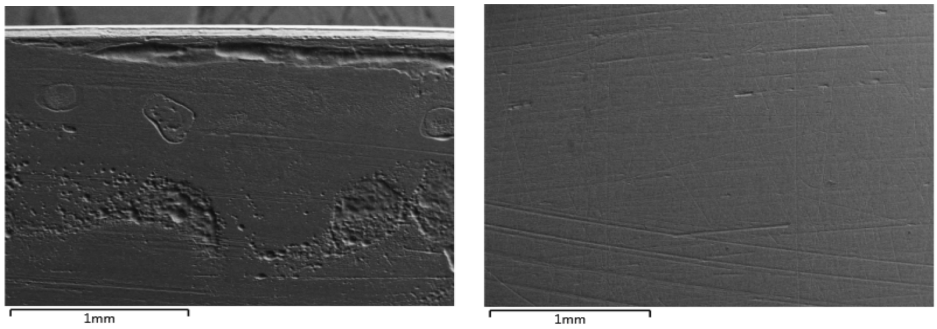

(a) **(b)**

Figure 4.54: SEM images post chemical cleaning (a) the upper crevice mouth of aluminium alloy 6082 sample (b) the middle of carbon steel X65 sample.

Chapter 5

Discussion

A discussion of the results from the experimental work including electrochemical behavior, weight loss measurements and corrosion rates, surface characterization and the comparison of the earlier studies of this project will be presented in this chapter. The experimental work will be discussed in addition to suggestions for further work.

5.1 Electrochemical behavior

Galvanic corrosion experiments of steel-aluminium couples with applied cathodic protection showed promising results. Throughout all of the experiments, both steel and the aluminium alloys experienced a cathodic current. The current on steel was approximately one and two order of magnitude larger than on aluminium [5],[7]. The cathodic current on AA5083 and AA6005 was slightly higher than on AA6082, where the latter showed an exponentially decreasing cathodic current. A very steadily potential more negative than the protection potential of steel was observed throughout the experiments [11]. The potential was in the same range as the Open Circuit Potential of the sacrificial anode. The pH measured on the samples gave an interesting observation. The steel indicated an alkaline environment on the surfaces with a pH of 10-11. The reduction reactions occurring on the cathodic steel surface gave formation of hydroxyl-ions, which in turn gave rise to an alkaline diffusion layer adjacent the cathodic surface. The aluminium alloys however, revealed an acidic/neutral pH of 6-7 on the surfaces. The macroscopic photographs of the samples involved in galvanic corrosion experiments showed a uniform layer of deposits on the surfaces. A thick white/grey deposit was seen on steel while a thin grey deposit was

covering the aluminium alloys. At these measured potentials a calcareous deposit layer will form on the steel surface [14], [16]. The higher measured pH on steel showed the precipitation of $Mg(OH)_2$ [17]. The acidic/neutral pH measured on the aluminium alloys at these potentials was in the passive region [19],[20], indicating a passivating aluminium oxide on the surfaces. The higher cathodic current on the steel samples was due to the larger cathodic surface area compared to the aluminium alloys, where reduction reactions occur only at the intermetallic particles in the Al-matrix [5].

Galvanic crevice corrosion experiments with applied cathodic protection were performed with a crevice size of both $100\,\mu m$ and $300\,\mu m$. For the latter crevice size, the current on the aluminium alloys 5083 and 6082 respectively, showed an initial anodic peak. The current on AA5083 decreased steadily towards zero. An initially increasing cathodic current was seen on steel before it decreased towards $-15\,\mu A/cm^2$ when coupled to AA5083. The same initially case was seen on the steel coupled to AA6082. The final current on AA6082 and steel showed an increased anodic and cathodic peak respectively. This behavior could be explained by dissolution of the oxide layer on Al as a consequence of the increased pH in the crevice due to higher reduction rates seen on the steel. The pH in the crevice was measured to be 10. An alkaline pH of this value is detrimental for Al [19]. The macroscopic photographs from the couplings in a crevice of $300\,\mu m$ revealed a uniform deposit layer on both the aluminium alloys and steel, as shown in figure 4.21 and figure 4.27. As described earlier, the white/grey deposits on the steel samples were calcareous deposits. On the other hand, the color of the deposit layer on AA5083 and AA6082 differed in this case from the deposits seen on the respective alloys in galvanic corrosion experiments. A thin light-grey uniform deposit was seen on AA5083, while a deposit similar of what was seen on steel was revealed on AA6082. This could be explained by the chemical composition of the alloy. The matrix of AA5083 consist of a higher content of Mg and Mn, which makes a more passivating oxide layer on Al with increasing pH [4]. The deposit on AA6082 seems to be a reflection of the deposit on steel. This could be the case if the crevice was sealed as a consequence of a thicker formation of calcareous deposits. Earlier studies [14] have stated that $Mg(OH)_2$ is mainly formed at 10°C and in the potential range as recorded.

The electrochemical behavior regarding galvanic crevice corrosion experiments for five days differed from the earlier observations. After approximately fifty five hours the current on AA5083 and the steel experienced an increased anodic and cathodic current respectively, as shown in figure 4.10. The macroscopic photographs revealed brown/orange deposits on the left corner on steel, as shown in figure 4.22a. The area was beneath the Teflon strip. It is possible to believe that a micro galvanic environment was made in be-

tween the Teflon and the sample surface. White deposits were mainly seen at the upper and lower crevice mouth. A thicker layer of deposits and corrosion products were seen on AA5083. Nearly half of the sample surfaces seemed exposed to seawater. The results clearly evidence the effect of crevice size. Another possible explanation is gas bubbles which blocks the flow of seawater [23]. Minor deposits can be seen when looking at the macroscopic photographs of the steel and AA6082 for the same type of experiment, as shown in figure 4.28. The corresponding electrochemical data in figure 4.13 showed a slightly increasing anodic current on AA6082. An initial increasing (but small) cathodic peak was observed on the steel before the current was stabilized. A possible reason is that less exposed surface area gave rise to the small currents.

Parallel experiments were performed of the steel-aluminium galvanic crevice couples of AA5083 and AA6082 for twenty days. The anodic current on AA5083 decayed with time after the initial anodic peak, as shown in figure 4.11. The electrochemical behavior was similar earlier studies [7], [9], though the current was significant lower on AA5083. The current on steel was in the cathodic range with an initial increasing peak before the current was stabilized. The potentials were in a range of -1088 mV_{SCE} and -1108 mV_{SCE}. Though, no significant impact on the currents were seen due to the potential differences between the parallels. The decay in currents with time could be explained by the depletion of oxygen in the crevice [22]. The measured pH on both steel and AA5083 was 9-10 in both parallels. The alkaline pH indicated the change of environment inside the crevice when cathodic protection was applied. A higher initially rate of reduction reactions on steel increased the pH in the cavity due to formation of hydroxyl-ions. Destabilization of the possible oxide film on the Al surface revealed the cathodic intermetallic particles in the Al-matrix [4], [5]. An alkaline etching of the Al-matrix surrounding the intermetallic particles was initiated due to the increased pH and the particles may be detached. With time as the currents on steel and AA5083 got stable it is reason to assume that a new oxide layer has been formed in addition to calcareous deposits [5]. The higher content of Mg in the matrix of AA5083 gives reason to believe that a passive Mg-oxide layer in addition to $Mg(OH)_2$ deposits on the metal surface. Taking the macroscopic photographs into account, the possible explanation of the electrochemical behavior seems reasonable. The calcareous deposits were mainly at the lower crevice mouth on steel but could also be seen at the upper part of parallel 1. AA5083 in parallel 1 clearly indicated partly exposure to seawater. Again, a possible reason could be gas bobbles trapped inside the simulated crevice. This indicated hydrogen gas evolution from the reduction reactions on steel. Recall that parallel 2 was restarted because of vehement gas evolution in the cell where the samples were not replaced. The macroscopic photograph clearly indicated corrosion prod-

ucts which covered the whole exposed surface of AA5083. This is an interesting point of view in accordance to the affect of gas evolution. Though, caution should be made when comparing the macroscopic photographs in addition to weight losses of this parallel with others.

A slightly higher anodic peak was seen on AA6082 in parallel 2, as shown in figure 4.14. The current was slightly higher than what was observed on AA5083. Though, the current on AA6082 was similar earlier studies at 25°C [9], but the initial anodic peak was wider in parallel 1 and 2 at 10°C. The impact of temperature on the currents could be explained by the kinetics of deposits. The kinetics of calcareous deposits is found to be slow at low temperatures on steel [14]. It is reason to believe that this is valid also for aluminium. The slightly higher anodic peak of AA6082 compared to AA5083 could be explained by the chemical composition of AA6082 which consist of more intermetallic particles in the surface matrix [5]. In addition to Fe the 6000-series consist of a higher content of the noble intermetallics Si and Cu which will act as cathodic sites in the Al-matrix. As earlier described, the destabilization of the possible oxide layer leads to revealing of the cathodic sites. This gave rise to alkaline etching of the surrounding matrix which lead to the anodic current peak before the passive oxide layer was renewed. The parallels had a potential range from -1090 mV_{SCE} to -1105 mV_{SCE} and the measured pH varied in between 10-11. The macroscopic photographs of parallel 1 showed an almost unexposed surface on both steel and AA6082. Again, this could be a consequence of gas trapped on the inside of the crevice, or the crevice was to small for the seawater to pass through. Minor deposits were seen at both upper and lower crevice mouth on AA6082. Parallel 2 on the other hand, revealed a thicker layer of deposit on AA6082. The result validates the slightly higher anodic current peak. It seemed like $Mg(OH)_2$ deposits as a homogeneous layer at the alkaline surface around the earlier cathodic sites in the matrix. Both the cathodic currents on steel in addition to the macroscopic photographs indicated that steel was protected. Only minor calcareous deposits were seen on the upper and lower crevice mouth.

The comparison of the electrochemical behavior of AA6005 at 25°C revealed the same initial anodic peak trend on Al as described earlier at 10°C. One exception was parallel 3 from [8] which experienced a cathodic current. The current on steel was cathodic in all of the experiments but varied in magnitude. A decayed in both anodic and cathodic current as a function of time could be seen in figure 4.15. The difference in magnitude of the currents could be explained by the wider potential range seen for the different experiments. A more anodic potential was seen from [7] which corresponded to the highest anodic peak seen for AA6005 and the highest cathodic peak on steel. As steel initially draw more protective current from the sacrificial anode, aluminum suffer of initial high anodic current. As the

earlier described mechanism in the crevice stabilizes, the currents on both Al and steel got more stable. Nevertheless, the potential was in the range of the protective potential of the anode. Parallel experiments is difficult to reproduce especially on Al because of the dependence of the composition of the alloy, particle distribution in the matrix, sample size and how the experiment is performed by the authors. The cathodic current on AA6005 from parallel 3 [8] could be explained by the sample size. A smaller sample size (20·20·2mm) was used by the authors regarding these experiments. The sample size might have affected the exposed sample area when immersed in the artificial seawater. A smaller sample would make it easier to expose the whole surface since the distance from the crevice mouth into the middle of the sample is shorter. In addition, a higher temperature affected the kinetics of the calcareous deposits [14], which covered the sample surface.

5.2 Weight loss measurements and corrosion rates

Based on the corrosion rates presented in table 4.1 carbon steel X65 seemed protected when connected to aluminium and the CP system independent of the experimental setup, as also seen in other studies [6]. Very small corrosion rates were measured on steel. Exceptions were the corrosion rates of the OCP and parallel 2 when coupled to AA5083 in galvanic crevice experiment. The highest corrosion rate involved in Open Circuit experiment was expected when looking at the potential of the steel in figure 4.1 where a stable potential was reached at approximately -700 mV_{SCE}. This potential favors corrosion of steel [13] where steel must be polarized to a potential between -850 mV_{SCE} and -1100 mV_{SCE} when submerged in seawater [11]. As described earlier, steel and AA5083 involved in galvanic crevice experiment parallel 2 experienced gas evolution. The steel did not indicate significant corrosion on the surface from a macroscopic view, but parts of the edges on the sample were dissolved and gave rise to the higher corrosion rate. The pH regarding the steel in all of the experiments varied between 9-11. Except the Open Circuit Potential, the potentials where steel was involved lay in the region of the protective potential from the sacrificial anode. Steel was in the immune region at these potentials and pH [13]. Furthermore, the kinetics of the calcareous deposit $Mg(OH)_2$ was favored at these conditions [14],[16],[17].

Corrosion rates of AA5083 were in the same order of magnitude regarding OCP, galvanic corrosion and galvanic crevice corrosion with a crevice of $300\,\mu m$, as shown in table 4.2. The Open Circuit Potential of AA5083 was stable at -755 mV_{SCE}, as shown in figure 4.2, where the potential corresponded to earlier studies [21]. At this potential and slightly alkaline pH in the artificial seawater pitting is expected [20]. The corrosion rate regarding crevice corrosion for five days stands out. Recall the anodic peak in current on

AA5083 and the reflection of a cathodic peak on steel after approximately seventy hours. The higher reduction reactions on the steel seemed to have increased the dissolution of AA5083, possibly due to the increased alkaline environment formed from the formation of hydroxyl-ions. The higher corrosion rate of parallel 1 was expected since the experiment ran for twenty days. Furthermore, at a potential of approximately -1108 mV_{SCE} and a alkaline pH of 9-10 slightly pitting corrosion was expected [20],[21]. Nevertheless, by comparing this value with the corrosion rate of the OCP one can see that galvanic crevice experiments lowers the corrosion rates as a function of time. As explained earlier, this is due to the stabilization of the corrosion mechanisms on Al in the crevice with time. Parallel 2 experienced gas evolution as described earlier, and the corrosion rate was not comparable with the other experiments. Taking the calculated corrosion rates by Faraday's law into account, the correlation between these and the measured values was good. Due to not taking into account the localized corrosion on the sample surfaces, the calculated values was lower, which correspond with other studies [6]. A linear trend of the corrosion rates could be seen in figure 4.16 which compared the measured corrosion rates. This indicated the corrosion rates to increase steadily with time. This was expected since cathodic protection is a form of corrosion control rather than corrosion inhibition. Steep curves regarding the calculated corrosion rates was seen the first days in figure 4.17. A steadily stabilization could be seen as a function of time. Recall that the calculated corrosion rates were based on the anodic current densities from the electrochemical data and therefore showed steeper curves especially for the five days crevice experiment.

AA6082 revealed a very low corrosion rate regarding the OCP, as shown in table 4.4. The same value was measured from the galvanic corrosion experiment. The result showed that cathodic protection of AA6082 is promising. The Open Circuit Potential of AA6082 was approximately stable at -910 mV_{SCE} and showed the same trend as earlier studies [21]. Assuming the experimental potential-pH diagram in figure 2.3b is valid for AA6082 as earlier stated [21], the alloy is in the passive area at the potential and the neutral pH measured in the galvanic corrosion experiment. The experiment with a crevice size of $300\,\mu m$ also revealed a low corrosion rate though the value was higher than for the OCP. The corrosion rate of parallel 1 was in the same order of magnitude as parallel 1 regarding AA5083. An slightly increased rate was seen on parallel 2 which corresponded to the increased anodic peak seen in the current. The mechanism for this behavior was explained earlier. Furthermore, at a potential of approximately -1100 mV_{SCE} and a alkaline pH of 10-11 slightly pitting corrosion was expected [20],[21]. The correspondence between measured and calculated corrosion rates was not equally adequate as seen for AA5083. A larger difference was seen of the calculated corrosion rates regarding parallel 1 an 2 in figure 4.17. Again,

this was due to the initially anodic peak in the current on AA6082 in parallel 2. In addition, AA6082 contained the highest Si-content of the respective alloys used in this project. A small Mg/Si ratio makes the alloy more susceptible to intergranular corrosion [10]. This phenomena was not studied in the thesis, but it could explain the effect of intermetallic particle distribution in the 6000-series on the corrosion rates. The sacrificial anode AlZnIn revealed a very low self corrosion rate, as shown in table 4.5. The highest corrosion rates were seen regarding the galvanic corrosion experiments. The corresponding macroscopic photographs indicated large areas with small pits tightly packed to each other. The same observations were seen regarding the other experiments as well.

The corrosion rate regarding the OCP of AA6005 was very small, as shown in table 4.3. An interesting observation was the corrosion rate of the galvanic corrosion experiment which was lower than the OCP. A light grey layer was seen on the macroscopic photographs, which indicated the passive oxide film on the sample surface. Figure 4.18 showed a comparison of the measured corrosion rates of AA6005 from OCP, galvanic corrosion and galvanic crevice corrosion experiments both with and without applied cathodic protection at 10°C and 25°C from earlier studies [7],[8],[9]. Lowest corrosion rates regardless the temperature were seen from the OCP and galvanic corrosion experiments with applied CP. A linear trend could be seen as a function of time. The temperature differences seemed not to significantly affect the corrosion rates regarding the galvanic crevice experiments. The calcareous deposits formed more rapidly at 25°C as earlier studies also have shown [14]. A uniform magnesium oxide layer formed on Al at 10°C [8],[16]. An alkaline etching of the Al-matrix surrounding the intermetallic particles due to increased pH in the crevice was seen [7],[8],[9]. As described earlier, a small Mg/Si ratio makes the alloy more susceptible to intergranular corrosion. From the chemical composition in table 3.2 a small Mg/Si ratio of 0.86 could be seen for both AA6005 and AA6082. Of the aluminium alloys involved in this thesis, AA6005 consist of the highest amount of copper. The noble intermetallic particles like Fe, Si, Cu and Cr acts as cathodic sites in the Al-matrix. Thus, AA6005 seemed more susceptible to corrosion when comparing the corrosion rates of AA6005 from the earlier studies [7],[8],[9] with the corrosion rates of AA5083 and AA6082 in this thesis.

Calculated corrosion rates by Faraday's law corresponding to the electrochemical data in figure 4.15 was shown in figure 4.19. The calculated corrosion rates of AA6005 in galvanic crevice experiments showed a significant deviation from the measured rates. In example, the green curve for galvanic crevice with CP of AA6005 [7] had a corresponding measured corrosion rate of 0.45 [mg/cm^2] in figure 4.18. The blue curve for galvanic crevice with CP parallel 1 [8] had a corresponding measured corrosion rate of 0.36 [mg/cm^2]. The

orange curve for galvanic crevice with CP [9] had a corresponding measured corrosion rate of 0.64 [mg/cm^2]. Recall that the electrochemical data for the experiment of [9] was plotted for seventy two hours in figure 4.15, but the calculated corrosion rate in figure 4.19 was performed in the original test duration of ninety six hours. The latter was done so the calculated corrosion rate would correspond to the measured value of the experiment of ninety six hours. Reasons for the differences is not easily explained. As earlier described, the comparison of the measured and calculated corrosion rates of AA5083 and AA6082 revealed more similar values. The larger differences regarding AA6005 must arise from other differences which will be discussed later.

5.3 Surface characterization

The formation of deposits in addition to the distribution of intermetallic particles on the sample surfaces has shown to be important factors due to the electrochemical behavior and corrosion rates as described earlier. Investigations in the Scanning Electron Microscopy (SEM) in addition to Energy Dispersive Spectroscopy (EDS) revealed the microscopic aspects of these factors. The microscopic investigations of steel from galvanic corrosion experiments confirmed the deposit layer to be mainly of $Mg(OH)_2$. When the calcareous deposits were scraped off, Ca-ions was found as small particles in the Mg-layer [16] near the metal surface, as shown in table 4.15. In addition, a small amount of Cl-ions and Na-ions was revealed, indicating that salts from the seawater deposit on the surface. The alkaline environment due to the formation of hydroxyl-ions from the reduction reactions when CP was applied increased the pH on the surface. Positive charged ions was drawn to the surface due to electroneutrality, and the formation of $Mg(OH)_2$ arose. The deposits on AA5083 involved in galvanic corrosion indicated a Al-oxide layer, as shown in figure 4.32. The surface morphology could be seen on the micrograph, revealing the additional intermetallic particles in the Al-matrix as shown in table 4.6. Thus, the oxide layer was thin. The deposits on both AA6005 and AA6082 involved in galvanic corrosion experiments also revealed a thin Al-oxide layer.

The steel samples involved in galvanic crevice experiments with a crevice size of $300\,\mu\mathrm{m}$ showed a thicker layer of deposits near the crevice mouth. A uniform layer of $Mg(OH)_2$ with small Ca particles was covering the exposed sample surfaces. A thin Mg-oxide layer was seen on AA6082 involved in the same experiment in addition to small Ca particles. The EDS analysis in table 4.16 showed a small amount of Ca and C. In a pH range between 6 - 7.58 $CaCO_3$ precipitates [14],[17]. AA5083 involved in galvanic crevice corrosion experiment for five days revealed a thicker deposit layer at the edge of the upper crevice mouth, as shown in figure 4.36. EDS analysis of spectrum 2 indicated a significant amount

of Ca and O in addition to C. The edge of the crevice mouth was closer to the bulk solution containing a less alkaline pH, which could explain the precipitation of $CaCO_3$ at the edge. The SEM image post chemical cleaning in figure 4.37 showed localized corrosion attacks where the calcareous deposits were prior cleaning. The behavior could be explained by the alkaline etching of the Al-matrix surrounding the intermetallic particles. As described earlier, the deposit of $Mg(OH)_2$ precipitates over the earlier cathodic sites [5].

The precipitation of $CaCO_3$ at the edge of the upper crevice mouth was also observed on AA5083 parallel 1 in the experiment for twenty days, as shown in figure 4.38. A $Mg(OH)_2$ layer with attached Ca-ions was also observed. A lot of other ions from the artificial seawater was revealed in the EDS analysis of the deposits. Earlier studies has indicated that sulphate-ions inhibits the formation of $CaCO_3$ [16], which could explain the single particle distribution of Ca in the Mg-layer. A higher content of fluoride was observed. Non literature of the affect of fluoride regarding calcareous deposits has been found. Localized corrosion was seen on both upper and lower crevice mouth post chemical cleaning. Alkaline etching of the Al-matrix surrounding the intermetallic particles could be seen in figure 4.39. Pitting potentials of -620 $mV_{Ag/AgCl}$ and -590 $mV_{Ag/AgCl}$ has been found for AA5083 and AA6082 respectively in natural seawater at 10°C [21] which corresponded to the experimental potential-pH diagram [20]. It is difficult to explain why pitting corrosion occur at the potential of the sacrificial anode at approximately -1100 mV_{SCE}. Some corrosion is of course expected regarding the OCP. Though, earlier studies have observed similar results at these potentials from cathodic polarization [21].

A uniform Al-oxide layer in addition to corrosion products was observed on AA5083 parallel 2. Recall that the parallel experienced gas evolution and the samples were not replaced before the experiment was restarted. SEM images post chemical cleaning revealed larger areas of the surface suffering of pitting attacks. Earlier observations of pitting have been centered at the crevice mouth, though in this parallel the whole surface suffered of pitting. Carbon steel did not show any significant corrosion attack from the hydrogen gas evolution. Lack of some pieces of the edges was the only visible difference in the steel surface. Thus, the steel seemed protected even though the potential got very cathodic during the gas evolution [13].

The long term parallels of AA6082 also revealed a thicker deposit layer at the crevice mouth. A $Mg(OH)_2$ layer in addition to small $CaCO_3$ particles was observed on parallel 2. The initial pH in the artificial seawater trapped inside the crevice was approximately 8.2. The precipitation of $CaCO_3$ could occur in this pH range [17]. As the environment inside the crevice changed and the pH increased, the deposition kinetics of $Mg(OH)_2$ got

faster in the alkaline environments at lower temperatures [14],[16], and possibly inhibit the precipitation of $CaCO_3$. Localized corrosion was observed post chemical cleaning where the deposits were thickest at the upper crevice mouth, as shown in figure 4.51. The SEM image in figure 4.52 revealed the alkaline etching of the Al-matrix surrounding the intermetallic particles, as earlier described. The depth of the pits was not measured. Though, the pit depths seems to correspond with earlier studies [21].

The formation of deposits in addition to intermetallic particle distribution in the alloys has shown to be important factors due to the electrochemical behavior and corrosion rates. Cathodic protection of steel-aluminium galvanic couples in galvanic corrosion experiments seems possible based on the electrochemical behavior, weight loss measurements and the surface characterization of the involved alloys. Both steel and the respective aluminium alloys showed a cathodic current throughout the experiments, where the currents on steel were one and two order of magnitude larger than on Al. Very small corrosion rates were observed regarding both steel and the aluminium alloys involved in galvanic corrosion experiments. The corrosion rates of the aluminium alloys corresponded to the OCP. Thus, some corrosion is expected due to initial corrosion attack which will be stabilized and passivated with time due to the protective properties of the calcareous deposits and repassivated oxide films. The electrochemical behavior of steel and the aluminium alloys in a simulated crevice showed that the currents decayed and was stabilized as a function of time. It is reason to believe that the very small final anodic currents on the aluminium alloys will turn cathodic at long term exposure for more than twenty days. Furthermore, the formation of calcareous deposits and repassivated oxide layers indicated the possibility to seal the crevice and reduce further crevice corrosion respectively. The depletion of oxygen both at the seabed and in the crevice would reduce the possible reduction reactions and the the currents decreases. A linear trend in the corrosion rates as a function of time is thus expected since cathodic protection of both steel and aluminium is a possibility for corrosion control rather than corrosion inhibition. Nevertheless, steel-aluminium galvanic couples can be protected against crevice corrosion with applied cathodic protection.

5.4 Experimental work

The experimental setup and procedure were based on the previous work of Røstbø [7] and the specialization project of the author [9]. New dimensions of the crevice device (sample holders) regarding crevice corrosion experiments were introduced by the author [9] in the specialization project to give more accurate results of the corrosion rates. In addition, a larger crevice size ($300\,\mu m$) was introduced in this thesis to investigate the affect of exposing the whole surface area of the samples in the crevice. The latter seemed to give better

results regarding exposure of the samples. Furthermore, a more uniform deposit layer was revealed on the samples, which seemed to give better protective properties. However, by using a crevice size of $100\,\mu m$ only half of the sample surface was exposed. The results gives a contradicting effect. With a small size the crevice could possibly be sealed by the deposits formed at the crevice mouth, which could inhibit further crevice corrosion. A thicker and more uniform deposit layer was developed with a larger crevice size, which protected the sample surfaces. Teflon strips were used to simulate a crevice between the samples. As earlier described, a problem regarding the use of these strips were the possibility of crevice corrosion between the sample and the Teflon. This could occur if the two sample holders were not tightened good enough. Crevice corrosion could also occur between the Miccro lacquer and the edge of the samples. The pH measurements by use of pH paper should not be regarded as accurate. A more sophisticated setup for pH measurements on the samples inside the crevice should be considered. Even though the crevice device was lifted up carefully before it was opened and the pH was measured, the environment inside the crevice would change as a consequence of convection in the solution.

Practical difficulties regarding the analytical weight were seen in the specialization project of the author [9], where the values on the weight were not always stabilized. Improvements regarding the measurements have been made. First, the analytical weight was calibrated before each measurement. Second, anti static tissues were used to clean the weight. In addition, after the cleaning and drying with the heating gun the samples were cooled. Cotton gloves were used to prevent static friction when the samples were placed on the weight. Each sample was weighted three times to see if the weight value changed. The largest difference between each weight round was stated to only be 0.1 mg, which was the error of the weight. This procedure was concluded to be satisfactory. Furthermore, corrosion rates were calculated from the anodic current densities regarding the aluminium alloys and the sacrificial anode, as described in appendix B. The aim was to investigate the correlation between the measured rates and the rates regarding the electrochemical data. As discussed earlier, the correlation was stated to be satisfactory regarding AA5083 and AA6082. A flaw in the calculation could be the molar mass used for the anode. For simplicity, the molar mass of aluminium was also used for the anode, in addition to the same valence z. A larger difference between the measured corrosion rates versus the calculated was seen regarding AA6005 when comparing the results from earlier studies. This is not easily explained. Comparing results from different authors are difficult according to the different ways of performing the experiments and measurements.

5.5 Further work

Based on the performed work and possible improvements as discussed earlier for the aim of this ongoing project, the following suggestions have been made for further work.

- Perform the experimental work in natural seawater, due to introduction of the biological factors of seawater and flow velocity.
- GDOS analysis of the intermetallic particle distribution in the aluminium alloys to better understand the factors which affect the alkaline etching mechanisms.
- Use a more reliable experimental setup to prevent experimental errors.
- Cross section analysis to measure the pit depths.
- Measure the potential and current along the crevice length by use of a more sophisticated crevice setup.
- Long term exposure for several months to see if the crevice is sealed due to formation of calcareous deposits.
- A more sophisticated setup for pH measurements inside the crevice.

Chapter 6

Conclusion

Studies of steel-aluminium galvanic couples have been performed in order to investigate whether or not cathodic protection is possible against crevice corrosion. In addition, investigations of steel-aluminium galvanic couples in the absence of a crevice were performed to validate the effect of cathodic protection. The electrochemical behavior of carbon steel X65 and the aluminium alloys 5083, 6005 and 6082 has been studied, in addition to weight loss measurements and surface characterization. The study showed as follows:

- Cathodic protection of steel-aluminium galvanic couples is possible in the absence of a crevice.
- Both steel and the aluminium alloys showed cathodic currents when galvanic coupled with the sacrificial anode in the absence of a crevice. The cathodic current on steel was one and two orders of magnitude larger than on the aluminium alloys.
- A uniform calcareous deposit layer of mainly $Mg(OH)_2$ covered the steel surfaces. Calcium ions were found as small particles in the Mg-layer near the steel surface. A uniform oxide film covered the surface on the aluminium alloys. The sacrificial anode experienced heavy pitting attacks.
- Galvanic crevice corrosion experiments with applied cathodic protection and a crevice size of $300\,\mu m$ gave a uniform layer of calcareous deposit on steel, mainly of $Mg(OH)_2$. A thin oxide layer was seen on the aluminium alloys. A thicker layer of deposit was seen at the crevice mouth.
- Partial exposure to the artificial seawater was seen on the samples involved in gal-

vanic crevice corrosion experiment with applied cathodic protection and a crevice size of $100\,\mu m$. Gas bobbles trapped inside the crevice could explain this, or the crevice size was to small. A thicker layer of deposits were seen at the crevice mouth on the samples which could possibly seal the crevice mouth.

- Cathodic currents were seen on steel in galvanic crevice experiments. Higher initial cathodic currents were observed before they decreased as a function of time. Initial anodic current peaks were seen on the aluminium alloys. The anodic currents decayed towards zero as a function of time in long term experiments.
- An increased alkaline environment was observed in the galvanic crevice experiments with a pH in the range of 9-11. The formation of hydroxyl-ions from the reduction reactions on steel gave the increased pH. Destabilization of the oxide film on aluminium revealed the intermetallic particles in the aluminium matrix. The intermetallic particles acted as cathodic sites in the Al-matrix. An alkaline etching of the Al-matrix surrounding the intermetallic particles was initiated due to the increased pH, and detachment of the intermetallic particles could occur. A renewed oxide film in addition to calcareous deposits formed at these areas afterwards.
- The potentials were in the range of the Open Circuit Potential of the sacrificial anode in both galvanic and galvanic crevice experiments when CP was applied.
- The currents decayed as a function of time when the environment inside the crevice was stabilized due to oxygen depletion and less reduction reactions on the surfaces.
- A linear trend was observed regarding the corrosion rates of the aluminium alloys involved in the experiments. Long term parallels suffered the highest corrosion rates. Localized pitting attacks were mainly seen at the crevice mouth on the aluminium alloys.
- Comparisons of earlier obtained results in this project revealed higher corrosion rates of aluminium alloy 6005 than seen of aluminium alloy 5083 and 6082 performed in this thesis. A higher content of the nobler intermetallic particles such as Cu and a small Mg/Si ratio in AA6005 could lead to intergranular corrosion.
- Some corrosion is expected due to initial corrosion attacks which will be stabilized in the crevice as a function of time.
- Steel-aluminium galvanic couples could be protected in the form of corrosion control against crevice corrosion by application of cathodic protection.

References

[1] NORSOK. *STANDARD M-121. Aluminium structural material*. NORSOK 2.ed., 2015.

[2] NORSOK. *STANDARD M-DP-001. Design principles material selection*. NORSOK, 1994.

[3] C. Knutsen, I. Kvale, J.H. Nordlien. *Aluminium Applied for Subsea Structures: Possibilities and Challenges*. The International Society of Offshore and Polar Engineers. Proceedings of the International Offshore and Polar Engineering Conference, pp. 46-52, 2001.

[4] K. Nisancioglu. *Corrosion and protection of aluminum alloys in seawater.* Corrosion behaviour and protection of copper and aluminium alloys in seawater, D. Féron, ed., pp. 145-155, CRC Press, 2007.

[5] R. Gundersen, K. Nisancioglu. *Cathodic Protection of Aluminum in Seawater.* Corrosion, Vol. 46, No. 4, pp. 279-285, 1990.

[6] M.J. Pryor, D.S. Keir. *Galvanic Corrosion. Current Flow and Polarization Characteristics of the Aluminum-Steel and Zinc-Steel Couples in Sodium Chloride Solution*. Journal of the Electrochemical Society, Vol. 104, No. 5, pp. 269-275, 1957.

[7] S. Røstbø. *Cathodic Protection of Steel-Aluminium Galvanic Couples for a New Generation of Lightweight Subsea Structures. Master's thesis.* NTNU, 2016.

[8] H. Solli. *Effects of three metal coupling on galvanic crevice corrosion. Master's thesis.* NTNU, 2017.

[9] K. Jacobsen. *Corrosion and Cathodic Protection of Steel-Aluminium Galvanic Couples in Subsea Structures. Specialization Project.* NTNU, 2017.

[10] K. Nisancioglu. *Corrosion Basics and Engineering*. Norwegian University of Science and Technology, 1994.

[11] NORSOK. *STANDARD M-CR-503. Cathodic protection*. NORSOK, 1994.

[12] DNV. *Recommended Practice DNV-RP-B401, Cathodic Protection Design*. DET NORSKE VERITAS (DNV), 2011.

[13] F. Galsgaard, L.V. Nielsen. *AC/DC interference corrosion in pipelines*. MetriCorr, 2006.

[14] T. Okstad. *Hydrogenutvikling ved katodisk beskyttelse av karbonstål i naturlig sjøvann. Master's thesis.* NTNU, 2005.

[15] S. Elbeik, A.C.C. Tseung, A.L. Mackay. *The formation of calcareous deposits during the corrosion of mild steel in sea water*. Corrosion Science, Vol. 26, No. 9, pp. 669-680, 1986.

[16] C. Barchiche, C. Deslouis, O. Gil, P. Refait, B. Tribollet. *Characterisation of calcareous deposits by electrochemical methods: role of sulphates, calcium concentration and temperature*. Electrochimica Acta, Vol. 49, No. 17, pp. 2833-2839, 2004.

[17] Y. Yang, J.D. Scantlebury, E.V. Koroleva. *A Study of Calcareous Deposits on Cathodically Protected Mild Steel in Artificial Seawater.* Metals, Vol. 5, No. 1, pp. 439-456, 2015.

[18] E. Deltombe, M. Pourbaix. *The Electrochemical Behavior of Aluminum - Potential pH Diagram of the System Al-H_2O at 25°C*. Corrosion, Vol. 14, No. 11, pp. 16-20, 1958.

[19] N.L. Sukiman, X. Zhou, N. Birbilis, A.E. Hughes, J.M.C. Mol, S.J. Garcia, X. Zhou, G.E. Thompson. *Durability and Corrosion of Aluminium and Its Alloys: Overview, Property Space, Techniques and Developments*. InTech, Chapter 2, pp. 52, 2012.

[20] Ph. Gimenez, J.J. Rameau, M.C. Reboul. *Experimental pH Potential Diagram of Aluminum for Sea Water*. Corrosion, Vol. 37, No. 12, pp. 673-682, 1981.

[21] R. Johnsen, O. Nese. *AA5083 and AA6082 Exposed to Seawater - Effect of Potential on Corrosion Behaviour*. NACE International, No. 8942, 2017, April 27.

[22] S. Joma, M. Sancy, E.M.M. Sutter, T.T.M. Tran, B. Tribollet. *Incongruent dissolution of copper in an Al-Cu assembling. Influence of local pH changes.* Surface and Interface Analysis, Vol. 45, No. 10, pp. 1590-1596, 2013.

[23] Z. Li, F. Gan, X. Mao. *A study on cathodic protection against crevice corrosion in dilute NaCl solutions*. Corrosion Science, Vol. 44, No. 4, pp. 689-701, 2002.

[24] A. Bergin. *Alternating Current Corrosion of Steel in Seawater. Master's thesis.* NTNU, 2015.

[25] ASTM International. *ASTM G1-03(2011). Standard Practice for Preparing, Cleaning and Evaluating Corrosion Test Specimens*. ASTM International, 2011.

[26] ASTM International. *ASTM D1141-98(2013). Standard Practice for the Preparation of Substitute Ocean Water*. ASTM International, 2013.

[27] K. Rottmann. *Matematisk Formelsamling*. Spektrum forlag, 13. ed., pp. 174, 2013.

Appendix A: Weight loss measurement - carbon steel X65

Chemical cleaning of carbon steel X65 was performed in accordance to the ASTM standard G1 [25] to remove corrosion products and calcareous deposits. The steel samples were chemically cleaned in a solution of hexamethylenetetramin and hydrochloric acid for five cycles. The samples were weighted on an analytical weight between each cycle to determine the weight loss. Accumulated weight loss was plotted as a function of number of cycles, as shown in figure A.1. The intersection of the two extrapolated trend lines gave the weight loss of the steel.

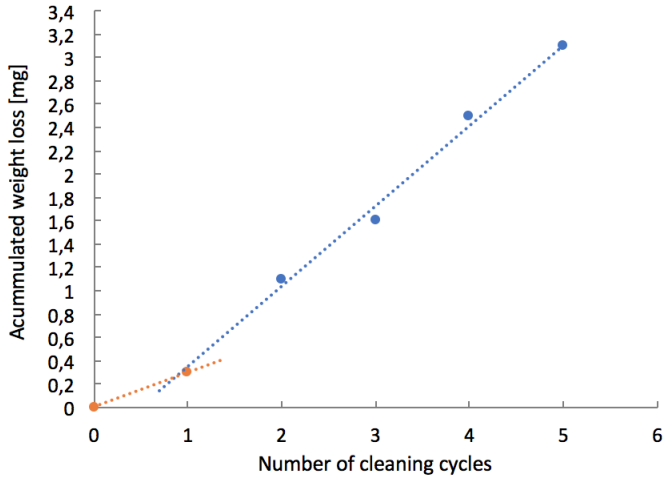

Figure A.1: Schematic graph of weight loss measurement of carbon steel X65. Accumulated weight loss [mg] as a function of cleaning cycles.

Appendix B: Weight loss calculations by Faraday's law

The trapezoidal rule: integration of current densities

Weight loss was calculated by the trapezoidal rule and Faraday's law to compare with the measured weight loss from the analytical weight. The trapezoidal rule was used as the numerical integration method of the anodic current densities from the electrochemical data, as shown in equation (B.1) - (B.3) [27]:

$$\left[\frac{Q}{A}\right] = \int_a^b f(x)dx \tag{B.1}$$

$$\int_a^b f(x)dx = \frac{\Delta x}{2}[f(x_0) + 2f(x_1) + 2f(x_2) + 2f(x_3) + ... + 2f(x_{n-1}) + f(x_n)] \tag{B.2}$$

where $f(x)$ is the anodic current densities [µA/cm^2], and Δx is given by:

$$[s] = \Delta x = \frac{b-a}{n} \tag{B.3}$$

Where b is the end-time in seconds [s] of the last measured electrochemical data point in the experiment, a is the time [s] for the first measured electrochemical data point and n is the number of measured data points in the experiment.

Weight loss by Faraday's law

The weight loss m can be calculated from Faraday's law by [10]:

$$m = \frac{Q \cdot M_m}{A \cdot z \cdot F} \tag{B.4}$$

where Q is charge [C], A is area [cm^2], M_m is the molar mass [g/mole], z is the valence of the respective ion of the metal and F is Faraday's constant 96485 [C/mole]. For simplicity, a molar mass M_m of 26.98 g/mole and a valence z of 3 was used in the calculations for both the aluminium alloys and the sacrificial anode AlZnIn. The last calculated data point of weight loss is given in the weight loss tables of the respective alloys in chapter 4.

Appendix C: Additional SEM and EDS data

Coupling of carbon steel X65 and aluminium alloy 5083

Galvanic corrosion: cathodic protection at 10°C for 3 days

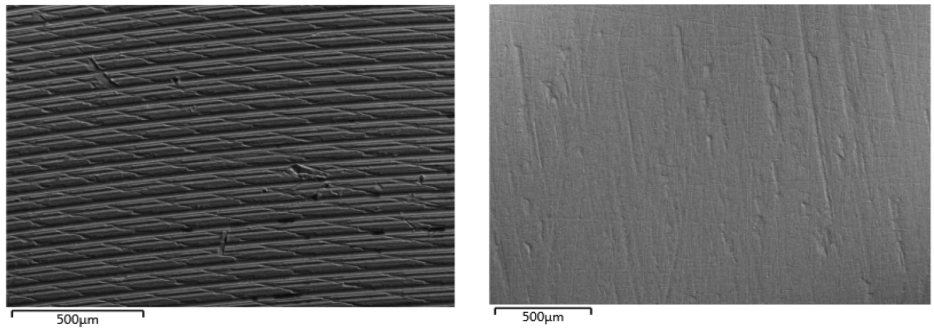

(a) **(b)**

Figure C.1: SEM images post chemical cleaning (a) SEM of the middle of aluminium alloy 5083 sample, (b) SEM of the middle of carbon steel X65 sample.

Crevice corrosion: cathodic protection at 10°C for 3 days

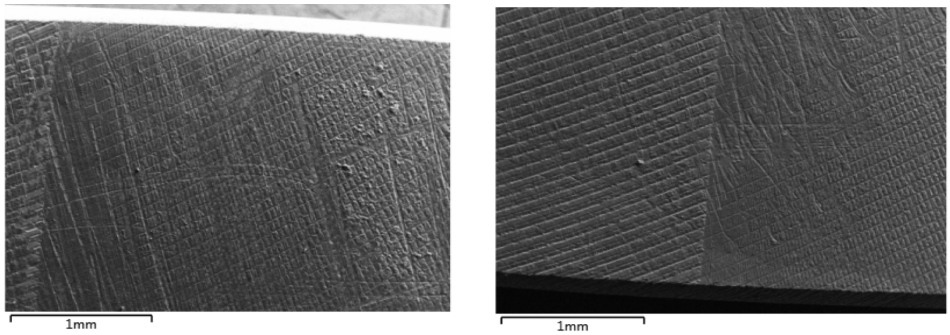

(a) **(b)**

Figure C.2: SEM images prior chemical cleaning of aluminium alloy 5083 sample (a) upper crevice mouth, (b) lower crevice mouth.

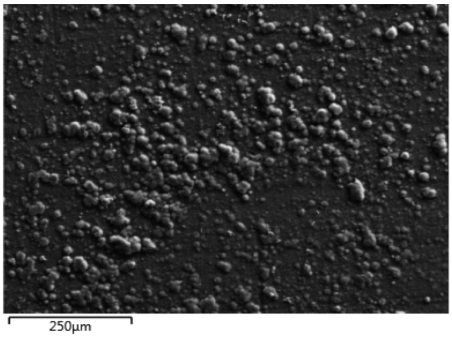

Figure C.3: SEM image of the middle of carbon steel X65 sample prior chemical cleaning.

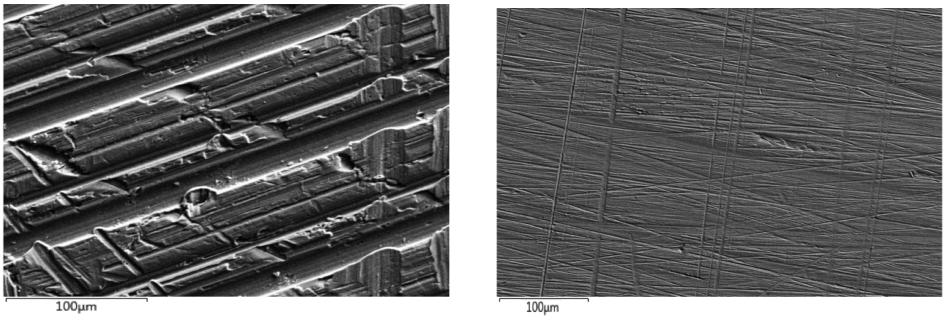

(a) **(b)**

Figure C.4: SEM images post chemical cleaning: (a) close up of the upper part of aluminium alloy 5083 sample, (b) the middle of carbon steel X65 sample.

Crevice corrosion parallel 1: cathodic protection at 10°C for 20 days

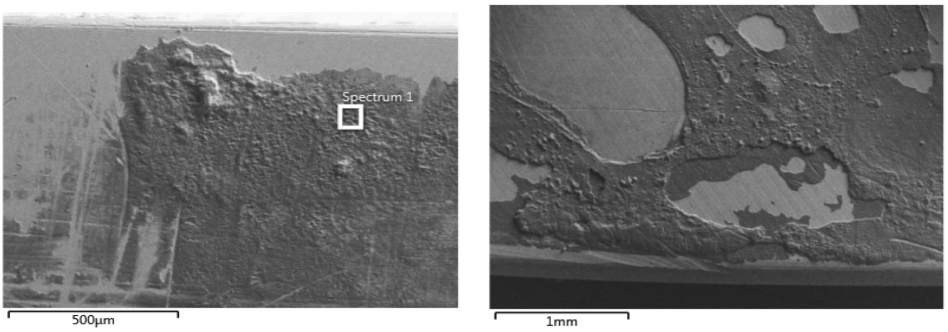

(a) **(b)**

Figure C.5: SEM images prior chemical cleaning: (a) the upper crevice mouth of carbon steel X65 sample, (b) the lower crevice mouth of carbon steel X65 sample.

Table C.1: EDS analysis for spectrum 1 in figure C.5a prior chemical cleaning.

Element	Spectrum 1 [wt%]
C	4.16
O	58.29
Mg	7.50
Al	27.33
Cl	0.19
Ca	0.78
Fe	1.74

Crevice corrosion parallel 2: cathodic protection at 10°C for 20 days

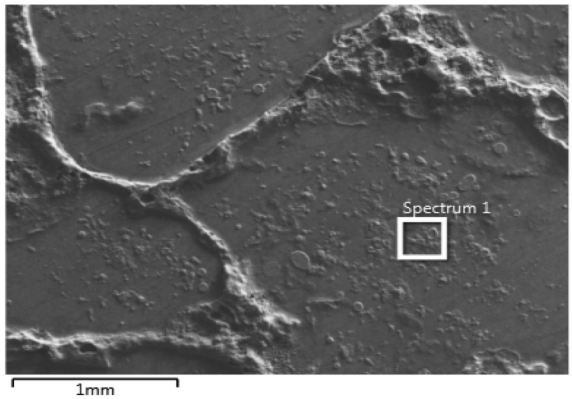

Figure C.6: SEM image of the upper crevice mouth of aluminium alloy 5083 sample prior chemical cleaning.

Table C.2: EDS analysis for spectrum 1 in figure C.6 prior chemical cleaning.

Element	Spectrum 1 [wt%]
C	4.57
O	49.29
Mg	1.70
Al	44.43

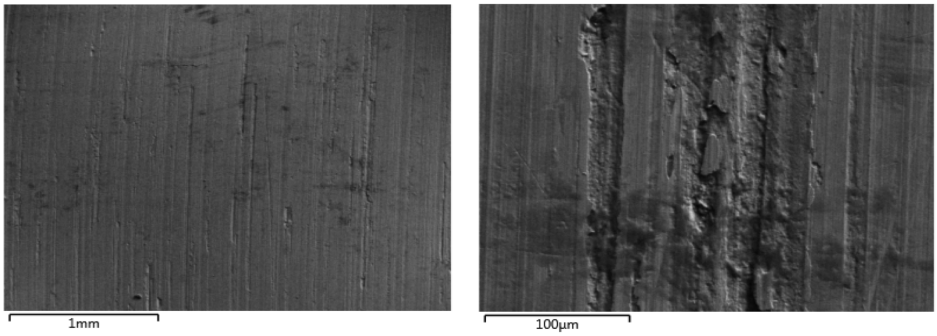

(a) **(b)**

Figure C.7: SEM images of carbon steel X65 sample prior chemical cleaning (a) SEM of the middle of the sample, (b) extra close up of the middle of the sample.

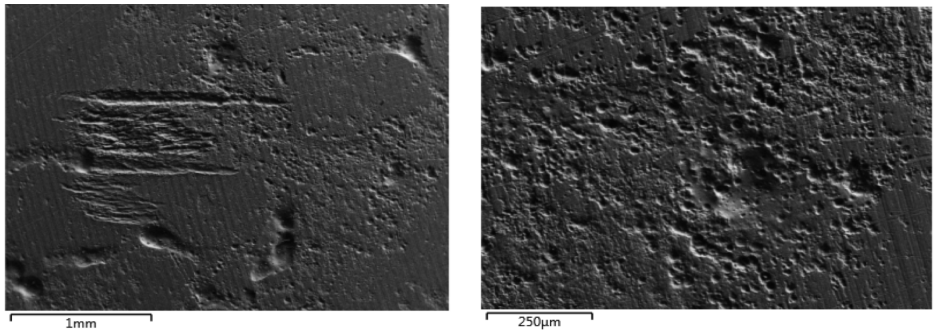

(a) **(b)**

Figure C.8: SEM images of aluminium alloy 5083 sample post chemical cleaning (a) SEM of the middle of the sample, (b) extra close up of the middle of the sample.

Coupling of carbon steel X65 and aluminium alloy 6005

Galvanic corrosion: cathodic protection at 10°C for 3 days

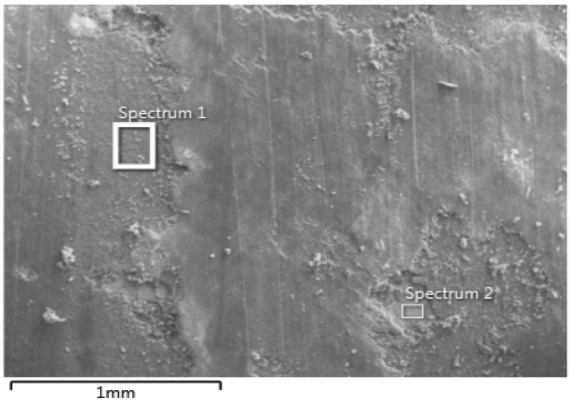

Figure C.9: SEM image of the middle of carbon steel X65 sample prior chemical cleaning.

Table C.3: EDS analysis for spectrum 1 and 2 in figure C.9 prior chemical cleaning.

Element	Spectrum 1 [wt%]	Spectrum 2 [wt%]
O	53.53	2.89
Mg	44.12	2.01
Cl	0.79	-
Ca	0.38	0.37
Fe	1.18	89.05
Mn	-	1.46
C	-	4.22

Coupling of carbon steel X65 and aluminium alloy 6082

Galvanic corrosion: cathodic protection at 10°C for 3 days

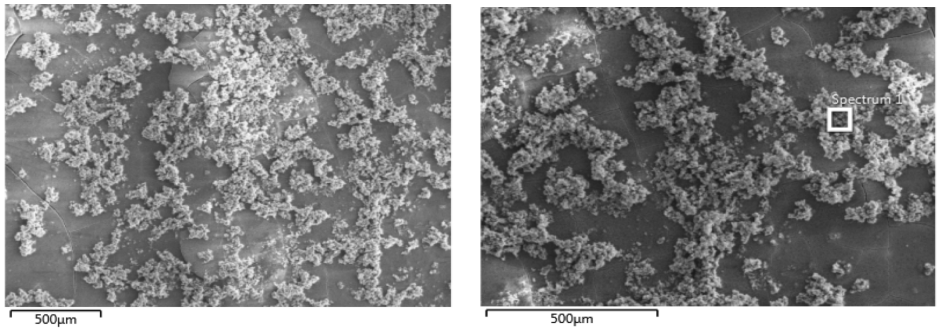

(a) **(b)**

Figure C.10: (a) SEM image of the middle of carbon steel X65 sample prior chemical cleaning, (b) close up of the calcareous deposit on carbon steel X65.

Table C.4: EDS analysis for spectrum 1 in figure C.10b prior chemical cleaning.

Element	Spectrum 1 [wt%]
Mg	41.53
Cl	3.77
O	50.96
Fe	1.11
Na	1.37
Al	0.80
Ca	0.45

Crevice corrosion: cathodic protection at 10°C for 3 days

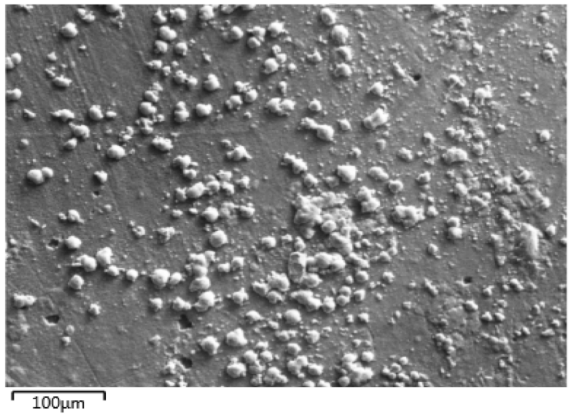

Figure C.11: Zoomed SEM image of spectrum 1 in figure 4.47 of aluminium alloy 6082 sample prior chemical cleaning.

Crevice corrosion parallel 1: cathodic protection at 10°C for 20 days

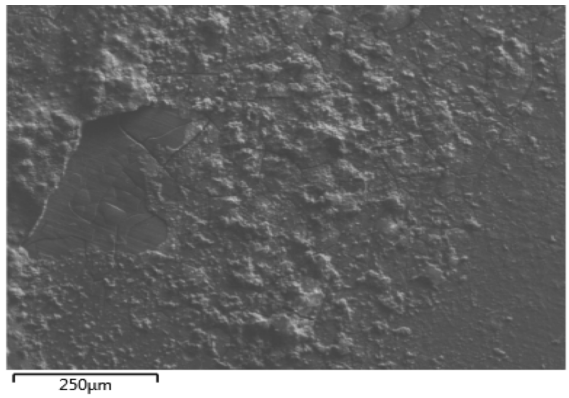

Figure C.12: SEM image of the lower crevice mouth of aluminium alloy 6082 sample prior chemical cleaning.

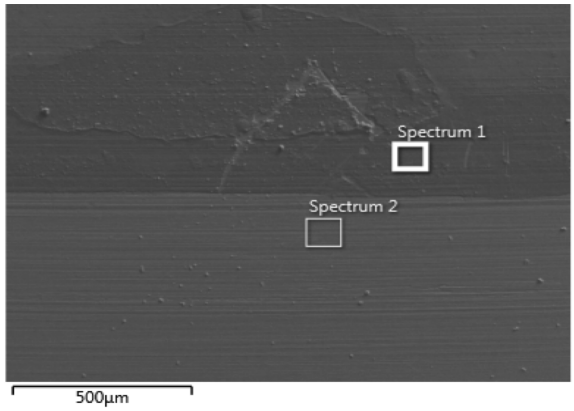

Figure C.13: SEM image of the upper crevice mouth of aluminium alloy 6082 sample prior chemical cleaning.

Table C.5: EDS analysis for spectrum 1 and 2 in figure C.13 prior chemical cleaning.

Element	Spectrum 1 [wt%]	Spectrum 2 [wt%]
O	45.37	0.95
Al	54.47	97.86
Ca	0.16	-
Si	-	0.72
Mn	-	0.46

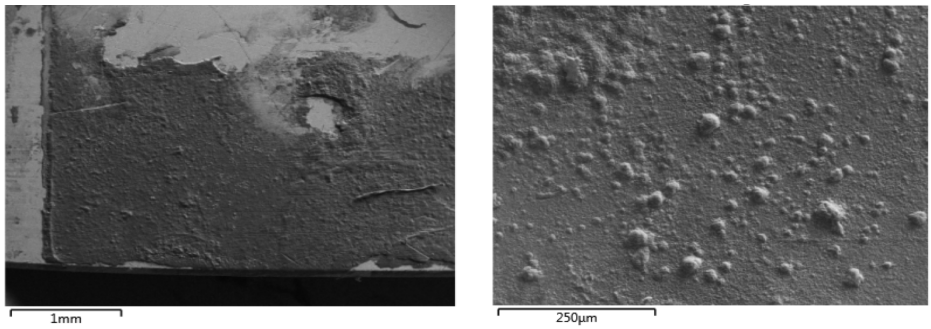

(a) **(b)**

Figure C.14: SEM image prior chemical cleaning (a) the lower crevice mouth of carbon steel X65 sample (b) close up of the lower crevice mouth of carbon steel X65 sample.

Crevice corrosion parallel 2: cathodic protection at 10°C for 20 days

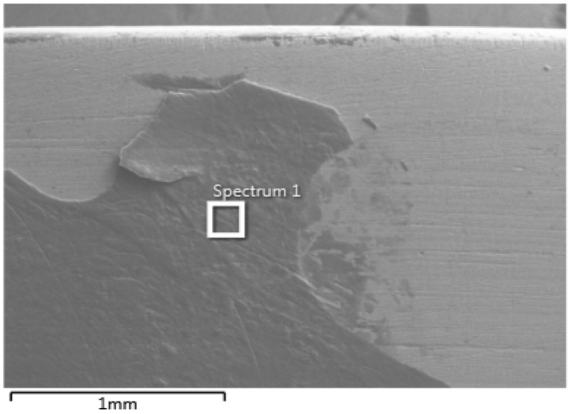

Figure C.15: SEM image of the upper crevice mouth of carbon steel X65 sample prior chemical cleaning.

Table C.6: EDS analysis for spectrum 1 in figure C.15 prior chemical cleaning.

Element	Spectrum 1 [wt%]
C	4.43
O	52.17
Mg	31.54
Al	8.07
Ca	2.28
Fe	1.51